A STAGE-BY-STAGE POST-STALL COMPRESSION SYSTEM MODELING TECHNIQUE: METHODOLOGY, VALIDATION, AND APPLICATION

by

Milton W. Davis, Jr.

Dissertation submitted to the Faculty of the
Virginia Polytechnic Institute and State University
in partial fulfillment of the requirements for the degree of

DOCTOR OF PHILOSOPHY

in

Mechanical Engineering

APPROVED:

W. F. O'Brien

J. Moore

R. G. Leonard

H. L. Moses

G. T. Patterson

December, 1986

Blacksburg, Virginia

A STAGE-BY-STAGE POST-STALL COMPRESSION SYSTEM MODELING TECHNIQUE: METHODOLOGY, VALIDATION, AND APPLICATION

by

Milton W. Davis, Jr.

Committee Chairman: Walter F. O'Brien
Mechanical Engineering

(ABSTRACT)

A one-dimensional, stage-by-stage axial compression system mathematical model has been constructed which can describe system behavior during post-stall events such as surge and rotating stall. The model uses a numerical technique to solve the nonlinear conservation equations of mass, momentum, and energy. Inputs for blade forces and shaft work are provided by a set of quasi-steady stage characteristics modified by a first order lagging equation to simulate dynamic stage characteristics. The model was validated with experimental results for a three-stage, low-speed compressor and a nine-stage, high-pressure compressor. Using these models, a parametric study was conducted to determine the effect of inlet resistance, combustor performance, heat transfer, and stage characteristic changes due to hardware modification on post-stall system behavior.

ACKNOWLEDGMENTS

The work described herein was sponsored by the Arnold Engineering Development Center (AEDC), Air Force Systems Command. The results were obtained by Sverdrup Technology, Inc., AEDC Group, operating contractor for the propulsion test facilities of the AEDC, Arnold Air Force Station, Tennessee.

The author wishes to thank his employer, Sverdrup Technology, Inc., for their financial and spiritual support during the three-year period over which this program has taken. The Graduate Study Program which allowed the author to spend a year (1983-1984) on the Virginia Tech campus pursuing his course work and satisfying the residency requirement eased the financial burden and made the obtaining of this degree possible.

The author wishes to thank his major professor, Dr. W. F. O'Brien for his technical support and especially for his moral support during some of the more difficult times of this process. The author wishes to acknowledge the other members of his committee, Dr. J. Moore, Dr. R. G. Leonard, Dr. H. L. Moses, and Dr. G. T. Patterson for their guidance and inputs into the effort reported within this dissertation. The author also wishes to thank and acknowledge persons within Sverdrup Technology, Inc., who were instrumental in the preparation of this dissertation: Dr. G. T. Patterson of the Analysis and Evaluation Section (not only a Committee Member but a fellow colleague) for his technical inputs and guidance; Dr. V. K. Smith, Manager, Technology Department, for his encouragement and constructive inputs during the review cycle; Mr. R. E. Smith, Jr., Sverdrup Chief Scientist, for his faith in the author

and positive encouragement; and Mr. A. Hale of the Computational Fluid Dynamics Section for his technical assistance, computational abilities, and moral support. The author also wishes to thank Linda W. Hershman and Linda Meredith of Lin-Hersh Enterprises, for their efforts in the typing of this dissertation and Edna Grant of Schneider Services International for her efforts in figure preparation.

The author wishes to thank and acknowledge his family for their support and understanding during the many long days and missed weekends that were necessary for the completion of this dissertation. Without their support, this dissertation would not have been completed.

TABLE OF CONTENTS

LIST OF FIGURES

NOMENCLATURE

A	Area
A/C	Point of Maximum Camber
a	Acoustic velocity
B	Greitzer's "B" parameter
C	Rotating stall point; Moore's model
c_p	Specific heat at constant pressure
C/S	Solidity
CV	Control Volume
c_v	Specific heat at constant volume
C_X	Axial velocity
E	Energy function
e	Internal energy
FX	Force of compressor blading and cases acting on fluid, including wall pressure area force
F_B	Force of compressor blading
f	Frequency or friction factor
far	Fuel-air ratio
G(g)	Characteristic function; Moore's model
H	Total enthalpy
h	Circumferential velocity disturbance; Moore's model
IMP	Impulse function
k	Coefficient of heat conductivity
L	Length
LVH	Lower Heating Value
L_c	Compressor length; Greitzer's model

L_T	Throttle length; Greitzer's model
M	Mach number
m	Mass of blades, platforms, and seals
$\dot{M}_T$	Mass flow function based on total condition
MOC	Method of characteristics
N	Compressor rotor speed
P	Pressure
$\overline{P}$	Average Pressure
Per	Perimeter
PR	Total pressure ratio
Q	Rate of heat addition to control volume
R	Gas constant
SW	Rate of shaft work
T	Temperature
TR	Total temperature ratio
t	Time
t	Nondimensionalized time
t/c	Thickness-to-chord ratio
U	Generalized notation for Navier-Stokes equations or wheel speed
u	Axial velocity
V	Generalized notation for Navier-Stokes equations or volume
v	Velocity component in direction of rotation
W	Mass flow rate
X	A point along the x-direction
x	Axial coordinate

Greek Symbols

α	Angle of attack
γ	Ratio of specific heats or stagger
ϵ	Energy term in Navier-Stokes equations
δ	Ratio of compressor entry total pressure to standard day, sea-level-static pressure
η	Efficiency
η_{ad}	Stage adiabatic efficiency
ρ	Density
σ	Normal stress
μ	First coefficient of viscosity
λ	Second coefficient of viscosity
ϕ	Flow coefficient or camber
θ	Angular location, ratio of compressor inlet total temperature to standard day, sea-level-static temperature
τ	Time constant
ψ_1, ψ_2, ψ_3	Terms in compatibility equations which account for frictional and energy dissipation terms
ψ^P, ψ	Stage pressure coefficient
ψ^T	Stage temperature coefficient (stage loading parameter)
Δ	A difference
δ	A difference

Superscripts

C	Corrector solution
P	Predictor solution or pertaining to pressure
T	Pertaining to temperature

Subscripts

actual	Pertaining to actual measured value
avg	Average value
B	Pertaining to bleed flow or blade
C	Compressor
Comb	Combustor
crit	Critical value
core	Pertaining to core engine/high-pressure compressor properties
design	Pertaining to design value
E1	Intersection of characteristic curve with previous time solution, exit boundary
E2	Intersection of streamline curve with previous time solution, exit boundary
entrance	Control volume entrance plane
Hys	Hysteresis value
I	Intersection of characteristic curve with previous time solution, inlet boundary
i	Spatial location
idle	Idle power setting
initial	Initial value
inlet	Pertaining to inlet
ISEN	Pertaining to isentropic flow conditions
max	Maximum value or maximum power setting
min	Minimum value
new	New time
old	Old time

P	Plenum
S	Static condition
SS	Steady state condition
S-S	Static-to-static
stall	Value at stall
T	Total conditions
T-S	Total-to-static
T-T	Total-to-total
total	Pertaining to total geometric or thermodynamic properties
tip	Pertaining to tip region
x	Axial component or direction
τ	Pertaining to torque coefficient

CHAPTER I

INTRODUCTION

An important component of the gas turbine engine is the compression system. The compression system performance strongly influences all other component performance. For most gas turbine engines, the compression system consists of one or more aerodynamically coupled axial compressors. These compressors may or may not be connected to the same shaft. An axial compressor consists of stages with a rotating component (rotor) and a stationary component (stator). The rotor is a series of airfoils which, when rotated, impart kinetic energy to the fluid. The stator diffuses the flow and redirects the flow for the next row of rotors. Thus, it is the function of the compression system to increase the static pressure and density of the fluid. Without stable aerodynamic operation, the compression system cannot deliver the desired increase in static pressure and density.

During operation of axial-flow multistage compression systems, instability phenomena known as surge and/or rotating stall have been observed. Surge is a violent planar disturbance in which the flow in the compressor reverses direction and empties the compressor volumes (Figure 1). This flow reversal relieves the back pressure on the compression system so that correct pumping action can take place. If, however, the original cause of surge has not been corrected, the compression system will undergo repressurization until it reaches the instability limit at which time surge will occur again. Surge typically occurs in a frequency range of 3 to 15 Hz. Rotating stall, on the other

hand, is not as apparently violent as surge but is more damaging to engine operation. Rotating stall occurs when a portion of the circumferential annulus is locally stalled by some destabilizing event such as a low-pressure region. Flow separation on a portion of the blades causes the angle of attack to increase on the adjacent blades, thus stalling them. The stalled region progresses from one blade passage to the next giving the appearance that the stalled region rotates in the direction of rotation (Figure 2). When rotating stall is present in a compressor rig, recovery can be produced by opening a throttle valve. When rotating stall occurs in an engine, no such throttle valve is possible. In fact, combustion has the effect of closing the turbine nozzle area, which appears as a throttle to the compressor. Thus, recovery from rotating stall is usually possible in an engine only by stopping the fuel flow and restarting the engine. With continued engine operation, rotating stall is "nonrecoverable". Since the primary focus of this model is on engine compression system performance, the term nonrecoverable stall is used. The "nonrecoverable" type of instability has promoted numerous experimental and analytical investigations over the last decade. Results of several of the experimental investigations can be found in References [1] through [5].

In experimental cases, results are often limited because of specific test hardware and/or economic constraints. Where more information is desired, validated compressor mathematical models can be used to provide performance and stability information not obtained during experimental testing. In addition, these mathematical models also provide

tools for studying the effects of external disturbances thus helping to determine a cause and effect relationship.

Mathematical modeling of axial compression systems has been pursued from the time that axial compressors began to be used in aircraft applications through present-day high-performance military turbine-engine systems. The modeling process has been evolutionary with periods of revolutionary insight providing stimulus for significant advances. Axial compressor instability problems have been a driver for better and more sophisticated models. System surge was the first problem to be addressed in the Forties and Fifties. Rotating stall was a known phenomenon in the Fifties, but significant compression system modeling was not undertaken until the late Sixties and early Seventies. Inlet pressure and temperature distortion effects on compressor stability spawned a multitude of parallel compressor modeling studies and techniques. Then, with the "stagnation stall" problem first associated with the F100 engine in the Seventies, there was and continues to be emphasis on the understanding of surge and rotating stall phenomena on an engine system level as well as a component level. Stagnation stall, or as it has now become known, "nonrecoverable stall", has produced the strongest incentive for the understanding of compression system instability. The associated test programs have produced revolutionary insights into the problem and have also produced many mathematical models.

Prior to describing the current work, previous works are reviewed to obtain an understanding of how the present effort complements and extends the concepts presented by others.

CHAPTER II

LITERATURE SURVEY

II.1 Prestall Compression System Models

II.1.1 Early Analytical Methods

The earliest compressor instability analysis dealt with the most violent form of compressor instability--surge. In works by Hartog [6] and Horlock [7], analysis of surge was performed with the knowledge of the intersection of the pressure ratio/mass flow curve with the throttle curve. The analysis indicated that when the slope of the compressor characteristic was greater than that of the throttle characteristic, unstable compressor operation was possible. This result provided an approximate prediction which was found to be lower than experienced flow rates at surge.

While investigating axial compressor stability problems, Pearson and Bower [8] noted the discrepancy which existed between compressor experiments and characteristic curve theory. This theory did not account for the dynamic effects caused by volumetric capacitance, fluid column inertia, and flow resistance in the compressor and its inlet and exit ducting. Their approach was to represent the compressor by an electrical analogy with a set of time-dependent equations. Individual stage characteristics were coupled or "stacked" to form a representative multistage unit. Compressor instability was assumed to occur when the impedance of any given part of the circuit representing the compressor was zero. Positive circuit impedance indicated stable operation, while

negative circuit impedance indicated unstable operation.

II.1.2 One-Dimensional Models

With the advent of the analog and digital computers, compressor performance and stability computations could be made by using numerical analysis techniques. One type of computer model of the compressor used one-dimensional, lumped-volume techniques. The time-dependent conservation laws of mass, momentum, and energy were applied separately or in combination to the lumped volumes, thus accounting for the dynamic behavior of the system. The conservation laws were expressed with one-dimensional mathematical models which only permitted spatially uniform flow to be considered. Stages were replaced by an actuator disc followed by a lumped volume equal to that of the stage, or group of stages. The required pressure and temperature rise across the actuator disc was usually supplied by a set of stage characteristics. The one-dimensional models were generally used to predict system instability for either undistorted flow or time-variant inflow distortions. Several examples are offered in the following paragraphs.

Gabriel, Wallner, and Lubick [9] developed a one-dimensional, 15-stage axial compressor model using only the conservation-of-mass principle. The compressor model was divided into four parts for which steady-state group characteristics were available. With low-frequency (less than 50 Hz) sinusoidal pressure variation applied to the inlet, the model predicted the experimentally observed stability limit. Because this model did not take into account momentum or energy transfer, the model could not simulate correct compressor behavior under

high-frequency pressure variations.

Kuhlberg, Sheppard, and King [10] developed a one-dimensional model based on the conservation of mass and momentum. They investigated a continuity model (based only on conservation of mass) and found that this model was unsuited for determining dynamic compressor response over the stable operating range of the compression system. With the addition of the momentum equation, it was possible to overcome the problems associated with the continuity model. Also investigated was a model based on the continuity, momentum, and energy equation. It was found that the model behaved in the same manner as the momentum-continuity model. Because of the complexity and lack of flexibility in the more complex model, they chose to use the momentum-continuity model for their analytical studies, which included surge-line prediction with and without inlet planar pressure distortions. In a study of oscillatory inflow effects on compressor stability, the continuity-momentum model predicted the stability limit as observed experimentally up to a frequency of 60 Hz. Beyond that frequency, the model deviated from experimental results.

A one-dimensional model based on all three conservation principles was developed by Willoh and Seldner [11]. Their model assumes that each compressor stage (rotor, stator, and included volume) can be represented by a compressor element coupled to a following lumped volume. The compressor element performance is obtained from steady-state stage characteristics. The gas dynamics of the following lumped volume are modeled through the application of continuity, momentum, and energy.

Although the model uses the conservation principles, some simplifications were made. Convection terms in the momentum equation were neglected and the Mach number at the compressor element exit and in the following lumped volume were assumed the same. The latter simplification resulted in dropping the distinction between static and total pressure in the lumped-volume element. This one-dimensional modeling technique was first implemented on an analog computer. A simulation of the J85-13 compression system was constructed, and predictions of compressor stability limits were obtained and compared to experimental results. Willoh and Seldner found that the predicted stability limit agreed closely with the stall line of the actual jet engine compressor. Daniele, Blaha, and Seldner later implemented this technique on the digital computer [12]. In addition to the simplifications used in the analog computer simulation, the digital simulation included a simplification which eliminated the temperature dynamics in the lumped-volume element. The results with this simplification were in agreement with those obtained by the analog simulation at corrected speeds of 80 percent and below. However, the results differed at the higher speeds.

Kimzey developed a one-dimensional technique which solved the full nonlinear form of all three inviscid conservation equations [13]. His model divided the compressor into a series of elemental control volumes representing a stage (rotor-stator) and solved the governing equations employing a fourth order Runge-Kutta numerical technique. Compressor stage force and shaft work were determined from empirical stage characteristics and applied as distributed functions within the control volume.

Using the one-dimensional formulation, three different single-spool compressors were modeled. These models were validated against experimental data and generally computed compression system stability within one-to-two percent of that observed experimentally. Studies were conducted with these one-dimensional models to determine the effects of time-variant planar pressure oscillations and rapid inlet temperature ramps. The computations generally compared favorably to those results observed experimentally.

Davis, using Kimzey's modeling concepts, reformulated the numerical solution technique to improve the numerical stability and extended the model to dual-spool compression systems [14]. Model reformulation using the MacCormack explicit differencing scheme successfully resolved most numerical instability problems associated with Kimzey's model. In the dual-spool configuration, this modeling technique used a pseudo-splitter near the exit of the fan to allow transmission of fan duct perturbations which are felt by the fan and ingested by the high-pressure compressor. The model was validated against experimental results for a current-day military axial compression system. The model predicted correct compressor response during surge-inducing external disturbances representing combustor fuel pulses, augmentor rumble, augmentor hard-lights, ingested gas products from armament firings, and time-dependent inlet pressure disturbances. In addition to the correct compression system behavior, the model predicted the stage at which the instability was initiated. The major deficiency of this modeling technique, as well as all the above techniques, is that results beyond stall/surge inception are not

valid. This is in part due to incorrect or nonexistent stage characteristic definition in the post-stall regions.

II.1.3 Parallel Compressor Models

One-dimensional models are used primarily to predict the compressor stability limit with steady and time-variant uniform flow entering the compressor. Efforts have also been made to predict the influence of external disturbances on compressor stability. One major class of model has been based upon "parallel compressor theory."

Pearson described the parallel compressor theory for circumferential distortion in his 1963 work [15]. The theory divides the distorted compressor into sections; each section is treated as an individual compressor working in parallel with the other sections. The theory incorporates the following assumptions: (1) all parallel compressor sections discharge to the same static pressure; (2) there is no fluid dynamic connection between sections, (i.e. crossflows are ignored); and (3) each section uses the undistorted stage characteristics. In its simplest form, the entire compressor is assumed to have reached instability when any one of the sectors reaches the stability limit. In more complicated forms, provisions for approximating crossflows and determining the effect of unsteady aerodynamics on compressor behavior have been incorporated. Examples of several parallel compressor models can be found in References [16] and [17].

II.2 Post-Stall Compression/Engine System Models

Prior to the mid-Seventies, all compression system modeling had been directed to determining the surge boundary and to identifying

external disturbances, which might influence the limits of that boundary. With the advent of the "stall stagnation" problems first occurring in the F100 system, new emphasis was placed on understanding compression system behavior during surge and rotating stall. This emphasis spawned several experimental and analytical investigations which have produced several theories and models for the study of post-stall behavior. A review of the major theories and their application to compression systems and/or turbine engines will be presented in the following sections.

II.2.1 Greitzer's Model

In 1976, E. M. Greitzer published a theory along with a mathematical model for post-stall compression system behavior. His initial work spawned several investigations and modeling studies over the next decade. Because his work was the first significant effort in post-stall modeling, and elements of it are used in the present work, an in-depth review is presented.

Greitzer developed a one-dimensional time-dependent, nonlinear mathematical model [18] of an axial compression system to predict the transient response of that system while undergoing a perturbation from steady operating conditions. His model was designed to investigate the phenomena of compressor surge and/or the compression system while rotating stall is present.

A schematic of the compression system modeled is presented in Figure 3. The system model consists of a compressor operating in a circular duct connected to an exit plenum which includes a throttling device. The compressor is represented by an actuator disc, thus

providing the pressure rise across the compressor, and a section of constant area pipe to account for the fluid dynamics within the compressor. The throttle is modeled by an actuator disc, across which the pressure drops, which is also attached to a constant area duct.

For the type of oscillations (low-frequency) expected to be calculated with this model, the flows in the ducts can be considered to be incompressible. This imposes "slug" flow in which the fluid in any one of the equivalent ducts will have the same axial velocity throughout that duct.

Since incompressible flow was assumed, Greitzer formulated his model with the momentum and continuity equations. The rate of change of mass flow within the compressor duct can be expressed as

$$-\Delta P + C = \frac{L_c}{A_c}\frac{d\dot{m}_c}{dt} \tag{1}$$

where

$\Delta P = P_{plenum} - P_{duct}$,

C = pressure rise across compressor,

L_c = effective length of compressor duct,

A_c = cross-sectional area of compressor duct, and

$\dot{m}_c$ = mass flow of compressor.

A similar equation can be written to describe the flow through the throttle

$$\Delta P - F = \frac{L_T}{A_T}\frac{d\dot{m}_T}{dt} \tag{2}$$

where

F = pressure drop across the throttle

and all other terms are similar to those of the compressor duct.

For the plenum, the velocities have been assumed small and the static pressure uniform throughout. The mass equation for the plenum can be written as

$$\dot{m}_c - \dot{m}_T = V_p \frac{d\rho_p}{dt} \tag{3}$$

where

$\dot{m}_T$ = mass flow rate of the throttle,

V_p = volume of the plenum, and

ρ_P = density of the plenum.

By assuming polytropic behavior in the plenum, the density change can be related to the plenum pressure by

$$\frac{d\rho_p}{dt} = \frac{\rho_p}{kP_p} \frac{dP_p}{dt} \tag{4}$$

where k = polytropic exponent and γ = ratio of specific heat. In addition, if the overall pressure and temperature ratios of the compressor are near unity (i.e. the compressor pressure rise is small), we can substitute (ρ/P) for (ρ_p/P_p) in the above equation. The mass conservation in the plenum then becomes

$$\dot{m}_c - \dot{m}_T = \frac{\rho V_p}{\gamma P} \frac{dP_p}{dt} \cdot \tag{5}$$

In Equation (1), the pressure rise across the compressor must be known for the mass flow rate to be calculated. At present, prediction of this pressure rise-flow correlation in certain flow regions is not possible, and one must rely on experimental results. In previous analyses, it was assumed that the pressure rise-mass flow relationship was the same transiently as it is in rotating stall. Here, it was observed that the stall cell takes some time to develop, up to ten rotor revolutions. These times are long enough to introduce significant changes in the compressor mass flow during such processes. Thus, since quasi-steady approximations would not be adequate, a first order time lag was imposed on the compressor pressure rise by the following equation

$$\tau \frac{dC}{dt} = C_{ss} - C \tag{6}$$

where

τ = time constant, and

C_{ss} = steady-state measured pressure rise.

The throttle expression (Equation (2)) requires the pressure drop across the throttle, F. The pressure drop can be written in terms of the velocity at the throttle discharge plane as

$$F = \frac{1}{2} \rho C_{x_T}^2 \tag{7}$$

or in terms of throttle mass flow as

$$F = \frac{\dot{m}_T^2}{2\rho A_T^2} \tag{8}$$

Thus Equations (1), (2), (5), (6), and (8) are the equations describing the compression system dynamics.

If these governing equations are non-dimensionalized, some interesting parameters are created. The mass flows are non-dimensionalized by $\rho U A_c$; the pressure difference by $1/2\ \rho U^2$, and the time variable of $1/\omega$,

where

U = mean rotor velocity

ω = Helmholtz frequency = $a\sqrt{\frac{A_c}{V_p L_c}}$, and

a = acoustic velocity.

Thus, the governing equations can be written as

$$\frac{d\tilde{\dot{m}}_c}{d\tilde{t}} = B\ (\tilde{C} - \Delta\tilde{P}) \tag{9}$$

$$\frac{d\tilde{\dot{m}}_T}{d\tilde{t}} = \frac{B}{G}\ (\Delta\tilde{P} - \tilde{F}) \tag{10}$$

$$\frac{d\Delta\tilde{P}}{d\tilde{t}} = \frac{1}{B}\ (\tilde{\dot{m}}_c - \tilde{\dot{m}}_T) \tag{11}$$

$$\frac{d\tilde{C}}{d\tilde{t}} = \frac{1}{\tilde{\tau}}\ (\tilde{C}_{ss} - \tilde{C}) \tag{12}$$

where (~) denotes non-dimensionalized variables and

$$B = \frac{U}{2\omega L_c} = \frac{U}{2a}\sqrt{\frac{V_p}{A_c L_c}} \tag{13}$$

$$G = \frac{L_T A_c}{L_c A_T} \tag{14}$$

$$\tilde{\tau} = \frac{2\pi NR\omega}{U} = \left(\frac{\pi R}{L_c}\right) \cdot \left(\frac{N}{B}\right) \tag{15}$$

where

N = number of rotor revolutions needed for full development of a stall cell, and

R = compressor mean rotor radius.

Thus Equations (9), (10), (11), (12), and (8) are solved in Greitzer's model. The parameter, B, becomes quite significant in describing the type of instability encountered.

II.2.2 The "B" Parameter

Greitzer exercised his model to determine the effect of the parameter, "B", on compressor instability. Some results of that study are presented in Figures 4 through 7. The compression system model was set with the throttle adjusted such that a uniform flow equilibrium point was no longer possible. With a low value of "B" (0.45), Figure 4, the compression system moved directly to an operating point on the stalled portion of the compressor operating curve. Operation along this stalled curve has been associated with the behavior of a machine in rotating stall. With a slight increase in "B" to a value of 0.6, the final compressor operating point became the same as before but took longer to achieve. As seen in Figure 5, the final operating point was reached through a series of decaying amplitude oscillations. At a value of "B" of 0.70, the compression system exhibited an entirely different

behavior as indicated in Figure 6. The oscillations grew in amplitude and exhibited a limit cycle behavior. Beyond a value of "B" of 0.70, the compression system response was similar in nature but the shape of the limit cycle changed. With very large values of "B", the time scales were no longer characterized by the Helmholtz frequency but were of the relaxation type with two distinct time scales (Figure 7): (1) a very long scale in which the plenum pressure is slowly built up or discharged; and (2) a much shorter scale in which the flow changes rapidly at almost constant pressure. This latter type of instability, typically seen in high-pressure ratio, high-speed machines, is controlled by the resistance elements of the system. The longer scale is set by the balance between resistance and restoring forces, or in other words, the rate that the plenum can empty through the throttle and the compressor.

It should be noted here that these values of the "B" parameter are associated with a particular compression system (i.e. the one Greitzer modeled and later verified experimentally [1]). Therefore, the quantitative results cannot be used as exact measures to determine what type of instability any compressor will exhibit but should be looked upon as a qualitative measure through which one can speak about compressor behavior in general.

In 1985, Gamache [5] modified Greitzer's model to investigate the effects of an external forced excitation (such as a sinusoidal pressure perturbation) on the recoverability of a compression system during post-stall events. Depending upon the timing and/or the strength of the external excitation, Gamache found that this forced excitation could cause the compression system to move into a nonrecoverable stall upon

the termination of the external excitation. In his dissertation he also concluded that the predicted forced or free-response behavior is heavily dependent upon the form or shape of the compressor post-stall characteristic.

II.2.3 Wenzel's Model

Wenzel developed a model of the TF34 engine in order to study "non-recoverable" stall [19]. Wenzel performed a parametric study to determine which compressor or engine parameters were most important to compression system recovery.

The model used quasi-steady compressor and fan maps to generate component performance. Dynamic behavior of the compressor characteristics was not modeled (i.e. by lagging the characteristics as in [18]). All volume dynamics were computed using the technique of Seldner, Mihaloew, and Blaha [20], (i.e., a one-dimensional technique which used simplified forms of the continuity, momentum and energy equations). The fuel control was a simple fuel-flow/compressor discharge pressure relationship with no dynamics modeled. For all events, mechanical speed and variable geometries were held constant at the initial settings. Neither the turbine nor any downstream component was explicitly modeled. Each speed-line characteristic was defined for unstalled flow and for stalled flow including reverse flow. The unstalled portions were based upon experimental data, whereas the form and shape of the stalled curves were postulated based upon Greitzer's experimental results [1]. These stalled characteristics were modeled such that they could be adjusted parametrically to determine the effect of shape and level of

recoverability. Temperature changes for stalled operation were calculated based upon pressure rise and a postulated efficiency which was also programmed as a variable.

The fan performance characteristics were constructed in a similar manner but with the temperature ratio assumed constant. Radial cross-flow between the hub and tip was allowed and was proportional to the pressure difference between the radial segments. Flow impedance between hub and tip was also programmed as a variable.

The model was exercised to determine the importance of various parameters on compression system recovery. Compressor instability was initiated by fuel pulses in the combustor, rapidly increasing the compressor discharge pressure. The fuel pulse was then ramped back down to a minimum after instability was initiated.

To quantify the effect of a certain parameter on system recoverability, turbine area was used as a stability rating criterion. At the time of instability, the nominal turbine area was changed by some delta area ($\Delta A/A$) which could be positive or negative. This increment was then adjusted until recovery was obtained. Thus, the turbine area was increased to affect recovery. (Note: An increase in turbine area relieves downstream resistance and thus relieves compressor back pressure). A set of nominal parameters was chosen as an initial (standard) set. Some parameters which were unknown were set at an arbitrary value.

Presented in Figure 8 is the result of a parametric study varying only the shape of the compressor characteristic. For a +/- 10 percent change in turbine area ($\Delta A/A$), a very small change in the parabolic nature of the positive characteristic was noted. However, the same

recovery resulted in a very large change in the negative stall characteristic. Therefore, Wenzel concluded that compression system recovery was very sensitive to the shape of the curve in the rotating stall region and not so sensitive to the shape in the negative flow region.

Wenzel performed other parametric studies in which he was able to quantify the relative importance of some factors governing compression system instability. Some parameters not well known (such as reverse flow characteristics and compressor stall/recovery hysteresis) were relatively unimportant to the recovery process. He noted that compressor discharge volume and inertness, positive flow between fan hub and tip regions, were important, highly sensitive parameters. These sensitive parameters would be difficult to measure experimentally but are the heart of any meaningful post-stall modeling effort.

II.2.4 Other Engine Models

Variations of Greitzer's 1976 modeling techniques have been applied in complete engine models [4], [21], and [22]. In general, the compression systems were represented by a single actuator disk followed by a lumped volume. The most complex a model of a fourteen-stage high-pressure compressor, was represented by three actuator-disk, lumped-volume combinations [19]. Pre-stall compressor characteristics were obtained from experimental results while post-stall characteristics were estimated based upon lowspeed compressor rig results. The primary value of these models is their use in analysis of engine performance prior to and during poststall events such as surge and rotating stall. They are used to determine what actions might be effective to produce

engine recovery or to prevent rotating stall. These engine models include only overall compression system behavior; thus, only overall compressor recovery actions can be investigated. Interstage changes and/or recovery actions cannot be evaluated. Study of interstage changes and/or recovery actions would require a stage-by-stage model.

II.3 Models for Analyzing Rotating Stall

In general, two types of analytical modeling of compression system behavior have been pursued. One is the study of the overall compression system behavior, usually from a one-dimensional viewpoint, which has been discussed in the previous section. The second type of study deals with rotating stall development and the general properties of the fluid within the stall cell. Several investigations have produced models which are capable of reproducing some aspects observed experimentally. These models are briefly summarized below.

Takata and Nagano [23] developed a model to describe rotating stall in axial-flow compressors. The flow was assumed inviscid and rotational with a compressor blade row being replaced by a semi-actuator disk (i.e., a cascade of flat plates at some stagger angle with finite length). The model was basically concerned with two-dimensional flow (axial, circumferential) but had the capability to be expanded to three-dimensions by adding spanwise variation. The modeling technique was expressed for a single-blade row and later converted for multiple-blade rows with and without axial spacing.

The performance of the blade row(s) was represented by cascade steady-state characteristics (pressure-loss coefficient and outlet-flow

angle as a function of inlet-flow angle) adjusted for dynamic behavior by lagging the steady-state pressure coefficient with a first-order equation of the form

$$\tau \frac{\partial \omega}{\partial t} + \omega = \omega_{ss} \tag{16}$$

where

ω = total pressure-loss coefficient,

ω_{ss} = steady-state value-of-loss coefficient, and

τ = characteristic time constant.

This equation was applied because of the delay time related to the response of the boundary layer on the blade surfaces.

A dynamic head loss for the blade row was calculated using these dynamic cascade characteristics. The flow field downstream was determined using the vorticity transport equation and the rotational Poissons' equation. Boundary conditions downstream were imposed upon the appropriate equation of motion thus obtaining equations to be solved at the exit boundary. All equations were solved using standard finite difference methods.

Takata and Nagano studied the effects of blade-row interference on stall-cell behavior. For the case of an inlet guide vane and rotor row, multiple stall cells were produced. It was postulated that this type of stall cell development was caused by the rotor row since the inlet guide vane was assumed not to have stalling characteristics. However, the isolated rotor model indicated that the number of cells in a rotor row did not change. Therefore, the interaction between

the inlet guide vane and the rotor row contributed to the change in the number of cells.

In an investigation with a rotor/stator combination it was found that the rate of change in the total pressure-loss coefficient of the first blade row must be small for an increase in the number of cells to take place. Thus, in general, it seems difficult for the number of cells to increase in a rotor/stator combination but more probable for an inlet guide vane/rotor combination.

Another model for the analysis of rotating stall in axial compressors was later developed by Sexton and O'Brien [24]. Much like the Takata/Nagono model, the Sexton model used a semi-actuator disc to represent the compressor rotor. The flow field upstream of the rotor row was calculated using two-dimensional, incompressible flow equations. The blade row interaction with the flow field was modeled by specifying the dynamic pressure-loss coefficient and turning angle. The major difference presented in this modeling technique was the application of an improved dynamic loss response model.

The dynamic response function was based upon Fourier transforms of the measured quasi-steady pressure loss and the measured dynamic pressure loss. The quasi-steady pressure loss was inferred from cascade experimental results. At high angle of attack, data was not available but was estimated using standard airfoil lift and drag definitions. The dynamic portion was experimentally measured with on-rotor high-response pressure transducers on a single rotating blade row in which rotating stall was induced. Calculations of dynamic total pressure

loss were made from these measurements. A dynamic response function was constructed from the following equation

$$TF = \frac{F(\Delta P_o)_{\text{dynamic loss}}}{F(\Delta P_o)_{\text{quasi-steady loss}}} \tag{17}$$

where

TF = transfer function, and

$F(\Delta P_o)$ = Fourier transform of pressure waveform.

By knowing the instantaneous incidence angle, the quasi-steady pressure loss becomes known.

To determine the sensitivity of the transfer function, a parametric study was conducted. The value of the transfer function was varied over a range at the fundamental frequency. The critical angle for rotating stall development was determined for a range of transfer functions. It was found that the critical incidence angle ranged from 14 degrees to 10.5 degrees for the corresponding range of transfer function of 0.4 to 0.6. Experimentally, it was determined that the critical angle was approximately 13 to 15 degrees for stable rotating stall.

Similarly, the phase angle corresponding to the fundamental frequency was varied over a range to determine its sensitivity. A change of 10 degrees in phase angle resulted in only a change of 1/2 degree in critical angle. However, stall-cell speed was greatly affected by changes in phase. For the same 10 degree change it was found that stall cell speed ranged from 28 percent of rotor speed to 44 percent. Experimentally, the stall-cell speed was found to be 52 percent of rotor speed.

Using the principles presented by Sexton and O'Brien, Cousins enhanced the two-dimensional rotating stall model and added the capability for predicting compressor stage characteristics [25]. With the specification of angle of attack, inlet guide vane discharge angle, and rotor blade velocity, Cousins' model produces a steady mean axial flow. Adding an axial perturbation to the mean axial flow produces a flow field that will either return to the mean velocity, indicating stable, unstalled operation or grow in strength to a limited size indicating a rotating stall cell. Since these calculations take place at a constant flow, one can define an average flow and pressure rise across the blade row producing a stage characteristic which encompasses both prestall and a portion of the post-stall operating regions (Figure 9). This model thus has promise for use as a post-stall stage characteristic prediction tool.

F. K. Moore developed a theory with a corresponding analytical model for the analysis of rotating stall in axial compressors [26]. In development of his theory, a small circumferentially steady disturbance was postulated to exist in the compressor. When rotating stall occurred, the static pressure rise across each blade row was assumed to have the form

$$\psi = \frac{\Delta P}{\frac{1}{2}\rho U^2} = F(\phi) - \tau(\phi)\dot{\phi} \qquad (18)$$

which simply stated that the quasi-steady characteristics are no longer valid but must be time lagged. This lagged characteristic, much like Greitzer's, resulted from flow separation or viscous processes within the flow passage.

To study recovery, a complete compressor performance characteristic with unstalled flow, reverse flow and a rotating stall region was incorporated into the analysis. Moore postulated a compressor characteristic as shown in Figure 10. The characteristic is a series of parabolic curves which are convex near stall inception and concave along the install characteristic near point C. Also indicated in the figure is a point, δ, which indicates the performance difference due to rotating stall. The characteristic shown is intended to be the pressure rise characteristic in the absence of rotating stall.

To illustrate some of the results obtained with this analysis, Moore posed a series of indirect problems in which he specified a rotating perturbation, found the resulting oscillations, and then inferred something about the compressor characteristic. Indicated in Figure 11 is the result of a growing oscillation. (Note: g and h can be thought of respectively as the axial flow coefficient perturbation and the transverse velocity coefficient perturbation.) Starting at point P, the oscillation grew until it encountered reverse-flow resistance and became momentarily unstalled. After three cycles the oscillation reached a limit and repeated itself. The amplification of the oscillation was caused by the deep-stall slope being positive; i.e., if it were negative it would damp. The limit cycle depends upon the throttle setting for any given case.

Keeping the throttle setting constant, Moore then investigated the "tallness" of the diagram (i.e., the height of the drop into stall compared to the diagram width, see Figure 10) as to its effect on

recovery. As the diagram becomes taller, the cycle tends to follow the unstalled and reverse flow legs very closely. In general, it was found that a tall diagram and a small value of external lagging favor recovery.

Through the study of the overall characteristic, Moore was able to conclude that recovery from rotating stall depends upon the compressor's steady characteristic "tallness" and, secondarily, the slope of the unstalled characteristic. He also concluded that the slope of the reverse-flow resistance was not nearly as significant as was the slope of the deep stall line (if that slope were positive). In addition, Moore concluded that recovery did not depend on compressor lag (dynamic hysteresis) but was affected by the external lags introduced in the entrance and exit geometries. Sudden changes in exit volume would favor recovery.

In 1983, F. K. Moore and E. M. Greitzer produced a two-dimensional theory for post-stall events in multi-stage axial compression systems [27] and [28]. The theory included a two-dimensional unsteady treatment of the compressor flow field coupled with dynamic response of the overall system. System dynamics were modeled by a lumped parameter method which was satisfactory as long as compressibility did not become a factor. Compressor performance was represented by an axisymetric characteristic with unsteady blade row response modeled as in Greitzer's previous theory. System hysterisis was included within the theory.

Some significant conclusions drawn by this investigation can be stated as follows: Surge and rotating stall can each exist in a pure form but rotating stall can not have evolved without having induced

surge-like unsteadiness into the system; the instantaneous rotating stall cell amplitude has a significant effect on the instantaneous compressor characteristic; and, other parameters such as length to radius ratio, in addition to the "B" parameter, can also have a significant effect on system response.

II.4 Limitations of Previous Modeling Efforts

The one-dimensional models described in section II.1.2 [9 through 14] use various combinations of the conservation laws. Even when all three nonlinear conservation laws are modeled [11], [12], and [13], these models are only able to predict compression system behavior up to the point of system instability. These models are limited by the often unavailable post-stall stage or compressor characteristics.

The parallel compressor models [16] and [17] share the same limitations. These models were constructed to analyze inlet and time-variant distortion effects on compression system behavior and do perform well in that application.

Greitzer produced the first system model capable of predicting surge and rotating stall [18]. He developed this model for a three-stage low-pressure compressor using a single compressor characteristic to represent the performance of all three stages. His model assumes incompressible flow which is appropriate for the low-speed system he modeled. However, if this modeling technique is to be useful in modeling high-pressure axial compression systems, it must be able to address compressibility. Thus, Greitzer's initial model is limited to low-speed

machines and must be modified to handle high-pressure compressors on a stage-by-stage basis.

Wenzel developed his modeling technique in a manner similar to that of Greitzer but did not modify his quasi-steady compressor characteristic for dynamic effects. However, since Wenzel's major objective was to study certain aspects of system recoverability, exact dynamic characteristics were not required. His model also used a single compression system characteristic, limiting recovery actions to system related parameters.

The engine models discussed in Section II.2.3 are based upon Greitzer's modeling technique. Since the compression system was represented by a single characteristic, these models are limited to overall compression system behavior and only overall compressor recovery actions can be investigated.

The rotating stall models discussed in Section II.3 each have some limiting capability [21] and [22]. However, since these models are of a different nature (two-dimensional and usually single-blade row or, at most, a single stage) and their use is for examining the details of the rotating stall cell, their further limitations will not be discussed. These types of models do have a direct connection to system models through the capability for predicting stage characteristics in the post-stall regions as was done by Cousins [25].

II.5 Purpose and Approach of Present Investigation

The purpose of this investigation is to investigate a compression system model capable of exhibiting observed system behavior during

post stall events (surge and rotating stall). In addition, the model should have the capability for providing information on a stage-by-stage basis for detailed analysis during surge and/or rotating stall.

To provide the desired new type of post-stall compression system model, an existing one-dimensional, time-dependent, stage-by-stage compression system model [14] was modified to handle post-stall events. The philosophy of the modification was to incorporate the basic post-stall concepts presented by Greitzer [18] into the existing stage-by-stage modeling techniques.

This dissertation describes the compression system modeling technique by presenting the governing equations, the numerical scheme which solves the governing equation, and the modifications necessary for the extension of the model to handle post-stall events. The model has been configured for a three-stage low-speed compressor similar to that used by Greitzer [1] and for a nine-stage, high-pressure compressor, typical of modern turbofan engines. These two model configurations have been used to validate the modeling technique by comparison with experimental results. The three-stage, low-speed compressor configuration provides the majority of validation evidence, because more experimental results exist for this system than for the high-pressure machines. However, because there exists some doubt as to the applicability of the post-stall modeling techniques to high-speed, high-pressure ratio systems, the modeling technique has also been validated for this latter type of machine.

Also presented in this dissertation is a parametric study designed to provide insight into external and internal factors which affect the

compression system's post-stall behavior. External disturbances such as inlet distortion and combustor performance are examined for their effect on system post-stall behavior. The effect of a rapid change in operating conditions is examined through a study which considers heat transfer effects inside the compressor. Finally, the effect of internal blading changes on stage performance and overall system behavior is examined.

CHAPTER III

ONE-DIMENSIONAL, TIME-DEPENDENT COMPRESSOR MODELING TECHNIQUE

The one-dimensional, time-dependent compressor modeling technique involves the solution of the nonlinear forms of the conservation laws. The models constructed by this approach can be used for the analysis of planar, transient, and dynamic effects on compressor operation and stability. A review of the governing equations, stage characteristic development, numerical techniques, and method of solution is presented in this section.

III.1 Governing Equations

Illustrated in Figure 12 is a representative single-spool compressor and ducting system. Included in this system are portions of the compressor inlet and the combustor volume. The compressor and ducting system is modeled by an overall control volume shown in Figure 12b. Acting on this fluid control volume is an axial force distribution, FX, due to the effects of the compressor blading and walls of the system. In addition, the rate of heat added to the fluid and shaft work done on the fluid are represented by Q and SW, respectively. These per-unit-length distributions are locally adjusted for each control volume. Mass transfer rate across boundaries other than the inlet or exit (such as in the case of interstage bleed) is represented by the distribution W_B. The time-dependent, inlet-boundary condition is the specification of total pressure and temperature. The exit-boundary condition is either the specification of static pressure or a unity Mach number. The overall control volume is divided into a set of elemental control volumes.

In the compressor section, an elemental control volume consists of a rotor followed by a stator and associated volume, representing a complete stage. The entrance and exit ducting sections of the overall control volume are divided into elemental control volumes to assure a frequency response as high as that in the compressor section. The governing equations are derived by the application of mass, momentum, and energy conservation principles to the elemental control volume in Figure 12c.

Applying the continuity principle to the elemental control volume yields

Continuity

$$\underbrace{W + \frac{\partial W}{\partial x}\,dx + W_B\,dx}_{\text{mass leaving control volume per unit time}} + \underbrace{\frac{\partial(\rho A dx)}{\partial t}}_{\text{time rate of increase of mass within the control volume}} = \underbrace{W}_{\text{mass entering control volume per unit of time}}, \tag{19}$$

which may be reduced to

$$\frac{\partial(\rho A)}{\partial t} = -\frac{\partial W}{\partial x} - W_B, \tag{20}$$

where W_B is the interstage bleed flow per distributed length.

Applying the momentum equation gives

Momentum

$$\underbrace{F_B dx + P_S A - \left[P_S A + \frac{\partial (P_S A)}{\partial x} dx \right] + P_S \left[A + \frac{\partial A}{\partial x} dx - A \right]}_{\text{axial forces acting upon the control volume}}$$

$$= \underbrace{\left[Wu + \frac{\partial (Wu)}{\partial x} dx \right]}_{\substack{\text{momentum leaving} \\ \text{control volume} \\ \text{per unit time}}} - \underbrace{Wu}_{\substack{\text{momentum entering} \\ \text{control volume} \\ \text{per unit time}}} + \underbrace{\frac{\partial}{\partial t} [\rho u A dx]}_{\substack{\text{time rate of} \\ \text{of increase} \\ \text{of momentum} \\ \text{within the} \\ \text{control volume}}} . \quad (21)$$

total time rate of change of momentum

Equation (21) may be reduced to

$$\frac{\partial W}{\partial t} = - \frac{\partial (IMP)}{\partial x} + FX, \quad (22)$$

where

$$IMP = Wu + P_S A , \quad (23)$$

and

$$FX = F_B + P_S \frac{\partial A}{\partial x},$$

an axial force distribution consisting of blade force and the axial force on the walls of the system.

Energy conservation yields

Energy

$$\underbrace{H + \frac{\partial H}{\partial x}dx + H_B dx}_{\substack{\text{enthalpy leaving}\\ \text{control volume}\\ \text{per unit time}}} + \underbrace{\frac{\partial}{\partial t}\left[\rho A\left[e + \frac{u^2}{2}\right]dx\right]}_{\substack{\text{time rate of increase}\\ \text{or energy within}\\ \text{control volume}}}$$

$$= \underbrace{H}_{\substack{\text{enthalpy entering}\\ \text{control volume}\\ \text{per unit time}}} + \underbrace{SWdx}_{\substack{\text{rate of shaft work}\\ \text{done on fluid in}\\ \text{control volume}}} + \underbrace{Qdx}_{\substack{\text{rate of heat}\\ \text{added to}\\ \text{fluid in}\\ \text{control volume}}}, \tag{25}$$

which may be reduced to

$$\frac{\partial(EA)}{\partial t} = -\frac{\partial H}{\partial x} - H_B + SW + Q\ , \tag{26}$$

where

$$E = \rho\left[e + \frac{u^2}{2}\right] \tag{27}$$

and

$$H = c_p W(T_t - T_{ref});\ T_{ref} = 0. \tag{28}$$

Equations (20), (22), and (26) represent the form of the nonlinear conservation equations used in the modeling technique.

Additional equations required include:

Equation of State

$$P_S = \rho R T_S\ . \tag{29}$$

Ratio of Specific Heats

$$\gamma = \frac{c_p}{c_v}. \tag{30}$$

Definition of Mach Number

$$M = \frac{u}{a}, \tag{31}$$

where a is the acoustic velocity,

$$a = \sqrt{\gamma R T_S}. \tag{32}$$

Definition of Total Temperature

$$T_T = T_S \left[1 + \frac{\gamma-1}{2} M^2 \right]. \tag{33}$$

Definition of Total Pressure

$$P_T = P_S \left[1 + \frac{\gamma-1}{2} M^2 \right]^{\frac{\gamma}{\gamma-1}}. \tag{34}$$

III.2 Stage Characteristic Definition

To provide the momentum and energy equations with stage forces and shaft work, respectively, a set of stage characteristics must be provided as input to the model. A stage flow coefficient (ϕ) is defined as

$$\phi = \frac{u}{U} \tag{35}$$

where u is the axial velocity and U is the wheel speed (ft/sec) at the mean-blade radius, The flow coefficient is related to the blade angle of attack, α, through the stagger angle, λ, by the relationship

$$\phi = \cot(\lambda + \alpha). \tag{36}$$

A decreasing flow coefficient means that the angle of attack is increasing, thus increasing the possibility of flow separation on the blade rows. A stage temperature coefficient (ψ^T) can be defined as

$$\psi^T = TR-1, \tag{37}$$

where TR is the stagnation or total temperature ratio. Similarly, a stage-pressure coefficient (ψ^P) can be defined as

$$\psi^P = PR, \tag{38}$$

where PR is the stagnation or total pressure ratio. The stage adiabatic efficiency can be defined as

$$\eta_{ad} = \frac{\Delta h_{ISEN}}{\Delta h_{actual}} = \frac{PR^{\frac{\gamma-1}{\gamma}} - 1}{TR-1}, \tag{39}$$

and can thus be defined in terms of the stage coefficients

$$\eta_{ad} = \frac{(\psi^P)^{\frac{\gamma-1}{\gamma}} - 1}{\psi^T}. \tag{40}$$

Two of the three relationships

$$\psi^T = \psi^T(\phi)\ ,\ \psi^P = \psi^P(\phi)\ ,\ \text{and}\ \eta_{ad} = \eta_{ad}(\phi) \tag{41}$$

are a set of stage characteristics which fully define the performance of a stage, assuming constant specific heat and γ. The three relationships represented by Equation (41) are redundant; any two of the three variables are sufficient to compute the third.

A typical set of steady-state stage characteristics for both pre- and post-stall operation is presented in Figure 13. The stage characteristics are divided into three distinct regions; pre-stall, rotating stall, and reverse flow. The pre-stall region is based upon the performance of a normal operating blade row where the flow is attached to each individual blade. The rotating stall region is based upon a flow weighted average of a fully developed rotating stall cell. The pressure

and temperature ratio in this region represent the average pressure and temperature rise across the stage for both stalled flow and unstalled flow. The reverse-flow characteristic region represents the pressure loss and temperature rise associated with full annulus reverse flow. The discontinuity at zero flow has been experimentally shown to exist for a three-stage low-speed compressor [5]. This aspect of the quasi-steady flow characteristic has been incorporated into the modeling technique.

Stage characteristic definition has been made with a current high-pressure compressor in mind. A slightly different but equivalent definition has been used for a three-stage, low-pressure compressor. Its definition will be discussed in Chapter IV when the system model is introduced.

III.3 Stage Characteristic Development

In previous modeling efforts [13] and [14], pre-stall stage characteristics have been experimentally based. If, however, experimental results are not available, a method for predicting stage performance is available. A current method for predicting overall as well as stage pre-stall performance utilizes the Combined Compressor Design and Evaluation Code (COCODEC).

COCODEC [29] is a computer program capable of calculating overall compressor performance. It provides a steady-state axisymmetric solution in determining both individual stage and overall compressor performance. Stage performance is determined from both total pressure loss coefficients and relative outlet flow angles estimated from the blading

geometry.

Blading geometry required to execute the program is summarized in Figure 14. Blade inlet and outlet angles may be substituted for camber and stagger angles as the indicator for the amount of turning imposed on the airstream. In addition to the blading geometry, both the flowpath boundaries and the position of the individual blade rows within that boundary must be specified.

COCODEC determines a solution to a radial equilibrium equation using the streamline curvature method of solution at a series of radially extending computing stations spaced axially in the flowpath. A computational mesh (Figure 15) is defined by the intersection of these computing stations with a number of streamlines whose radial positions are determined by the program. A number of data items are calculated at each of these mesh points. Considering a computing station that immediately follows a blade row, mesh point output items would include flow properties, blade performance, blade loading, both pressure and temperature rise across the blade row, and overall compressor performance up to the current computing station. This detail permits the extraction of steady-state stage characteristics.

COCODEC is capable of calculating a complete set of speed characteristics for a compressor, but provides no indication of the point on a speed characteristic at which the compressor stalls. The point at which the overall compressor experiences surge or rotating stall must be based upon experimental results. These results also provide the limiting flow rate for the distinction between pre-stall and post-stall stage characteristics.

Steady-state stage performance in the post-stall regions (rotating stall and reverse flow) is not as well defined as in the pre-stall case. First, steady-state performance in the rotating stall region must be looked upon in a global sense. Even though the flow is not steady in a one-dimensional sense at any stage, overall averaged performance can be said to be steady if the rotating stall cell is completely formed. Secondly, not many measurements have been taken on a stage-by-stage basis for high-speed compression systems. Many experimental investigations have been carried out on low-speed compressors which were designed to determine the size and extent of the rotating stall cell development. Steady-state characteristics have been synthesized from some of this unsteady data. The best available set of characteristics were synthesized on a three-stage low-speed rig at Massachusetts Institute of Technology and reported in Reference [5].

Since little post-stall experimental stage data exists for the high-speed/high performance compression systems typical of today's turbofan engines, estimates of stage performance in the post-stall region must be made. Besides the very limited experimental results, there do not exist any complete design tools such as COCODEC to predict post-stall behavior from blade geometry. Studies are currently in progress on the research level at selected Universities that will provide this basic design tool, [25] and [28]. Therefore, post-stall characteristics in the rotating stall and reverse flow regions are presently estimated by using the overall shape suggested by low-speed compressor rig studies and matching overall transient performance during surge and/or rotating stall.

III.4 Dynamic Stage Characteristic Treatment

In the preceding section, the discussion of the stage characteristic centered around the pre-stall and reverse flow steady-state performance and the globally steady rotating stall average performance. In a dynamic event such as rotating stall or surge, steady characteristics are not necessarily correct. For the pre-stall and post-stall reverse flow characteristics, steady characteristics can be used as they exist. The transient events in the pre-stall and reverse flow regions occur within 20 revolutions. However, in the rotating stall region, rotating stall may develop in 2 to 8 revolutions [30] and the globally steady characteristic is no longer applicable. To provide a dynamic stage characteristic, a first-order time lag on the stage forces has been incorporated into the modeling technique in the rotating stall region only. The first-order lag equation

$$\tau \frac{dFX}{dt} + FX = FX_{ss} \tag{42}$$

where

FX = blade force and pressure area force of the casing.

FX_{ss} = steady-state force, and

τ = time constant,

was used by Grietzer in his 1976 work [1]. It has been later applied by others, [21] and [22], and has been successfully applied to models for the overall compression system characteristic.

III.5 Combuster Representation

Because combustor performance can greatly influence compression system stability, the combustor volume with heat addition capability

has been included in the post-stall modeling technique. A schematic of the computational grid of a compression and representative combustion system is presented in Figure 16. The overall control volume is subdivided into elemental control volumes, with each elemental control volume in the compressor representing a stage. However, in the combustor no such relationship exists and each elemental control volume size was chosen to give adequate frequency response. The modeled combustor is one-dimensional with heat release taking place within the whole control volume. In an actual combustor there is a primary zone of combustion where the chemical reaction takes place near stoichiometric conditions. Secondary air is mixed with the products to lower the flame temperature to design levels. The one-dimensional modeling technique chosen approximates the final combustion state and does not model the mixing process explicitly. Overall fuel flow rate is input into the code, and then a total heat release is determined by the equation

$$Q_{total} = LHV \left[\frac{far}{1 + far} \right] W_{comb\ inlet} \tag{43}$$

This total heat release is then evenly distributed across the combustor control volumes.

During the post-stall events, the proper fuel/air ratio may not exist (as in the reverse flow situation). When this happens, combustion is assumed to cease with the heat release immediately going to zero. When conditions are again right for combustion in each control volume, heat release is assumed to take place. In the case of reignition, there is an imposed ignition delay.

The combustion process occurs as long as the fuel/air ratio is within a flammability zone. Figure 17 shows the flammability characteristics for a kerosene-type fuel in air at atmospheric pressure [31]. In this figure, equivalence ratio is defined as the ratio of the actual fuel/air ratio to that at stoichiometric conditions. Using this data as a basis, the rich fuel/air ratio for blowout occurs around an equivalence ratio of 3.0 (fuel/air ratio approximately 0.17). When reignition occurs, it takes place much nearer to stoichiometric conditions. The ignition delay is exponentially related to initial temperature, thus causing an exponential increase in heat release dependent upon temperature. A first order lag equation of the form

$$\tau \frac{dQ}{dt} + Q = Q_{ss} \tag{44}$$

is used to approximate the exponential ignition delay. Reignition is allowed to occur when the fuel/air ratio falls within a flammable range illustrated in Figure 17. Ignition delay is simulated with Equation 27 with a τ_{comb}=0.02 sec which is based on the total ignition delay time for JP4 at 800 K (Figure 18).

III.6 Numerical Technique

The governing Equations (20), (22), and (26) of the compressor modeling technique are hyperbolic in mathematical character. Thus, a numerical technique that has been applied successfully to hyperbolic equations was used in the model formulation. A predictor/corrector method was chosen which was first employed by R. W. MacCormack in 1969 on work dealing with hypervelocity impact cratering [32]. It is an explicit numerical method that is second-order accurate both in time

and space when applied to the time-dependent, compressible Navier-Stokes equations. This method has since become known as the MacCormack second-order finite-difference scheme.

The compressor model is not only an initial value problem but a boundary problem as well. Because the treatment of the boundaries can be a cause of stability problems, method-of-characteristics boundary formulations were employed. The numerical computational volume is divided into three areas; inlet, exit, and interior. MacCormack's scheme is applied at the interior; a method of characteristics (MOC) scheme is applied at the inlet; and either an MOC scheme for unchoked flow or an isentropic sonic nozzle scheme for choked flow is applied at the exit.

III.6.1 MacCormack's Scheme and Application to the Modeling Technique

MacCormack's differencing scheme has, in the past, been typically applied to the viscous form of the conservation equations. The basic concept will be presented using these equations, but will be specialized to the terms describing the compressor model (Equations (20), (22), and (26)). The unsteady compressible form of the conservation equations for one-dimensional flow neglecting body forces and heat sources may be written in conservative form as

$$\frac{\partial U}{\partial t} + \frac{\partial V}{\partial x} = 0 \ , \tag{45}$$

where

$$U = \begin{Bmatrix} \rho \\ \rho u \\ e \end{Bmatrix} \text{ and } V = \begin{Bmatrix} \rho u_2 \\ \rho u^2 + \sigma_x \\ (e + \sigma_x)u - k \frac{\partial \varepsilon}{\partial x} \end{Bmatrix} ,$$

$$\sigma_x = P_S - (\lambda - 2\mu) \frac{\partial u}{\partial x} , \quad \varepsilon = \frac{e}{\rho} - \frac{u^2}{2} ,$$

k = coefficient of heat conductivity, and

λ and μ = coefficients of viscosity.

Applying the predictor portion of MacCormack's technique to Equation (45) gives

$$U_i^{(P)} = U_i - \frac{\Delta t}{\Delta x_{i-1}} \left[V_i - V_{i-1} \right] , \tag{46}$$

where subscript, i, denotes a spatial location and superscript, P, denotes the predicted value. Correcting the predicted value then gives

$$U_i^{(C)} = 1/2 \left\{ U_i + U_i^{(P)} - \frac{\Delta t}{\Delta x_i} \left[V_{i+1}^{(P)} - V_i^{(P)} \right] \right\} . \tag{47}$$

The corrected value (denoted by superscript, C) then becomes the value of the dependent variable for the next instant in time. Backward differences are used in the predictor step and forward differences in the corrector step. To avoid biasing the solution because of the order of differencing in the predictor/corrector steps, the method has been modified to reverse the order of differencing every other time step. At the completion of the two-step process, first derivatives are approximated effectively by central differences.

Applying this method to the governing equations of the compressor model gives

Mass

Predictor:

$$\rho A_i^{(P)} = \rho A_i - \frac{\Delta t}{\Delta x_{i-1}} \left[W_i - W_{i-1} - W_{B_{i-1}} \right] . \tag{48}$$

Corrector:

$$\rho A_i^{(C)} = 1/2 \left\{ \rho A_i + \rho A_i^{(P)} - \frac{\Delta t}{\Delta x_i} \left[W_{L_{i+1}}^{(P)} - W_i^{(P)} - W_{B_i}^{(P)} \right] \right\} . \tag{49}$$

Momentum

Predictor:

$$W_i^{(P)} = W_i - \frac{\Delta t}{\Delta x_{i-1}} \left[IMP_i - IMP_{i-1} + FX_{i-1} \right] . \tag{50}$$

Corrector:

$$W_i^{(C)} = 1/2 \left\{ W_i + W_i^{(P)} - \frac{\Delta t}{\Delta x_i} \left[IMP_{i+1}^{(P)} - IMP_i^{(P)} + FX_i^{(P)} \right] \right\} . \tag{51}$$

Energy

Predictor:

$$EA_i^{(P)} = EA_i - \frac{\Delta t}{\Delta x_{i-1}} \left[H_i - H_{i-1} + SW_{i-1} + Q_{i-1} \right] . \tag{52}$$

Corrector:

$$EA_i^{(C)} = 1/2 \left\{ EA_i^{(P)} - \frac{\Delta t}{\Delta x_i} \left[H_{i+1}^{(P)} - H_i^{(P)} + SW_i^{(P)} + Q_i^{(P)} \right] \right\} . \tag{53}$$

The bleed flow, the force on the compressor blading and casing, and the shaft work and heat transfer terms are distributions over a particular axial length. These distributed terms have to be consistent with the differencing equations so that the equations can account for the

mass, momentum, and energy transfer across each elemental control volume. When backward differencing is employed, the distributed term should be associated with the upstream calculating station. When forward differencing is employed, the term is associated with the calculating station of interest.

In most previous works, the MacCormack method has been applied to computational fluid dynamic problems (i.e., internal or external flow without source terms). The compression system model not only adds source terms to the governing equations, but also uses nonuniform axial spacing. The addition of source terms does not cause any instabilities in the compression system model. However, the nonuniform radial spacing resulting in large axial area changes can and does cause numerical instabilities if that area change is too large. In the present work, this instability limited the modeling of the combustor to small changes in cross-sectional area from one control volume to the next.

III.6.2 Boundary Treatment

In all numerical solutions to boundary value problems, boundary specifications can influence the stability and accuracy of the solution. As indicated by Moretti [33], a boundary value problem in which a permeable subsonic boundary has constant properties is an ill-posed problem. Moretti suggests that a stretching of the permeable boundary to infinity, where the velocity vanishes and other properties take on their stagnation values, is one way for dealing with a constant property specification at the boundaries. Since a practical solution is limited to some finite domain, this approach has to be modified to some extent. Also, while

working with numerical solutions to the Navier-Stokes equations in inlet regions, Olsen, et al, [34] found it necessary to allow the boundary conditions to become functions of time.

Abbett has performed a comparative study [35] of numerical techniques for computing the boundary-flow conditions at solid walls and shock-boundary points in supersonic, inviscid flow. This effort investigated 30 different calculation procedures for determining boundary-flow conditions for four sample problems. The type of calculation procedures investigated included: reflection, explicit one-sided difference, extrapolation, method of characteristics (at boundary points only), combined equations, and Euler predictor/simple wave corrector. The conclusions of the study were based on comparisons of each method with a pure MOC solution (i.e., all points, interior as well as boundary points were calculated using MOC). When a full MOC was not utilized, Abbett concluded that the MOC boundary solution coupled with some higher order differencing scheme for the interior points (such as MacCormack's method) gave the best results in calculating steady flow in supersonic flow fields. Abbett's conclusion is also valid for the present compressor modeling technique, since both the present model and supersonic flow problems employ hyperbolic equations to describe the fluid flow.

Using the unsteady compressible form of the conservation equations for one-dimensional flow without body forces and heat sources, the following set of equations can be derived using the method of characteristics.

$$\underbrace{\frac{dP_S}{dt} - \rho a \frac{du}{dt} = a^2\psi_1 - \rho a\psi_2 + \psi_3}_{\text{compatibility equation}} \text{ for } \underbrace{\frac{dx}{dt} = u - a}_{\substack{\text{characteristic} \\ \text{equation}}} , \tag{54}$$

$$\underbrace{\frac{dP_S}{dt} + \rho a \frac{du}{dt} = a^2\psi_1 + \rho a\psi_2 + \psi_3}_{\text{compatibility equation}} \text{ for } \underbrace{\frac{dx}{dt} = u + a}_{\substack{\text{characteristic} \\ \text{equation}}} , \tag{55}$$

where

$$\psi_1 = 0 ,$$

$$\psi_2 = \frac{1}{\rho}\frac{\partial}{\partial x}\left[(\lambda + 2\mu)\frac{\partial u}{\partial x} \right] \text{ (momentum viscous damping terms)} ,$$

$$\psi_3 = (\gamma - 1)\left[(\lambda + 2\mu)\left[\frac{\partial u}{\partial x}\right]^2 + \frac{\partial}{\partial x}\left[k \frac{\partial T_S}{\partial x} \right] \right]$$
(energy dissipation and conduction terms) .

The compatibility equations reduce to the following set of relationships:

$$dP_S - \rho a du = 0 \text{ for } \frac{dx}{dt} = u - a , \tag{56}$$

$$dP_S + \rho a du = 0 \text{ for } \frac{dx}{dt} = u + a . \tag{57}$$

III.6.2.1 Inlet Boundary Solution

The inlet boundary thermodynamic properties for any time can be calculated by specifying certain boundary conditions (P_T and T_T) and using the characteristic relationships of Equation (56). The characteristic equation is first solved by approximating the total derivatives by differences

$$x_{new} - x_I = (u - a)\,\Delta t . \tag{58}$$

Illustrated in Figure 19 is the determination of the intersection of the characteristic curve (Point X_I) with the geometry of the previous time step (Line AB). The slope of the characteristic curve runs through the point of interest (i.e., Point C of Line CD) and a point which lies along the geometry of the previous time step, where all thermodynamic properties are known at the calculation stations. The thermodynamic relationships at Point X_I can be determined by linear interpolation of the properties between Points A and B. Once this point is known, the compatibility Equation (56) can be approximated by differences

$$P_{S_{X_{new}}} - P_{S_{X_I}} = a\, u_{x_{new}} - u_{x_I} . \tag{59}$$

An iterative technique is employed since there are one equation and two unknowns,

$P_{S_{X_{new}}}$ and $u_{X_{new}}$.

A guess at inlet Mach number is made, and along with the thermodynamic relationships

$$P_T = P_S \left[1 + \frac{\gamma-1}{2} M^2 \right]^{\frac{\gamma}{\gamma-1}} \tag{60}$$

and

$$T_T + T_S \left[1 + \frac{\gamma-1}{2} M^2 \right], \tag{61}$$

Equation (59) is solved using the interpolated values of density and acoustic velocity in the previous time frame. With P_T, T_T, and P_S known, a new value for inlet Mach number can be obtained. The process is continued until the Mach number does not change within a specified tolerance. To obtain a more accurate value of P_S , the above iterative technique

is applied to Equation (59), with density and acoustic velocity now being an average between the interpolated value in the old time step and the previous iterated value at the new time step. All thermodynamic properties are calculated using these relationships and the equation of state.

During post-stall events, flow reversal may occur at the inlet boundary. In this case, specification of constant total conditions at the inlet is inappropriate. Therefore, when flow reversal is sensed at the inlet boundary, the inlet boundary acts as an exit boundary and the specification of static pressure becomes the proper boundary condition. Thus, reverse-flow inlet boundary conditions are calculated using the method-of-characteristics exit boundary solution technique described below.

III.6.2.2 Exit Boundary Solution

For subsonic exit conditions, static pressure can be specified as the exit boundary condition. A characteristic scheme, such as used in the inlet boundary scheme, can then be employed. In addition to using the characteristic relationships of Equation (57), a set of streamline equations is used:

$$dP_S - a^2 dp = 0 \text{ for } \frac{dx}{dt} = u \; . \tag{62}$$

A procedure similar to that for the inlet solution is used with each compatibility equation solved along its characteristic curve or streamline curve, as illustrated in Figure 20. With the specification of static pressure and the two compatibility equations, an iterative procedure is not needed. This type of boundary specification is used when exit

static pressure variation is known (such as an exit pressure ramp leading to compressor surge).

For the case when an exit sonic condition is used, simulating choking in the turbine, an imaginary, zero length convergent nozzle is employed as presented in Figure 21. Flow within this nozzle has been assumed to be steady (i.e., at any time the steady-state flow equations govern the flow within the nozzle) and isentropic. Using the concept of mass flow function, $\dot{M}_T$, based on total conditions,

$$\dot{M}_T = \frac{W\sqrt{T_T}}{P_T A} , \tag{63}$$

the thermodynamic properties at the nozzle exit and inlet can be calculated. At sonic conditions the mass flow function has a constant value, which implies that the mass flow function at the nozzle inlet (Station N+1) also remains constant since the nozzle flow is governed by isentropic, steady-state equations. It is further assumed that isentropic flow exists in the preceding elemental control volume, thus specifying total pressure and temperature (P_T and T_T at Station N+1) to be equal to that at the previous calculating station (Station N). Boundary flow rate can then be calculated if the flow function at Station N+1 is specified based on the given area. This boundary condition allows compressor transients (such as inlet pressure and temperature perturbations) to take place without having to know how exit static pressure varies during those transients.

III.6.3 Model Solution Procedure

Figure 22 outlines the overall digital computer simulation procecure. At time zero (Step A), initial values of the dependent variables

(ρA, W, and EA) are specified for every control volume. The solution is started from a steady, uniform flow condition. With the specification of boundary conditions, all thermodynamic variables can be calculated (Step B) at the inlet, interior, and exit planes. Using the method of characteristics scheme or sonic exit condition scheme, the inlet and exit conditions for the next step in time can be calculated (Step C).

Knowing all the interior thermodynamic properties from Step B, the force and work terms (Step D) necessary for the momentum and energy equations (Equations (22) and (26)) can be calculated for input into the predictor step of MacCormack's method (Step E). New values for force and work can be determined from the predicted solution (Step F) and then used in the corrector step of MacCormack's method (Step G). The new values of the dependent variables determined in Step G are then used to compute the thermodynamic properties (Step B) for that time step. The sequence is repeated with boundary conditions changing in accordance with the specified event being simulated.

The momentum and energy Equations (22) and (26) require axial force and shaft work distributions representing the force of the compressor blading and casing on the fluid and the shaft work input per stage. These functions are constructed from the quasi-steady stage characteristics.

III.7 Stability Criteria and Frequency Disturbance Limitations

With any explicit differencing scheme which approximates partial differential equations, some stability criteria must be set. The system of equations used by the model is hyperbolic in nature and represents the one-dimensional compressible flow equations with source terms. A

stability criterion that has been used in the past with these equations is the Courant, Friedricks, and Lewey (CFL) stability restriction [36]. The restriction states that the finite-difference domain of influence must be at least as large as the physical domain of influence (i.e., a sound wave cannot travel more than one elemental control volume length in one time increment). Expressing this mathematically gives

$$\frac{(|u| + a)\Delta t}{\Delta x} \leq 1. \tag{64}$$

For the maximum time step, Equation (64) can be written as

$$\Delta t_{max} = \frac{\Delta x_{min}}{a + |u|_{max}} . \tag{65}$$

For the high-pressure compressor with combustor model, the maximum time was based on $\Delta x = 0.1$, $a = 2683$ ft/sec (static temperature of 3,000°R), and $u = 75$ ft/sec (conditions in a typical combustor control volume). This gave a maximum time step of

$$\Delta t_{max} = 3.63 \times 10^{-5} \text{ seconds}$$

The time step used for the high-pressure compressor, single-spool model was 3×10^{-5} seconds. A similar calculation was performed for a model of a three-stage low-speed compressor (discussed in Chapter IV). The time step used for that configuration was 1.5×10^{-4} seconds.

The model's response to a disturbance is dependent upon the elemental control volume length. Disturbance propagation through a control volume must be accomplished in a relatively short period of time to allow all of the fluid to respond to the disturbance. According to Kimzey [13],

maximum frequency response is limited by minimum disturbance wavelengths of 10 Δx_{max}. Thus, using Kimzey's definition,

$$f_{max} = \frac{(u + a)_{min}}{10\ \Delta x_{max}} , \tag{66}$$

the maximum frequency response for the high-pressure compressor, single-spool compressor model was estimated to be 630 Hz based on velocities encountered in the inlet ducting system and nominal duct lengths of 0.25 ft. According to Ward [37] a criterion for maximum frequency is that the propagation time through the control volume must be less than one-third the period of disturbance. Expressed mathematically this becomes

$$f_{max} \leq \frac{a}{6\pi\Delta x} , \tag{67}$$

where a and Δx are average quantities. Using this definition, the maximum frequency for the single-spool compressor model was estimated to be 385 Hz. Therefore, the maximum disturbance frequency which can be imposed on the model with accurate results probably lies somewhere in between these frequencies.

CHAPTER IV

MODEL VALIDATION

The modeling technique described in the previous section has been applied to a three-stage low-pressure compressor research rig and a single-spool, high-pressure compressor typical of today's turbofan engines. To completely validate the modeling technique, interstage and overall compressor experimental data would be necessary. Of the two systems modeled, the three-stage, low-speed compressor research rig has the most complete set of experimental results for validation purposes. However, since high-speed/high-pressure ratio machines are of great importance, the modeling technique will also be validated with available experimental results for that type of compressors.

IV.1 Low-Speed Research Compressor Rig

The model was applied to a low-speed research compressor rig as described by Gamache [5]. The compressor rig consists of three non-repeating stages with a constant cross-sectional area annulus. The hub and tip diameters are 53.63 cm and 60.96 cm, respectively, producing a hub-to-tip ratio of 0.88. Major design performance characteristics are summarized below:

Speed, N	= 5926 RPM
Mean Blade Speed, U	= 177.8 M/sec
Mass Flow Rate, W	= 8.73 Kg/sec
Flow Coefficient, C_x/U	= 0.619
Total Pressure Ratio	= 1.489

Pressure Coefficient, $\Delta P/\frac{1}{2}\rho U^2$ = 2.61

Efficiency, η = 86.2%.

The major emphasis of Gamache's work [5] was to describe the performance of this compressor rig during steady reverse flow. He configured the rig to hold constant speed while forcing the flow to traverse across the compressor in the reverse direction. By accomplishing this for many flow values, he was able to obtain overall and stage performance for the reverse flow region. With the previous work of Eastland [38], a complete set of steady stage pressure characteristics and corresponding overall steady performance is available for this rig.

IV.1.1 Stage Characteristic Synthesization

Stage characteristics can be defined in many different ways to denote the basic performance characteristics of pressure rise, efficiency and temperature rise as functions of airflow rate through the machine. For this machine, the pressure rise across a stage was defined by the following coefficient,

$$\psi^{P}_{s-s} = \frac{\overline{P}_{i+1} - \overline{P}_{i}}{1/2\ \rho U^2} \tag{68}$$

where

ψ^{P}_{s-s} = pressure coefficient based upon static pressures

$\overline{P}$ = average static pressure

ρ = compressor inlet density

U = mean wheel speed

i = stage entrance, and

$i+1$ = stage exit

The temperature rise was not given for each stage, but was given for the overall system in terms of a torque coefficient. Stage temperature rise characteristics were synthesized as a total temperature ratio based upon the overall torque characteristic. Measured stage pressure and synthesized temperature rise characteristics for the three-stage, low-speed research compressor are presented in Figure 23. Pressure rise characteristics are based upon experimental stage performance which indicates each individual stage behavior during unstalled operation, rotating stall and reverse flow. Stage temperature rise characteristics have been synthesized to be the same for each stage due to the lack of stage experimental data indicating otherwise.

Since these characteristics are indicative of stage performance during globally steady conditions (i.e. rotating stall has become fully developed), they may be "stacked" and compared to system overall steady performance. Presented in Figure 24 are the "stacked" synthesized stage characteristics and comparison to overall experimental results. Comparisons are made with the total-to-static, total-to-total, and static-to-static pressure coefficients and the overall torque coefficient. These coefficients are defined in the following manner:

Total-to-Static Coefficient

$$\psi^{P}_{T-S} = \frac{\overline{P}_{exit} - P_{T_{entrance}}}{1/2\ \rho U^2}, \qquad \text{Forward Flow} \qquad (69)$$

$$\psi^{P}_{T-S} = \frac{P_{T_{exit}} - \overline{P}_{entrance}}{1/2\ \rho U^2}, \qquad \text{Reverse Flow} \qquad (70)$$

Total-to Total Coefficient

$$\psi^{P}_{T-T} = \frac{P_{T_{exit}} - P_{T_{entrance}}}{1/2\ \rho U^2}, \qquad \text{Both Directions} \qquad (71)$$

$$\psi^{P}_{s-s} = \frac{\overline{P}_{exit} - \overline{P}_{entrance}}{1/2\ \rho U^2}, \qquad \text{Both Directions} \qquad (72)$$

Torque Coefficient

$$\psi_{\tau} = \phi \left[\frac{T_{T_{entrance}} - T_{T_{exit}}}{1/2\ \frac{U^2}{cp}} \right]. \qquad (73)$$

Overall "stacked" pressure performance agrees quite favorably with experimental results in the unstalled and rotating stall regions. In the reverse flow region agreement is not as good. The "stacked" pressure characteristics are lower than experimental results indicate. This trend appears in all pressure characteristics which may indicate the inaccuracy in obtaining average static pressure rise through each stage during reverse flow. The "stacked" total temperature rise agrees quite well with the overall torque coefficient. This is not unexpected since the temperature rise characteristics were synthesized by making this comparison. The experimentally determined torque coefficient near zero flow does not indicate a true steady flow measurement of temperature because the compressor had just previously run at a hot operating condition (rotating stall). In this case, the measured temperature was indicating residual metal-to-air heat transfer which disguised the true temperature rise associated with the mechanical work input to the compressor.

This comparison of overall steady performance parameters indicates that stage characteristic synthesization has produced a reasonably accurate set of stage characteristics which can be used in the present dynamic modeling technique described in Chapter III.

IV.1.2 Dynamic Stage Characteristic Treatment

The quasi-steady stage characteristics presented in the last section must be modified for post-stall dynamic behavior prediction. This was accomplished by the technique described in Section 4 of Chapter III in which the first order lag equation (42) was applied. The dynamic lag equation was only applied in the region where rotating stall might exist. (See Figure 25). In the reverse flow area, near flow shut-off, experimental results suggest that the transition between rotating stall and reverse flow does not necessarily occur at zero flow. To account for this behavior, stage-force lagging was continued into the reverse flow area until the flow coefficient, ϕ, reached a value of -0.075. During the rest of the reverse flow process, the stage forces were calculated using the quasi-steady reverse flow characteristic. Once the compression system could again begin filling the plenum and forward flow reacceleration began, stage-force lagging was applied to the quasi-steady stage force for flows in the rotating stall regions.

Experimental investigations have indicated that the transition from rotating stall to normal compression system operation does not occur at the same airflow as that which causes the system to transition into rotating stall from normal operation. This phenomena has been labeled hysteresis. To account for this behavior, the stage-forces were lagged

to a higher flow coefficient during forward flow reacceleration than during flow reversal. A factor of 1.3 (i.e. $\phi_{Hys} = 1.3\phi_{crit}$) was chosen for the three-stage low-speed compressor configurations based upon experimental evidence presented by Greitzer [1].

A comment on the blade-force lagging constant, τ, is appropriate at this point. The larger the constant, the more lagging of the blade forces. This input allows the model to obtain any solution desired for a given set of input condition. By increasing this constant, the model moves from predicting surge cycles with significant reverse flow, to surge cycles with no reverse flow, to the rotating stall condition where overall performance becomes stagnated (nonrecoverable stall). However, the fact that one can "dial in" any solution does not invalidate the effectiveness of the model as an analysis tool. Once a certain post-stall behavior is obtained, investigations can be made, while holding the lagging constant, τ, at the initial value, to determine the effects of other system parameters on post-stall system response. This, in fact, was the procedure used in the present validation process.

IV.1.3 Dynamic Model Comparison to Experiment Results

The low-speed compressor rig which Gamache [5] used to run his reverse flow experiments was not set up for any other purpose; thus surge and a large number of rotating stall events were not obtained. However, this rig is similar to the one Greitzer used in his first set of experimental investigations [1]. Both compression systems consisted of three stages with a constant area annulus. The major differences were in the blading. Greitzer's original rig consisted of three repeating stages,

using NACA 400 series airfoils with a hub-to-tip ratio of 0.7, while Gamache's rig consisted of three nonrepeating stages with a hub-to-tip ratio of 0.88. The speed capability of both machines was the same. Greitzer performed an extensive experimental investigation to determine system response during poststall events for a variety of compressor/ plenum configurations. This set of experimental results is excellent for validating the dynamic compression system modeling technique.

The model was configured to the geometry specified for Greitzer's compressor/plenum rig, but used the stage characteristics developed by Eastland and Gamache as presented in Figure 23. A schematic of the compressor rig used by Greitzer is presented in Figure 26 and the instrumentation set used is presented in Figure 27. For comparison purposes, Greitzer's "B" parameter was used as the correlation parameter between the model and the experimental results. Three cases will be compared to experimental results corresponding to "B" parameters of 0.65, 1.00, and 1.58.

The first experimental transient (with "B" of 0.65,) was conducted at a mean corrected blade speed of 59.0 meters/sec with a small plenum volume of 15.0 cubic meters. The throttle was slowly closed to the point of rig instability and then held constant. The system became unstable at the uniform flow stall point, before traversing to another operating point where damped, globally stable operation occurred. This post-stall behavior can be seen in Figure 28. At this new globally stable operating point, the compressor exhibited rotating stall.

The present mathematical model was configured in a similar way with a "B" parameter value of 0.66 at instability initiation. This was

accomplished by setting the mean blade speed at 59.02 meters/sec with a plenum volume of 6.84 cubic meters. This difference in plenum volume was necessary for model similarity because of the use of characteristics for different compressor blading for the reasons previously described. The imaginary sonic boundary condition (Section III.6.2.2) was employed to model the throttling action. The throttle was closed just enough to cause instability and then held constant. The compressor blade-force dynamic lagging constant, τ, was chosen (0.27) such that the overall system performance traversed immediately to the new operating point indicative of fully developed rotating stall. This modeled post-stall behavior is presented in Figure 29. Comparison to the general nature of the experimental results (Figure 28) indicates correct simulated overall system behavior.

Greitzer reconfigured the compressor rig by increasing the plenum volume from 15 cubic meters to 39.4 cubic meters while holding the speed constant at 59 meters per second. This configuration produced a "B" value of 1.00. At this condition, the system exhibited surge cycles as presented in Figure 30. Surge frequency was of the order of 1.5 Hz as can be seen in the time histories. The system trajectories are circular in nature when displayed on a compressor map. This type of surge has been denoted by Greitzer as "classic" surge.

The dynamic model was configured to produce a "B" value of 1.00 by increasing the plenum size to 15 cubic meters from 6.84 cubic meters, while holding the speed constant at 59.02 meters per second. The blade force time constant was held to its initial value of 0.27 (i.e., the same level as for the case where "B" = 0.66). At this condition the

model also exhibited surge cycles as presented in Figure 31. Comparing the time histories of the flow and pressure coefficients, one can observe that the changes in these values are of a similar nature and frequency to those observed experimentally (Figure 30). Comparing the model results as depicted on a compressor map, one can observe that the surge trajectories are circular in nature and are quite similar to those observed experimentally (Figure 30).

The above experimental configuration resulted in a "B" value of 1.00 at low speed and large plenum value. By decreasing the plenum volume of the experimental rig back to 15 cubic meters and increasing the speed to 92.9 meter/sec, a "B" value of 1.03 was obtained. Experimental surge trajectories for this case are presented in Figure 32.

The present model could also be reconfigured for a high-speed, small plenum volume configuration. The plenum volume was reduced to its original level of 6.84 cubic meters and the speed was increased to 92.98 meters per second, producing a "B" value of 1.04. As expected, the model produced a result similar to those observed experimentally at this same value of "B" even though it was obtained with different performance parameters and configurations (Figure 33).

Greitzer reconfigured his rig to produce a maximum reported "B" value of 1.58. This was accomplished by holding the corrected speed to 92.9 meters per second and increasing the plenum volume to 34.9 cubic meters. For this experimental case, a slightly different system behavior was observed, as illustrated in Figure 34. The surge trajectories become larger with near-zero flow during the surge cycle.

By changing the throttle closure point, Greitzer discovered that the nature of the surge cycles could be affected. Indicated in Figure 35 are surge cycles for the same compressor configuration (B = 1.58) but at a smaller throttle setting. This type of surge cycle has been called as "deep surge".

Deep surge is characterized by change in compressor mass flow that is quite rapid over part of the trajectory and rather slow over the rest. At the initiation of surge, mass flow decreases to negative values at a fairly constant pressure ratio. Once reverse flow has become established, a slow blowdown process occurs where the compressor acts as a very high-loss throttling device. A large pressure drop occurs because of the high angle of attack on the blades during reverse flow. Once the pressure has dropped, the mass flow reaccelerates back to a positive flow because conditions are now correct for pumping to occur. Slow repressurization takes place in the plenum during which the compressor moves back to its original operating point along the steady-state characteristic.

The dynamic model was configured for a "B" value of 1.58 by increasing the specified plenum to a value of 15.51 cubic meters while holding the corrected mean-blade speed to 92.9 meters/sec. The blade-force time constant, τ, was held at 0.27. The throttle, $\dot{M}_T$, was decreased to a value just small enough to cause compression system instability. Resulting overall system response is presented in Figure 37. The model behavior is indicative of the "classic" type surges as was expected (Figure 34). The model indicated that the frequency of surge events occurred at 0.5 Hz.

Decreasing the throttle closure to 60 percent of the minimum value for system instability had the same affect on compression system post-stall behavior as was observed experimentally. Model overall system response is presented in Figure 37. Model trajectories are indicative of the deep surge type of post-stall behavior with an increase in the frequency to 1 Hz.

The above validation was accomplished with results from a low-speed compression system, because they represented the most documented set of post-stall experimental results. However, present turbine engine systems employ high-speed/high-pressure compression systems. This raises the question of the applicability of low-speed, post-stall results for comparison with results from high-speed machines. To address this question a model of a nine-stage high-speed/high-pressure compressor was constructed and qualitatively validated with experimental results from high-speed compressor rigs.

IV.2 High-Speed/High-Pressure Compression System

The modeling technique described in Chapter III was applied to a nine-stage, single-spool, high-pressure, high-speed compressor. To completely validate the modeling technique, interstage and overall compressor experimental data would be necessary for that compression system. However, complete compression system performance (overall or interstage) was not available. Thus, model validation consisted of qualitatively comparing the nine-stage compressor model results with experimental data from other high-speed compressor rig tests.

IV.2.1 Stage Characteristic Synthesis

Stage characteristics for the nine-stage high-pressure compressor were synthesized as outlined in Chapter III, Sections 2 and 3. Experimental stage performance was not available. However, stage-blade geometry was obtained thus allowing the use of COCODEC to predict stage performance for pre-stall operation. Stacking of the pre-stall synthesized stage characteristics in a steady manner provides a prediction of overall performance. Presented in Figure 38 is a comparison of model prediction of compression system steady performance to that obtained experimentally. In general, agreement between stacked characteristics and experimental results was excellent (i.e. pressure ratio and airflow agreed within 5 percent).

Experimental post-stall characteristics for this system do not exist. Therefore, estimates of stage performance in post-stall regions were made using the stage performance suggested by low-speed compressor rig studies. A typical set of stage characteristics used for this machine was presented in Figure 13.

IV.2.2 Available High-Speed/High-Pressure Compression System Experimental Results

Since validation of the high-speed compression system model must be made qualitatively, experimental results from two high-speed compressor rigs will be presented first followed by presentation of the model results and qualitative comparison.

Pratt and Whitney designed and tested a high speed research (designated HSR) compressor rig for post-stall investigations [4]. The compressor consisted of three stages capable of producing an overall

pressure ratio of 2.8 at a rotor speed of 22,000 RPM. Compressor discharge volume could be changed to allow different post-stall events to occur. Presented in Figure 39 is the overall system response to throttle closure at a corrected speed of 56 percent. The compression system experienced surge at a frequency of 18 Hz. Reducing the corrected speed to 54 percent, the compressor experienced rotating stall as indicated in Figure 40. Presentation of overall performance in this form can only show the average performance of the system without presenting any of the details of the rotating stall cell itself. However, what is of interest is the apparent boundary between surge behavior and rotating stall. Since the geometry is identical in each case, a "B" parameter could be defined which would describe that boundary for effects other than rotational speed. These results are very similar to that observed in low-speed rig tests.

Another high-pressure compressor rig test was conducted by General Electric [39] under the NASA sponsored Energy Efficient Engine program. The compressor is an advanced technology 10-stage compressor capable of high-speed and high-pressure ratio. It was instrumented with inlet and exit transient airflow rakes (total) and static pressure measurements) as well as inlet, exit, and interstage pressures and temperatures. The compressor was throttled by a metered discharge valve.

At a corrected speed of 70 percent, the throttle was adjusted to allow the compressor to experience rotating stall. Presented in Figure 41 is the average overall compressor performance unstalled and in rotating stall at several throttle settings. Although the transients to these

final states are not shown, their effective final quasi-steady operating points are indicated along the install characteristics.

At 98.5 percent speed, this same compressor was throttled to instability, producing high-speed surge cycles. Indicated on Figure 42 is the response of the compressor after instability inception. The compressor failed to return to its initial unstalled operating point during the surge transients because the initial reverse flow mixed with the inlet flow causing an increase in inlet pressure and temperature. Since the mechanical speed was held constant, this reduced the corrected speed to near 70 percent. However, as was the case in the low-speed rig tests [1], the surge trajectories are similar in nature with periods of full reverse flow and subsequent recovery and repressurization. Presented in Figure 43 are key compressor performance parameters as a function of time during the surge cycles near 70 percent corrected speed. At the initiation of the surge cycle, the exit pressure and flow rate dropped significantly followed by flow reversal. This caused a flow blockage at the inlet which produced a rapid increase in inlet pressure followed by a sharp drop. Following flow breakdown and reversal, there was a period where the system remained at a low flow rate and low-pressure ratio. Subsequent analysis of interstage measurements indicated that rotating stall was present. The system then began to recover with an increase in exit pressure and flow rate, and a decrease in temperature. The system continued to surge since the throttle was held in the same position.

IV.2.3 Nine-Stage Compressor Model Results

Since model validation with the nine-stage compressor is of a qualitative nature instead of a one-by-one analysis of individual cases, model results will be analyzed by comparing general characteristics observed in the experimental data that has been presented in the previous section. All comparisons will be made for a model configuration of a nine-stage high-pressure compressor with a representative combustor, but which does not involve combustion. This comparison will be analogous to the high-speed compressor-rig data presented in the last section.

The model was run at an initial corrected speed of 100 percent of design at sea-level standard day inlet conditions (P_T = 14.696 psia and T_T = 518.67 R). Mechanical speed was held constant but corrected speed varied with inlet temperature during post-stall events. The dynamic stage force time constant was set at 0.02, which allowed surge to be the dominant post-stall event. Presented in Figure 44 are the model surge trajectories as they appear on a compressor map. Because the throttle was held constant after initiating the post-stall event, the compressor experienced a series of surges as the combustor volume repressurized. A very rapid flow reversal process occurred at the initiation of the event. After reversal had taken place, pressure throughout the machine began to drop as evidenced by the dropping pressure ratio. Once the combustor and compressor volumes emptied, the compressor began to pump, causing the flow to accelerate toward positive flow. As was the case with flow reversal, this process is fairly rapid. Once positive flow had been established, the modeled compression system was

able to increase the pressure and move performance back toward the demanded pressure ratio.

Presented in Figure 45 are time histories of the major compressor performance parameters. These model results are similar to those experimental results obtained with the General Electric (G.E.) energy efficient high-pressure compressor (Figure 43). Comparison of several of the time-history plots reveals a one-to-one correspondence in the sequence of events. At the time of the initial instability, the exit total pressure increases rapidly indicating the flow blockage of the throttle. When flow reversal occurs, inlet total pressure and temperature rapidly increase, following the compressor exit condition. The inlet pressure spike is a result of the compressor exit high-pressure air flowing back through the compressor. As the flow reverses, the pressure drops because of the high flow resistance of the compressor. Thus, the momentary elevated inlet pressure spike is at a reduced level compared to that of the initial compressor exit pressure. The inlet temperature reflects the initial exit temperature plus any increase due to work input into the fluid.

Another way to view the surge process is illustrated in Figure 46. This figure shows the flow and temperature distributions during a single surge cycle. At the initial time, just prior to surge, the airflow is fairly constant but reflecting some unsteady adjustment due to the closing throttle. The initial temperature distribution reflects the temperature increase due to the compression process. By the third time step (approximately 14 milliseconds later), the flow reversal process is complete with the inlet flow having become strongly negative for a time.

The temperature distribution indicates the changing temperature environment during the surge cycle which involves the increase in the inlet temperature to the compressor exit temperature during blowdown and the reingestion of that high temperature flow during reacceleration of the flow. Note that during the entire surge cycle the rear portion of the combustor volume never experiences reverse flow. This result becomes important when combustion is present, and will be discussed in Chapter V.

Surge frequency as predicted by the model is of the order of 10 to 12 Hz which is typical of engine surge frequencies observed experimentally. This does not compare well with the low-speed rig experimental results because of the size of the combustor attached to the compressor. Combustor volumes of typical turbine engines are usually much smaller than the plenum volumes used behind compressor rigs. Thus, one would expect the surge frequency of the compressor rigs to be much lower than turbine engine results. This is the case for Greitzer's experimental results and the G.E. energy efficient compressor rig. The P&WA HSR rig surge frequency was somewhat higher (approximately 17 to 18 Hz) and the plenum volume was near that of a typical combustor. Surge frequencies for aircraft turbine engines are of the order of 9 to 11 Hz. Thus, model surge frequencies agree well with actual engine results.

Rotating stall at high engine speeds is not common in modern engine compression systems. To investigate rotating stall the nine-stage model was run at 70 percent speed where rotating stall has been observed in high-pressure machines. Increasing the stage force time constant, τ, will increase the lag of the stage forces and retard the flow reversal

process. If flow reversal does not take place, the forces necessary for recovery may not be generated. In this case, the model will "zero in" on the steady-state compressor characteristic which represents a one-dimensional average of the rotating stall performance. Presented in Figure 47 is the model-predicted overall compression-system performance trajectories on the compressor map. The flow reversal process began as it did in the surge event. The flow went through one complete surge cycle. However, during the second cycle the flow did not completely reverse, which set rotating stall into motion. In this case, the stage forces are quite heavily lagged generating the scenario outlined above. The trajectories to the final state did not appear to "spiral in" as did the rig results presented in Figure 40. In the case of the rig results, there was a facility inlet which created a high resistance to reverse flow. This did not allow restoring forces to be generated, resulting in rotating stall. In the case of the model, rotating stall was created by lagging the steady-state pressure characteristics such that restoring forces were also not generated, but in such a manner that only a partial surge cycle was generated. However, the model did finally come to a steady-state performance prediction at a pressure ratio of approximately 15 percent of design and a flow rate of 10 percent of design. This state represents the development of a completely formed rotating stall.

Presented in Figure 48 are the time histories of the major performance parameters during the rotating stall event. Airflow oscillates about the new operating point and compressor exit pressure settles into

a new low value. Both airflow and exit pressure behavior are similar in nature to that experienced with the P&WA HSR rig (Figure 40) and the G.E. energy efficient compressor (Figure 43). Inlet pressure and temperature oscillate about the initial condition indicating the unsteady nature of the initial process.

IV.3 Comment on the Validation Process

The modeling technique described on Chapter III has been validated by comparison with experimental results. To completely validate the technique, interstage as well as overall compression system performance measurements during post-stall events would be necessary. Only in the case of a low-speed compressor rig has there been adequate experimental results to properly validate this stage-by-stage compression system modeling technique. This was accomplished by using measured pressure stage characteristics and synthesized temperature characteristics for a three-stage, low-speed compressor rig. Comparison of model overall performance during post-surge events to the general nature of the experimental results indicate correct simulated overall system behavior. Dynamic stage behavior during post-stall events were not available. However, with the assurance that overall system behavior is correctly represented, one can have a good level of confidence in the individual stage behavior predicted by the model.

In addition, a qualitative validation was performed for high-speed systems by using a nine-stage, high-pressure compressor model. Stage characteristics were synthesized using a design code for pre-stall characteristics and estimates of stage performance in post-stall regions

as suggested by low-speed compressor rig studies. Comparison with overall experimental results from other high-speed compressor rigs indicates that model overall performance correctly simulates the general nature observed for high-speed machines experiencing surge or rotating stall.

Thus, the model can be used to investigate the effects of internal and external disturbances or stage performance changes on post-stall behavior that might be encountered or experienced by both low-speed and high-speed compression systems. Some disturbances and stage changes are investigated in the next chapter.

CHAPTER V

PARAMETRIC STUDY

To indicate the unique capabilities and potential usefulness of this stage-by-stage, post-stall compression system modeling technique, a parametric study was conducted to assess the influence of some external and internal disturbances on compression system operability. Such disturbances are produced by distortion screens, combustion instabilities and rapid power-lever transients, and are known to have detrimental effects on compression system stability. These effects are analyzed using both the three-stage, low-speed compressor model and the nine-stage, high-speed, high-pressure compressor model.

In addition, possible stage characteristic modifications representing changes which would occur from modifications in actual stage geometry are studied with respect to their effect on system stability and recoverability. Such modifications as tip clearance, camber, and the addition of tip treatment are known to change pre-stall stage performance and stall characteristics. Certain modifications are postulated, based upon experimental results, and the effects on stability and recoverability are analyzed.

V.1 Effect of Inlet Resistance on Post-Stall Behavior

During testing of compressor rigs or full-scale turbofan engines, distortion screens or distortion generators have been utilized to present unfavorable spatial pressure and temporal flow patterns to the compression system. The purpose of a spatial distortion mechanism is to produce pressure or temperature patterns that might be experienced by the

compression system during actual operating conditions. To completely analyze the effects of a distortion-generating mechanism, a two- or three-dimensional model would be necessary. Excellent two- and three-dimensional models have been constructed based upon parallel compressor theory [16, 17] but these models lack the capability for simulating post-stall events. However, the one-dimensional modeling technique described in this dissertation can provide insight into the effect that a distortion-producing device has on compression-system recoverability, since that device can be represented as a resistance in the inlet. The modeling technique has the capability to allow a resistive element to be included in any control volume. In an inlet duct, the resistive force can be represented as a frictional body force and can be calculated using the Darcy-Weisbach friction factor by the following equation:

$$Fr = \left[\frac{\gamma}{2} f P_s M^2 \right] \frac{Per}{4} \qquad (75)$$

where

f = friction factor

Ps = static pressure

M = Mach number, and

Per = wetted perimeter

All model computations are made with a friction factor of 0.02 representing a fairly smooth surface and turbulent flow (based upon Moody Diagram). When the effects of a distortion device were desired, additional friction loss was added to one control volume in the inlet.

To quantify the effects of a distortion-producing device (such as a screen) on compression system post-stall behavior, the three-stage,

low-speed compressor model was used with a screen simulated in the inlet duct. A typical inlet pressure distribution is presented in Figure 49. The pressure drops in control volumes 1 through 4 and 6 through 10 are the result of nominal frictional forces (f = 0.02). However, the pressure drop in control volume 5 is a result of additional friction (f = 0.1) representing the loss through a distortion screen.

To clearly show the strong effect of a distortion screen on system post-stall behavior, a base case was chosen in which deep surge existed (Figure 37). For this case, the model compressor was operated at a mean wheel speed of 92.98 meters per second with a large plenum, producing a "B" parameter of 1.58. The throttle was closed to a position 60 percent smaller than what would have just caused instability. The stage force lagging time constant was held constant (τ = 0.27) for all cases investigated.

The deep surge cycles produced by this configuration without a distortion screen simulation present are represented in Figure 50. The time marks are only for the first surge cycle and will be helpful in the analysis of the post-stall events.

The effects of a distortion screen on system post-stall behavior are presented in Figures 51 through 53. A higher-than-nominal friction factor was used in the fifth control volume (one diameter upstream of the compressor inlet) to represent the pressure loss due to a distortion screen. Presented in Figure 51 is the post-stall, compression system behavior when a friction factor of 0.1 was chosen. This friction factor level resulted in a pressure drop of 1.3 percent across the simulated screen. The compressor still exhibited deep surge cycles; but during

the surge, the flow did not reaccelerate as much as in the previous case (Figure 50). A new pressure coefficient/flow coefficient relationship was established during the repressurization phase. Increasing the friction factor to 0.15, which increased the pressure drop to 2.8 percent produced the nonrecoverable (rotating stall) condition after one partial surge cycle as illustrated in Figure 52. Further increasing the friction factor in the fifth control volume to 0.3 (4.7 percent pressure drop) produced the nonrecoverable condition without flow reversal as presented in Figure 53. This overall behavior is similar to the experimental behavior observed at a "B" parameter of 0.66 (Figure 28).

Analysis of this series of post-stall events can be facilitated by an examination of the energy and forces generated in the inlet ducting along with the compressor stage forces. Presented in Figure 54 is the energy distribution for the inlet during each of the previously presented post-stall events. The time marks correspond to the marks on Figures 50 through 53 for ease in identifying where these distributions occur during the events. As the pressure drop across the screen increases from the nominal case ($f = 0.02$) to the most severe case ($f = 0.3$), the energy available to the compressor ($X/R = 4.4$) is reduced from 96 percent of the initial inlet value to 91 percent. This decrease in energy is a direct result of losses due to the frictional forces which are presented as equivalent retarding forces in Figure 55. In the cases where nonrecoverable stall is the final state, the frictional forces are at a level of 40 to 60 Lb_f. Examining the forces in the compressor (Figure 56), one finds that the initial stage forces generated are of the same

magnitude as those frictional forces when a distortion screen is present. When a distortion screen is not present, the forces in the compressor, which are on the order of 50 to 60 Lb_f, are large enough to overcome the nominal frictional forces of -4 to -5 Lb_f, resulting in deep surge cycles. However, as inlet viscous forces are increased, dynamic forces generated within the compressor are not adequate to overcome the resistance of the frictional forces, resulting in the development of the nonrecoverable state or rotating stall.

V.2 Effect of Combustion in a Combustor on Post-Stall Behavior

During operation of a turbofan engine, compression system stability is strongly influenced by the stability of the combustor. Fuel pulses are known to initiate compression system surge and/or rotating stall. Whether the combustor stays lit or pulsates may determine the nature of the post-stall compression system behavior. Actual engine results were examined to determine the direction of this study. Presented in Figure 57 are typical compression system post-stall behavior for current-day turbofan engines with the performance of the combustor noted by the ultraviolet detector output signal. This detector produces a signal based upon the ultraviolet radiation released during combustion and can be used to determine whether combustion is present. The post-stall events include surge with combustion, surge with no combustion, surge driven by repeated blowouts and reignition, and rotating stall with burning in the combustor.

To analyze combustion effects, the nine-stage, high-pressure compressor model with a representative combustor (Figure 16) was utilized.

At high speeds, experimental results have indicated that deep surge is the predominant post-stall event for this class of machine. The model was configured to run at 100 percent speed with an initial fuel flow which provided a combustor exit temperature of approximately 3000°R. The compressor stage force lagging time constant was set such that deep surge would be predominant (τ = 0.02). The compression system was moved to instability by rapidly increasing the fuel flow (fuel pulsing) to approximately 10 percent over the initial value. Once this step increase was accomplished, the fuel flow was left at the new constant level for 0.5 seconds then reduced to its original level. The compressor exhibited deep surge cycles during the fuel pulse, then returned to its initial stable operating point when the fuel pulse was terminated. The surge cycles depicted in Figure 58 are quite similar to those obtained without combustion (Figure 44). However, in this case the surge cycles are being driven by the continual blowout and reignition process in the combustor as illustrated in Figure 59. During flow reversal, the fuel-air ratio reaches a rich blowout limit (FAR = 0.15) at which time the combustor can no longer sustain combustion. The combustor remains out during the blowdown and reacceleration phases and reignites during the repressurization phase. Reignition is scheduled according to Equation (44) with a time constant based upon the reignition of JP4 at 800°R (Figure 18). Because blowout occurs during the flow reversal process prior to any significant reverse flow, the compressor inlet temperature does not reflect the elevated combustor temperature, but only the temperature rise due to normal compression and the work input during flow reversal. This

process can be readily seen in Figure 60. At the initial time (just prior to the reversal process, t = 0.104), the temperature distribution indicates the temperature rise through the compressor and the linear temperature distribution in the combustor. At the next time period (t = 0.109), flow reversal has taken place from the inlet through the compressor to a portion of the combustor. This process elevates the temperature in the compressor and inlet ducts to that of the initial compressor exit temperature. However, the major portion of the combustor volume did not experience flow reversal. Combustor blowout occurred prior to complete reversal. Therefore, the temperature associated with combustion is not reflected in the inlet region during this process. During the reacceleration phase, the inlet temperature returns to the original value ($T_{T_{inlet}}$=518°R) while the elevated temperature air is pumped through the compressor resulting in a compressor exit temperature near 2000°R instead of the normal 1200°R. If combustor reignition occurs before this high temperature air is passed through the combustor, high values (>4000°R) of combustor exit temperature are experienced. Actual magnitudes of this exit temperature are in doubt because of the use of a simple combustion model. A combustion model with at least equilibrium chemistry and combustor efficiency degredation is needed to quantify the combustion process during post-stall events.

During compression system flow reversal, the model indicates that the initial portion of the combustor may also experience flow reversal. Since, in the actual engine, this region contains fuel atomizing nozzles, it can be assumed that a portion of the fuel may be drawn into the compressor. At this operating condition, compressor exit temperature is

high enough to cause ignition of this unburned fuel. To simulate this scenario, ten percent of the initial fuel flow rate was introduced into the last four stages of the compressor during compressor flow reversal, and ignited according to the ignition schedule provided by Equation (41). The heat release in the compressor as well as the combustor, during this process is illustrated in Figure 61. As in the previous case, the compressor experiences a similar series of deep surges (Figure 62) driven by an elevated fuel pulse. As the compressor begins to experience flow reversal, the combustor blows out with reignition occurring during the repressurization phase. This again places the compressor in an unstable position, thus driving the surge cycles. However, because of fuel ignition in the compressor during compressor blowdown, the compressor inlet temperature is approximately 300°R higher than previously noted (Figure 59). Airflow and temperature distributions for the first surge cycle are presented in Figure 63. Fuel ignition in the rear four stages of the compressor causes the temperature in these stages to approach 2200°R at time of combustion. But, since flow reversal is slowing down during the blowdown phase, this elevated temperature gas does not completely reach the compressor inlet. As in the previous case, the hot air is reingested into the compressor causing an elevated temperature during combustor reignition. Due to the over-simplified combustor model, a quite unrealistic temperature spike is created in the combustor but is rapidly washed out of the system.

At high speeds, the combustor will either pulsate or blow out as can be seen in Figure 57a. When the combustor blowout occurs, rotor speed will begin to decay. At some time later, the combustor may

reignite at a much lower compressor speed. As illustrated in Figure 57a, the compression system may experience rotating stall and operation may become nonrecoverable.

To simulate this post-stall event, the model was run at 70 percent speed with initial fuel flow set to produce a combustor exit temperature of approximately 2000°R. The stage force lagging constant was set at a value slightly higher than that used for the 70 percent rotating stall case without combustion present (Figures 47 and 48) to ensure that the nonrecoverable state was achieved. The throttle was set at a value to just cause instability. The fuel was pulsed to a level approximately 50 percent higher than the initial setting. Fuel air ratio cutoff was set at 0.08 which produced continuous combustion in the combustor. Very uncharacteristic surge cycles were predicted. Further manipulation of the lagging time constant, throttle, or fuel pulse did not produce the desired results. However, when a combustion efficiency degradation was implemented along with a smaller throttle closure, the nonrecoverable state could be achieved as illustrated in Figure 64. The compression system experienced one surge cycle, at which time the combustor blew out. However, during reignition, combustion efficiency was designated to be only 0.5 instead of 1.0 as in all previous cases. The compression system thus proceeded to the nonrecoverable state and exhibited a limited oscillation as illustrated in Figure 65. Combustor heat release remained constant during this phase but at only 50 percent of its initial value. Inlet temperature increased only 70 degrees during the one surge cycle. At this low speed, flow reversal is not quite as violent as during high speeds.

Presented in Figure 66 is the temperature distribution during this event. During fuel-pulsing, just prior to flow reversal, the combustor exit temperature reached approximately 2500°R. During flow reversal, the combustor blew out with the exit temperature dropping below 2000°R prior to reignition. During reignition, the combustor efficiency had been degraded to 50 percent, producing an exit temperature of approximately 2000°R. However, as the compression system operating point moved to the nonrecoverable state, combustor exit temperature reached a maximum of approximately 3500°R during the flow oscillations. Although this combustor exit temperature distribution may not be accurate, it does serve to point out why the nonrecoverable state is so undesirable. Turbines on present turbofan engines are designed to withstand combustor exit temperatures of 2500 to 3000°R. With continuously pulsating combustion producing exit temperatures of the order predicted with this model (3500°R), the turbine life would be consumed quickly.

V.3 Effect of Heat Transfer on Post-Stall Behavior

Operation of high-speed, high-pressure compressors result in a high-temperature rise through the compressor. A portion of the resulting large amount of thermal energy is stored in the compressor blades, rotors, and disks. Thus, during throttle transients such as a bodie maneuver (max power to idle then back to max power) heat transfer between the compressor metal and the airflow takes place. The release of energy during the transient from maximum power to idle moves the transient operating line toward the nominal surge line, at the same time that an increase in the compressor loading lowers the surge margin. This loss

in surge margin can result in a compression system instability during throttle readvance to maximum power. This phenomenon has been investigated by MacCallum and Pilidis [40]. A turbine engine model prediction of the loss in surge margin is illustrated in Figure 67. From their modeling study, they concluded that the following thermal effects contribute to the loss in stall margin during reacceleration: (1) nonadiabatic flows causing density changes due to heat transfer, (2) changes in boundary layer development on the blade airfoils, (3) changes in the boundary layer development near the end walls, (4) changes in tip clearances, and (5) changes in seal clearances.

Since the modeling technique presented herein is one-dimensional and cannot explicitly model boundary layer development and changes in tip and seal clearances, only the effect of nonadiabatic flows can be analyzed. An investigation by Crawford and Burwell [41] quantified the magnitude and nature of the heat transfer during turbine engine bodie maneuvers using actual engine test results. A calculation of stage thermal energy was made based upon the following equation

$$Q_{stage} = mC_p (T_{max} - T_{idle})_{stage} \tag{76}$$

where

m = mass of the blades, platforms and seals

C_p = specific heat of the metal

T_{max} = stage total temperature at max power, and

T_{idle} = stage total temperature at idle power.

Stage temperature distribution was obtained from a stage "stacking" model run for the given conditions. Stage temperature distributions for

maximum and idle power along with the corresponding stored thermal energy are presented in Figure 68. With a calculation of transient airflow, heat-transfer rates (Btu/sec) were calculated. Typical stage heat-transfer rates calculated from experimental results obtained from current-day high-pressure compressors are presented in Figure 69. Using these rates as a guideline, the effect of heat transfer due to a bodie maneuver was analyzed with the nine-stage, high-pressure compressor model.

The model was operated at 70 percent speed with the throttle set such that a compressor instability would occur. The stage force lagging constant, τ, was set at a value of 0.078. This value was chosen such that surge would be the dominant post-stall event without heat transfer occurring, but at a value high enough so that nonrecoverable stall could also occur if condition warranted. A stage specific heat transfer (Btu/lbm) was chosen for each stage based upon the calculated temperature distribution represented in Figure 69. Heat transfer rates were calculated knowing the airflow rate and were brought to their maximum level exponentially over a time period of approximately one second. The postulated heat transfer distribution through the compressor is illustrated in Figure 70. Since the throttle was set such that an instability would occur, the heat-transfer rates are shown to be oscillating during the first second of the dynamic event because the compressor is experiencing surge during this period. However, once the stage heat-transfer rates had reached their maximum values, the compressor moved to the nonrecoverable state as illustrated in Figure 71. This process can be better illustrated with time history plots as presented in Figure 72. The surge

cycles are readily identified with an indication of the developing heat transfer reflected in the inlet temperature spikes during flow reversal.

To understand the effect of heat transfer, an analysis of compressor stage performance is necessary. Presented in Figure 73 are the stage energy and force during the first surge cycle (minimum heat transfer) and the last surge cycle (maximum heat transfer) prior to the system operating point becoming nonrecoverable. In the first surge cycle, the second time distribution indicates force and energy during flow reversal (Figure 73a). However, during the last surge cycle, the second time distribution (Figure 73b) is much like the initial distribution, indicating more effect on the stage forces than during the first surge cycle. This change of the forces during the flow reversal process is a direct result of the density changes imposed upon the compressor flow due to heat transfer from the blades to the gas path.

This study presupposes that a compressor instability will occur during a bodie maneuver. Even if such is not the case, the model has indicated that because of the heat transfer generated within the compressor at time of throttle readvance, the compression system is more likely to enter the nonrecoverable state (rotating stall) than during a throttle advance when the compressor was in the original thermal equilibrium.

V.4 Effect of Possible Stage Hardware Modifications on Post-Stall Behavior

Once a particular compression system is built, the performance and stability behavior are fixed within certain limits. There are only a limited number of external changes that can be made to improve either performance or stability. If these changes can not produce the desired

result, certain internal or blade changes can be made which improve performance and stability. However, these types of changes can be costly and difficult to implement. For the designer to evaluate these types of changes, the present stage-by-stage model would be helpful to determine the type of changes to make and the degree of change necessary. In this section, tip clearance reduction, increased blade camber and tip treatment modifications will be examined for their effects on system post-stall behavior.

The amount of clearance between the rotating blade tip and the case wall has been proven experimentally to influence the overall performance of turbomachinery. The flow near the tip is three-dimensional and dominated by viscous effects producing a boundary layer which limits both the performance and efficiency of rotating blades. An experimental investigation by Hunter and Cumpsty [42] indicated that there is as much as a 20 percent increase in stall pressure rise for a reduction in tip clearance from 5% to 1% (Figure 74). In general, decreasing the tip clearance raises the compressor pressure rise performance along the speed characteristic, but much more so near stall.

Another change that the designer might wish to examine would be a change in blade camber. For isolated blade rows, more camber increases the peak lift coefficient. This translates to an increase in stage performance as illustrated in Figure 75 and presented by Koch [43] for a low-speed compressor. This change not only increases the pressure coefficient at stall but also increases the pressure characteristics all along the speed line, thus increasing the performance at all pre-stall operating conditions.

A final possible change that will be considered is the effect of some type of tip casing treatment. Takata and Tsukuda [44], utilizing a low-speed compressor rig, investigated the effects of certain types of tip-casing treatment on the performance of a single rotor row. Of the several types of treatment investigated, they found that a deep skewed slot tip treatment most improved the stage characteristics. Presented in Figure 76 is the deep skewed slot modification and its effect on stage performance. Although stage pressure rise is not increased by this technique, the amount of airflow reduction necessary for stall to occur was increased by 20 percent. This provides more stall margin reducing the chances for stall occurrence. In addition, a portion of the rotating stall characteristic is presented indicating a higher average pressure level during rotating stall.

The discussion of these possible hardware changes has basically dealt with the increase in performance in normal prestall operation, and the increase in the stall margin. However, these investigations have said very little about the effect on post-stall behavior. To evaluate these changes on post-stall behavior, the three-stage, low-speed model was chosen. A low-speed condition first presented in Section IV.1.3 (Figure 28) was chosen in which rotating stall was the end result. Overall performance during this event is represented in Figure 77. During these hardware modification studies, all variables ("B" parameter, force lagging constant, τ, speed and plenum configuration) were held constant except for the changes in the quasi-steady characteristics.

In reviewing the experimental evidence, one can conclude that reducing the tip clearance and/or increasing the blade camber have a

similar effect on the quasi-steady prestall characteristic. That is, both modifications raise the pressure rise capability at stall about 20 percent with increasing camber having a greater effect all along the stage characteristic. Therefore, a stage characteristic change can be postulated which might be a result of an increase in chamber, a reduction in tip clearance, or a combination of both. Illustrated in Figure 78 is a 25 percent increase in first-stage pressure coefficient for both the prestall and the rotating stall regions. Although experimental results indicate this type of change for the prestall characteristic only, it will be assumed that a similar effect occurs for the rotating stall region as well. Similar modification for stages two and three were also made. With changes to the characteristics of less than 25 percent or to only one or two stages, the compression system still exhibited the nonrecoverable state during a post-stall event. However, with a 25 percent increase for all stages, the compression system exhibited continuous surge cycles of the "classic" type as illustrated in Figure 79.

Takata's and Tsukuda's single rotor tip treatment experiment provides another possible stage characteristic modification [44]. Presented in Figure 80 is a postulated first-stage pressure characteristic based upon deep skewed tip casing treatment. The maximum stall pressure rise is extended for a 20 percent reduction in airflow, effectively increasing the stall margin for the first stage. The rotating stall characteristic is assumed to be similar in shape, but at a higher pressure as was indicated experimentally. With this change only to the first stage, the compression system exhibited continuous surge cycles as illustrated in

Figure 81. When similar changes were made to the second and third stages individually, the results were nearly identical. However, when changes to all three stages were incorporated collectively, the compression system resisted the stall condition altogether at the throttle setting which had previously caused instability. Not until the throttle was closed further did the system traverse beyond the stability limit.

The types of hardware changes investigated created higher stage forces either during prestall operation or at the stability limit. In some instances these forces were able to prevent the nonrecoverable state. The most effective mechanism seems to be tip casing treatment since the study indicated that treatment only need be done on one of the stages to increase the system recovery capability.

CHAPTER VI

SUMMARY

Compression system stability is essential for proper operation of turbine engines in aircraft application. During operation of axial-flow, multi-stage compression systems, surge and rotating stall have been observed. Although surge is a violent planar disturbance, the compression system and engine can recover to its former stable operating condition by relieving the surge-producing mechanism. Rotating stall, on the other hand, is not as violent but is more damaging to engine operation. Once rotating stall becomes completely established, a stable, but stalled condition can be produced from which the compressor cannot recover unless the engine is shut down.

During experimental studies, results are often limited because of test hardware and/or economic constraints. Where more information is desired, validated compression system mathematical models can be used to provide performance and stability information not obtained during experimental testing. These models also provide tools for studying the effects of external disturbances or possible hardware changes on compression system performance and stability.

The objective of the present investigation has been to provide a compression system model capable of exhibiting observed system behavior during post-stall events. That objective has been met by the creation, validation, and application of a one-dimensional, stage-by-stage, compression system model with post-stall capability. This model provides a tool for analyzing surge and rotating stall on a stage-by-stage basis

as well as on the overall system level. The following significant results and observations have resulted from this effort:

1. The model solves the nonlinear form of the conservation laws using the second-order accurate MacCormack finite-difference scheme.
2. The solution of the momentum and energy equations requires the modeling of stage forces and shaft work not only in the pre-stall cases but also during the post-stall events of surge and rotating stall. Stage forces and shaft work are obtained from a set of steady-state stage characteristics (pressure and temperature rise as a function of mass flow rate) that are lagged by a first-order lag equation to provide dynamic characteristics during surge and rotating stall. If experimental stage characteristics are not available, characteristics may be synthesized using a compressor design code (COCODEC) for prestall characteristics with estimates of post-stall characteristics which are based upon previous experimental results.
3. The model was validated for a three-stage, low-speed compression system for which experimental (pre-stall and post-stall) stage characteristics were available. Overall system post-stall behavior was compared to a very similar system for which post-stall system performance results were available. The three-stage, low-speed model was validated for post-stall events which encompassed rotating stall, classic surge and deep surge.
    a. The model was used to predict the nonrecoverable state (rotating stall) at the same condition (speed, plenum

volume, and "B" parameter) as was experienced experimentally. This was accomplished by the proper choice of the stage force lagging constant.

b. Holding the stage force lagging parameter constant, the model configuration was changed in the same manner (increasing the plenum volume) as in the experimental case to produce classic surge cycles. These surge cycles were very similar to those produced experimentally. The surge trajectories were circular in nature (with a frequency of 1.5 Hz.) when displayed on a compressor map.

c. Deep surge was predicted by the model when the speed was increased and the throttle was closed slightly, as was found experimentally. Deep surge cycles were similar to those observed experimentally with the occurrence of complete flow reversal, blowdown, reacceleration, and repressurization.

4. Since high-speed/high-pressure ratio compression systems are of great importance, the modeling technique was also validated for a typical high-pressure compressor by comparing model results with available experiments.

   a. Deep surge cycles were predicted by the model at high speeds, as has been observed with similar systems at similar operating conditions during testing. Model prediction of airflow, pressure, and temperature during the surge event were similar to those experienced with

the General Electric energy-efficient, high-pressure compressor. Inlet temperature and pressure during reverse flow reflect the elevated compressor exit temperature and pressure after the flow has traversed the compressor in the reverse direction.

b. The model has the capability to predict the nonrecoverable state (rotating stall) at any speed with the proper choice of the stage force lagging time constant. However, in any case, this event is more likely to occur at low speeds. The high-pressure compressor was run at 70 percent speed, and the nonrecoverable state was induced. The compression system exhibited an initial surge cycle, then traversed to the nonrecoverable state through a series of airflow and pressure-ratio reductions, to a final operating condition representing globally-stable rotating stall.

5. To indicate the potential usefulness of this stage-by-stage, post-stall compression system model, a parametric study was conducted to assess the influence of external and internal disturbances on system operability. In addition, possible stage characteristic changes representing possible hardware changes were studied as to their effect on system stability and recoverability.

   a. The effect of inlet resistance on compression system post-stall behavior was studied by evaluating the effect

that an inlet distortion producing mechanism, such as a screen, had on recoverability using the three-stage, low-speed compressor. When the amount of pressure drop occurring across a screen was increased, the model predicted that the system could experience nonrecoverable stall, when it had experienced deep surge prior to the introduction of the screen at the same rotational speed.

b. The effect of combustion on post-stall behavior was analyzed by using the nine-stage, high pressure compressor model with a representative combustor. Blowout and reignition of the combustor during surge cycles may not only be the result of surge but may aggravate the situation by keeping the surge-producing mechanism in place. If a portion of the combustor fuel is drawn into the compressor and burned during flow reversal, the compressor inlet will experience a more elevated temperature during this process than would be observed without combustion. If the combustor stays lit during rotating stall, the combustor exit temperature may exceed the design limit of the turbine even if a 50-percent degradation in combustor efficiency is assumed.

c. Blade to gas path heat transfer which would occur during a bodie maneuver was analyzed for its effect on compression system post-stall behavior. Heat transfer during nonequilibrium transients was found to be detrimental

to recovery, increasing the tendency for rotating stall to occur. Stage forces were lowered as a direct result of the density changes imposed upon the compressor flow due to heat transfer from the blades to the gas path.

d. Stage characteristic changes brought about by hardware modification were analyzed for their effect on system recovery. Reduction in tip clearance, increases in rotor blade camber and tip casing treatment were considered as possible hardware modifications. These changes were designed to improve performance and stability margin. By using the three-stage, low-speed compressor model, these changes were found to improve recoverability as well. The most promising change seems to be tip casing treatment. By simulating the effects of a deep-skewed slot treatment on a single stage, the model indicated that the system would exhibit classic surge cycles (i.e. be recoverable), instead of rotating stall (nonrecoverable) as previously had been observed at this condition without tip treatment.

CHAPTER VII

RECOMMENDATIONS

The post-stall compression system model has been created and validated against experimental results. In the course of development, certain limitations were imposed because of deficiencies in the numerical simulation. These limitations should be removed and further improvements made to facilitate applications to future compression systems. Therefore, the following recommendations are offered:

1. Stage Characteristics

Stage characteristics are at the heart of this modeling technique. Future experimental efforts should be directed to obtaining accurate stage-performance characteristics in the rotating-stall and reverse-flow regions, as well as the unstalled region. Theoretical methods for obtaining characteristics should be enhanced, developed, and validated to augment the experimental information.

2. Numerical Simulation

During the course of model construction, it was discovered that the MacCormack explicit numerical technique would not handle large changes in area from one calculating station to another. This type of area change occurs in the combustor. Satisfactory model results during surge or rotating stall could not be obtained. To overcome this limitation radical changes in modeled combustor area were not allowed, thus allowing only a representative combustor to be modeled instead of the actual

geometry. To remove this limitation, another numerical technique more tolerant of area changes should be explored and adapted.

3. Combustor Modeling

Modeling of the combustion process in the combustor is handled by a simple heat-release equation based upon fuel-air ratio and the lower heating value of the fuel. Only simple combustion efficiency degradations were modeled during post-stall events. Blowout and reignition are based upon limited experimental results and may not always occur at the proper combustor conditions. A more rigorous model of the combustion process should be developed and utilized to provide more accurate component interactions during post-stall events.

4. Dynamic Engine Model

The principles of the dynamic compression system model should be incorporated into a dynamic engine model which could then handle post-stall events. This would provide an engine analysis tool for purposes of analyzing test results and understanding their meaning. It would also provide a predictive tool to be used for facilitating future engine test programs.

REFERENCES

REFERENCES

1. Greitzer, E. M. "Surge and Rotating Stall in Axial Flow Compressors - Part II: Experimental Results and Comparison With Theory," ASME Journal of Engineering for Power, Vol. 98, No. 2, April 1976, pp. 199-217.

2. Day, I. J. "Axial Compressor Stall," Ph.D Dissertation, Christ's College (Cambridge University), 1976.

3. Burwell, A. E., and G. T. Patterson. "Dynamic Engine Behavior During Post Surge Operation of a Turbofan Engine," AIAA Paper No. AIAA-85-1430. Presented at AIAA/SAE/ASME/ASEE 21st Joint Propulsion Conference, Monterey, California, July 8-10, 1985.

4. French, J. V. "Modeling Post-Stall Operation of Aircraft Gas Turbine Engines," AIAA Paper No. AIAA-85-1431. Presented at AIAA/SAE/ASME/ASEE 21st Joint Conference, Monterey, California, July 8-10, 1985.

5. Gamache, R. N. "Axial Compressor Reversed Flow Performance," Ph.D Dissertation, Massachusetts Institute of Technology, May 1985.

6. Den Hartog, J. P. Mechanical Vibrations. New York: McGraw-Hill Book Company, Inc., 1940.

7. Horlock, J. H. Axial Flow Compressors. Huntington, New York: Robert E. Krieger Publishing Company, 1973.

8. Pearson, H., and T. Bowmer. "Surging of Axial Compressors," The Aeronautical Quarterly, 1:195-210, November 1949.

9. Gabriel, D. S., L. E. Wallner, and R. J. Lubic. "Some Effects of Transients in Inlet Pressure and Temperature on Turbojet Engines." Paper presented at the Twenty-Fifth Annual Meeting of the Institute of the Aeronautical Sciences, New York, January 28-31, 1957.

10. Kuhlberg, J. F., D. E. Sheppard, and E. O. King. "The Dynamic Simulation of Turbine Engine Compressors," AIAA Paper No. 69-486, presented at the AIAA/SAE Joint Propulsion Specialist Conference, Cleveland, Ohio, June 1969.

11. Willoh, R. G., and K. Seldner. "Multistage Compressor Simulation Applied to the Prediction of Axial Flow Instabilities," NASA TMX-1880, Lewis Research Center, Cleveland, Ohio, September 1969.

12. Daniele, C. J., R. J. Blaha, and K. Seldner. "Prediction of Axial-Flow Instabilities in a Turbojet Engine by Use of a Multistage Compressor Simulation on the Digital Computer," NASA TMX-3134, Lewis Research Center, Cleveland, Ohio, January 1975.

13. Kimzey, W. F. "An Analysis of the Influence of Some External Disturbances on the Aerodynamic Stability of Turbine Engine Axial Flow Fans and Compressors," Arnold Engineering Development Center TR-77-80, Arnold Air Force Station, Tennessee, August 1977.

14. Davis, M. W., Jr. "A Stage-by-Stage Dual-Spool Compression System Modeling Technique," ASME Paper No. 82-GT-189, Presented at ASME Gas Turbine Conference, London, England, March 1982.

15. Pearson, J. "Wakes in Axial Compressors," Journal of the Royal Aeronautical Society, 63:415-416, July 1963.

16. Mazzawy, R. S., D. A. Fulkerson, D. E. Haddad, and T. A. Clark. "F100(3) Parallel Compressor Computer Code and User's Manual Final Report," NASA CR-135388, Lewis Research Center, Cleveland, Ohio, May 1978.

17. Tesch, W. A., and W. G. Steenken. "Blade Row Dynamic Digital Compressor Program, Volume I, J85 Clean Inlet Flow and Parallel Compressor Models," NASA CR-134978, Lewis Research Center, Cleveland, Ohio, March 1976.

18. Greitzer, E. M. "Surge and Rotating Stall in Axial Flow Compressors - Part I: Theoretical Compression System Model," ASME Journal of Engineering for Power, Vol. 98, No. 2, April 1976, pp. 190-198.

19. Wenzel, L. M., and W. M. Bruton. "Analytical Investigation of Nonrecoverable Stall," NASA TM-82792, February 1982.

20. Seldner, K., J. R. Mihaloew, and R. J. Blaka. "Generalized Simulation Technique for Turbojet Engine System Analysis," NASA-TND-6610, 1972.

21. Chung, K., K. R. Leamy, and T. P. Collins. "A Turbine Engine Aerodynamic Model for In-Stall Transient Simulation," AIAA Paper No. AIAA-85-1429, Presented at AIAA/SAE/ASME/ASEE 21st Joint Propulsion Conference, Monterey, California, July 8-10, 1985.

22. Hosney, W. M., S. J. Bitter, and W. G. Steenken. "Turbofan Engine Nonrecoverable Stall Computer--Simulation Development and Validation," AIAA Paper No. AIAA-85-1432, Presented at AIAA/SAE/ASME/ASEE 21st Joint Propulsion Conference, Monterey, California, July 8-10, 1985.

23. Takata, H., and S. Nagano. "Nonlinear Analysis of Rotating Stall," Journal of Engineering for Power, October 1972.

24. Sexton, M. R., and W. F. O'Brien. "A Model for Dynamic Loss Response in Axial-Flow Compressors," ASME Paper 81-GT-154, March 1981.

25. Cousins, W. T. and W. F. O'Brien. "Axial-Flow Compressor Stage Post-Stall Analysis," AIAA Paper No. AIAA-85-1349, Presented at AIAA/SAE/ASME/ASEE 21st Joint Propulstion Conference, Monterey, California, July 8-10, 1985.

26. Moore, F. K. "A Theory of Rotating Stall of Multistage Axial Compressors," NASA CR-3685, July 1983.

27. Moore, F. K. and E. M. Greitzer. "A Theory of Post-Stall Transients in Axial Compression Systems: Part I - Development of Equations," ASME Paper No. 85-GT-171, March 1985.

28. Greitzer, E. M. and F. K. Moore. "A Theory of Post-Stall Transients in Axial Compression Systems: Part II - Application," ASME Paper No. 85-GT-172, March 1985.

29. Browell, R. W., L. D. Reynolds, and W. P. Core. "COCODEC: Combined Compressor Design and Evaluation Code." Union Carbide Corporation, Nuclear Division, CTC-INF-1039, May 1972.

30. Greitzer, E. M. "Review--Axial Compressor Stall Phenomena," Journal of Fluids Engineering, Vol. 102, June 1980, pp. 134-151.

31. Oates, G. C., Editor. "The Aerothermodynamics of Aircraft Gas Turbine Engines," AFAPL-TR-78-52, July 1978.

32. MacCormack, R. W. "The Effect of Viscosity in Hypervelocity Impact Cratering." AIAA Paper No. 69-354, presented at the AIAA Hypervelocity Impact Conference, Cincinnati, Ohio, April 30-May 2, 1969.

33. Moretti, G. "Importance of Boundary Conditions in the Numerical Treatment of Hyperbolic Equations," The Physics of Fluids, Supplement II (1969), pp. 13-20.

34. Olson, L. E., P. R. McGowan, and R. W. MacCormack. "Numerical Solution of the Time-Dependent Compressible Navier-Stokes Equations in Inlet Regions," NASA TM-X-62338, Ames Research Center, Moffett Field, California, March 1974.

35. Abbett, M. J. "Boundary Condition Calculation Procedures for Inviscid Supersonic Flow Fields," AIAA paper presented at the AIAA Computational Fluid Dynamics Conference, Palm Springs, California, July 19-20, 1973.

36. Courant, R., K. O. Friedricks, and H. Lewy. (1928), Translated from German to: "On the Partial Differential Equations of Mathematical Physics, IBM J. Res. Dev., Vol. II, pp. 215-234, 1967.

37. Ward, G. G. "Compressor Stability Assessment Program (Techniques for Constructing Mathematical Models of Compression Systems and Propulsion Systems)," Air Force Aero Propulsion Laboratory TR-74-107, Volume II, Wright-Patterson Air Force Base, Ohio, December 1974.

38. Eastland, A. H. J. "Investigation of Compressor Performance in Rotating Stall: I--Facility Design and Construction and Initial Steady State Measurements," MIT Gas Turbine and Plasma Dynamics Laboratory Report No. 164, June 1982.

39. Hosney, W. M. and W. G. Steenken. "Aerodynamic Instability Performance of an Advanced High-Pressure-Ratio Compression Component," AIAA Paper No. AIAA-86-1619, Presented at AIAA/ASME/SAE/ASEE 22nd Joint Propulsion Conference, Huntsville, Alabama, June 1986.

40. Maccallum, N. R. L. and P. Pilidis. "The Prediction of Surge Margins During Gas Turbine Transients," ASME Paper No. 85-GT-208, Presented at ASME Gas Turbine Conference, Houston, Texas, March 1985.

41. Crawford, R. A. And A. E. Burwell. "Quantitative Evaluation of Transient Heat Transfer on Axial Flow Compressor Stability," AIAA Paper No. AIAA-85-1352, Presented at AIAA/SAE/ASME/ASEE 21st Joint Propulsion Conference, Monterey, California, July 1985.

42. Hunter, I. H. and N. A. Cumpsty. "Casing Wall Boundary Layer Development Through an Isolated Compressor Rotor," ASME Journal of Engineering for Power, Vol. 104, No. 4.

43. Koch, C. C. "Stalling Pressure Rise Capability of Axial Flow Compressor Stages," ASME Paper No. 81-GT-3, Presented at the International Gas Turbine Conference, Houston, Texas, March 1981.

44. Takata, H. and Y. Tsukuda. "Stall Margin Improvement by Casing Treatment--Its Mechanism and Effectiveness," ASME Journal of Engineering for Power, January 1977.

APPENDIX

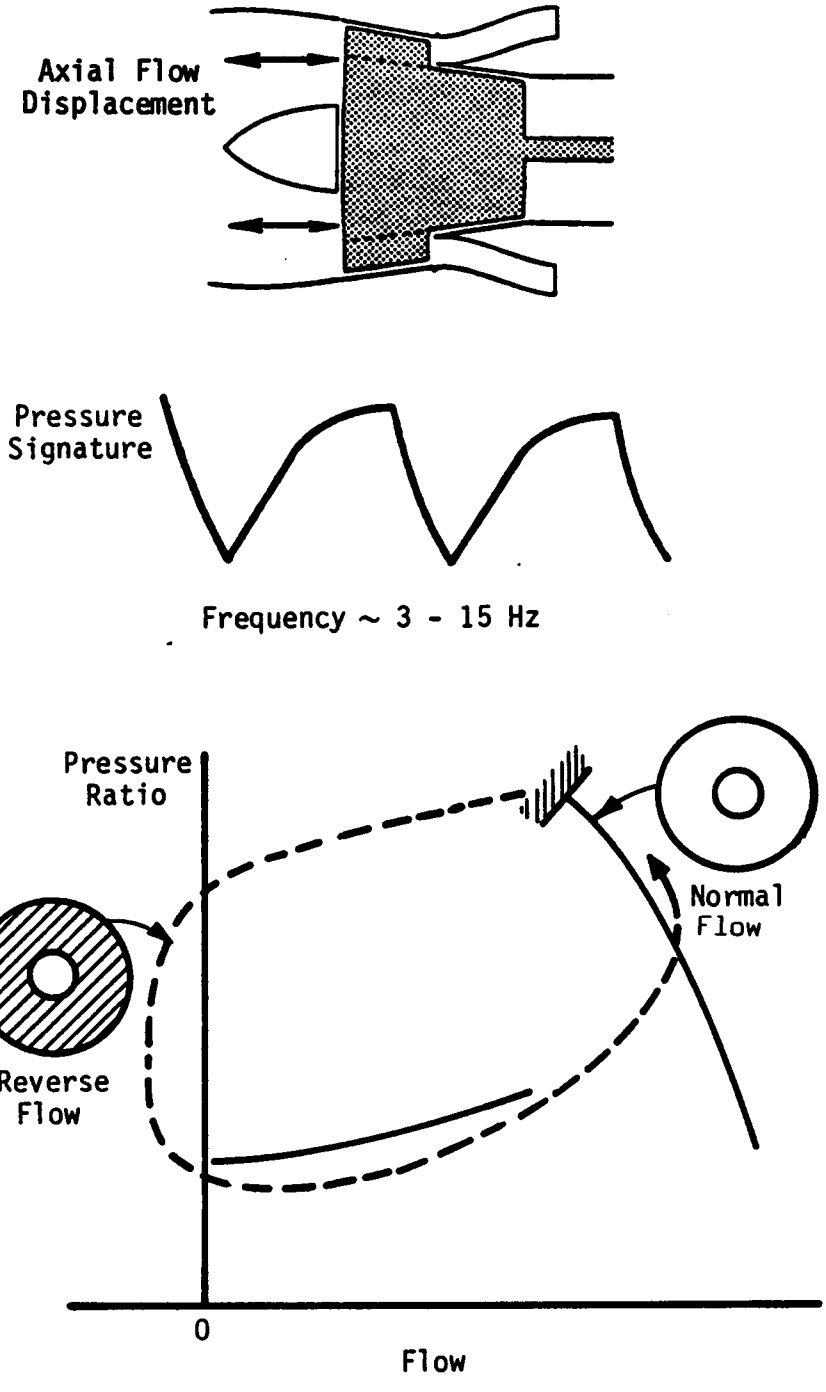

Figure 1. Compressor Surge--Axially Oscillating Flow.

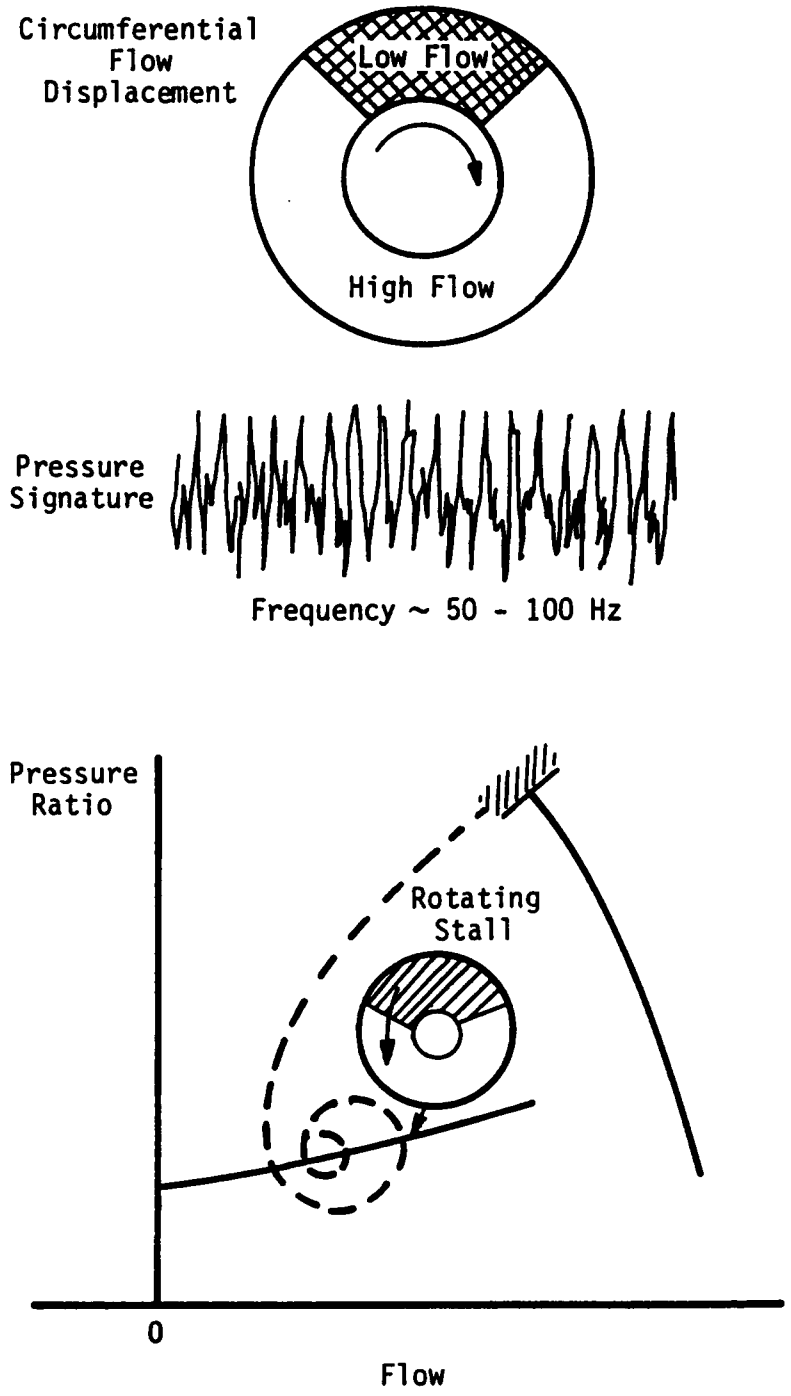

Figure 2. Compressor Rotating Stall--Circumferentially Nonuniform Flow.

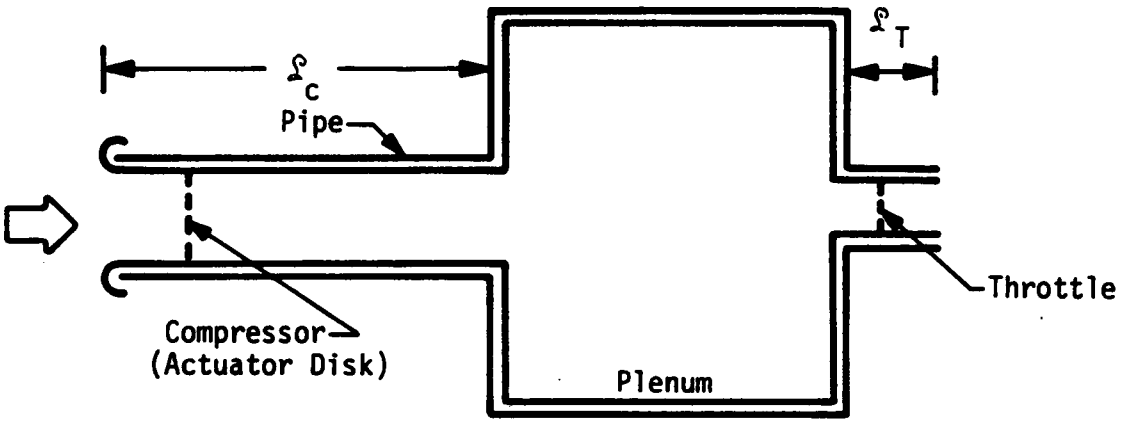

Figure 3. Equivalent Compression System [18].

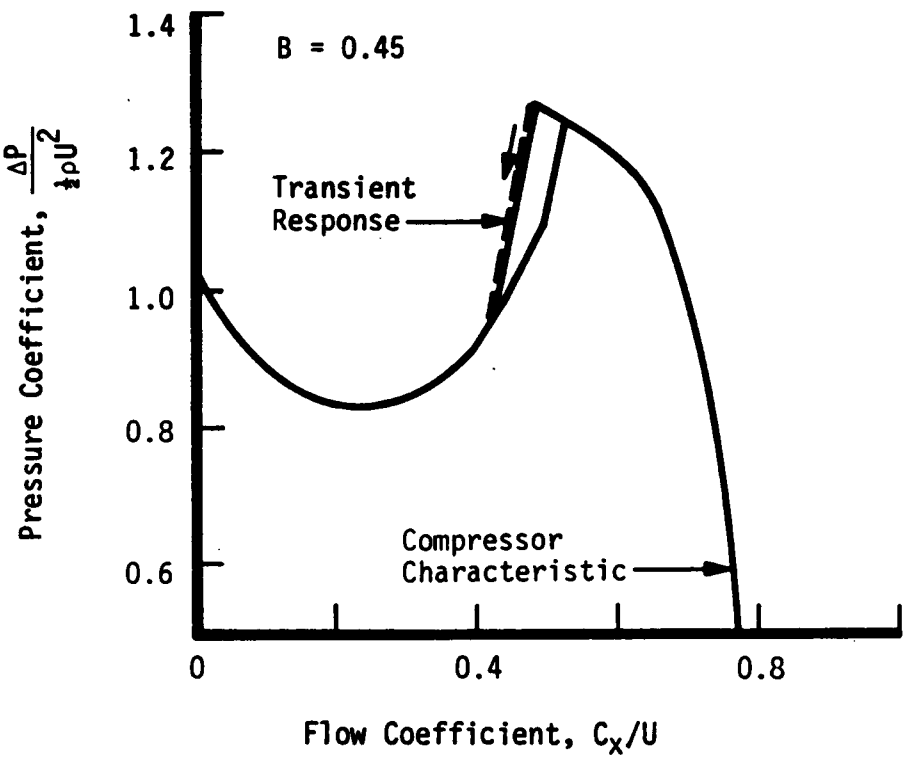

Figure 4. Transient Compression System Behavior: B=0.45 [18].

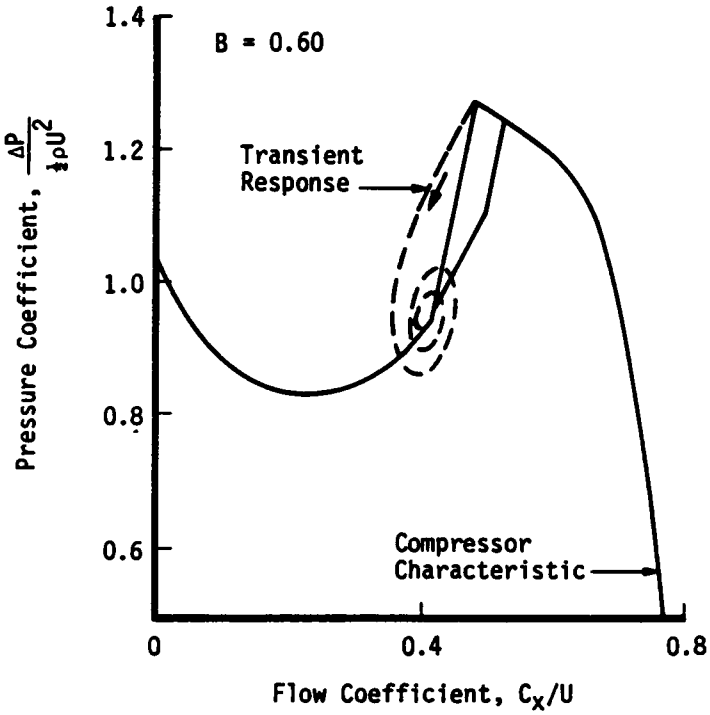

Figure 5. Transient Compression System Behavior: B=0.60 [18].

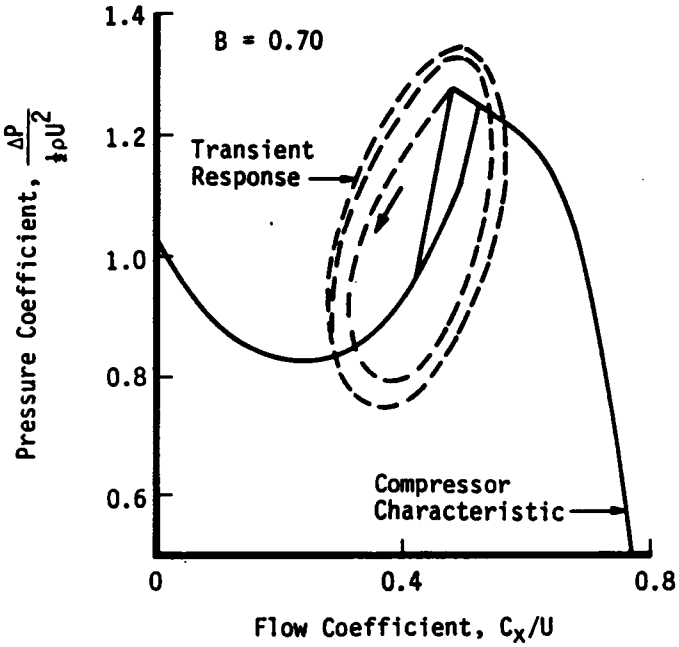

Figure 6. Transient Compression System Behavior: B=0.70 [18].

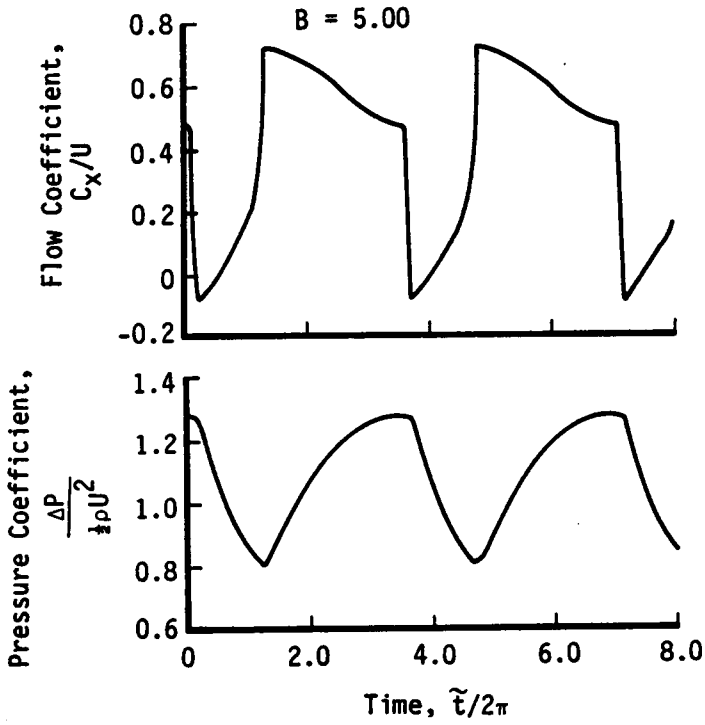

Figure 7a. Transient Compression System Behavior: B=5.00 [18].

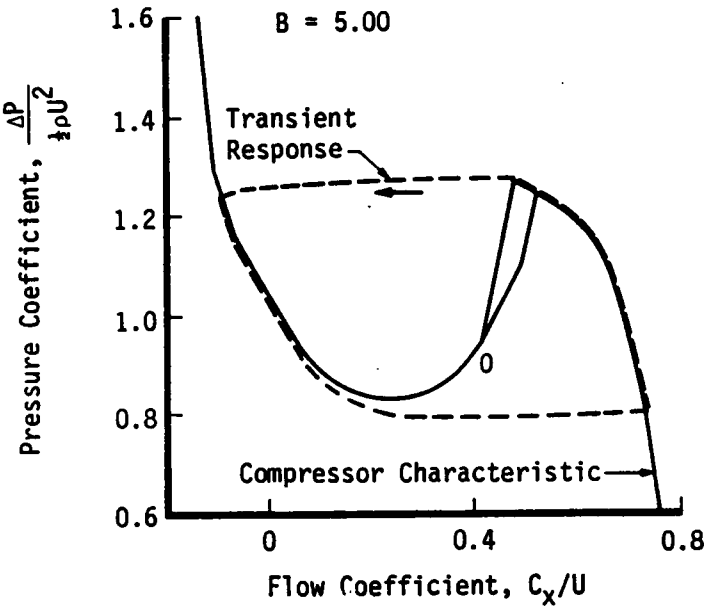

Figure 7b. Transient Compression System Behavior: B=5.00 [18].

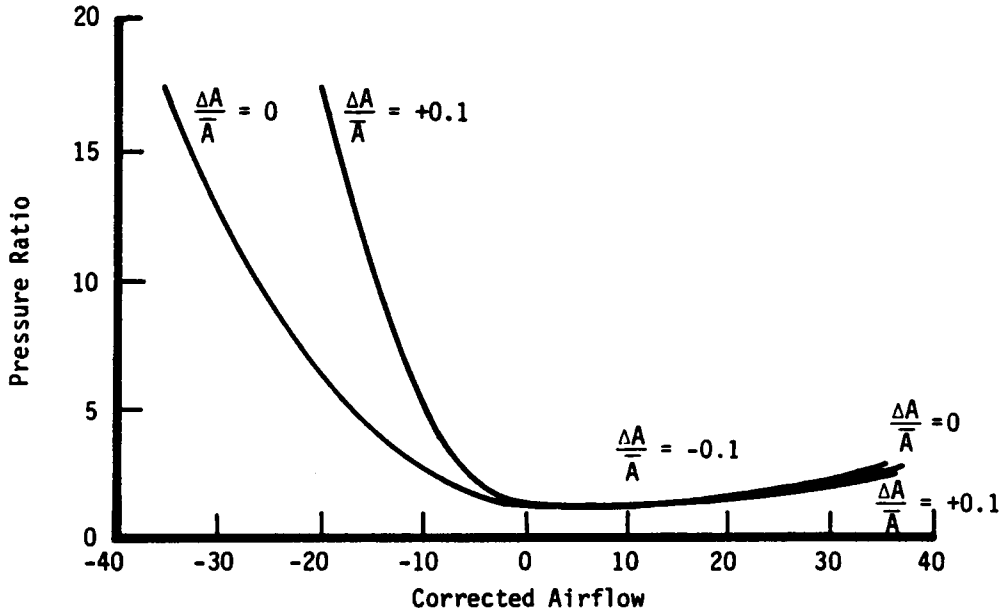

Figure 8. In-Stall Compressor Map Showing the Effects of Varying the Post-Stall Characteristic [19].

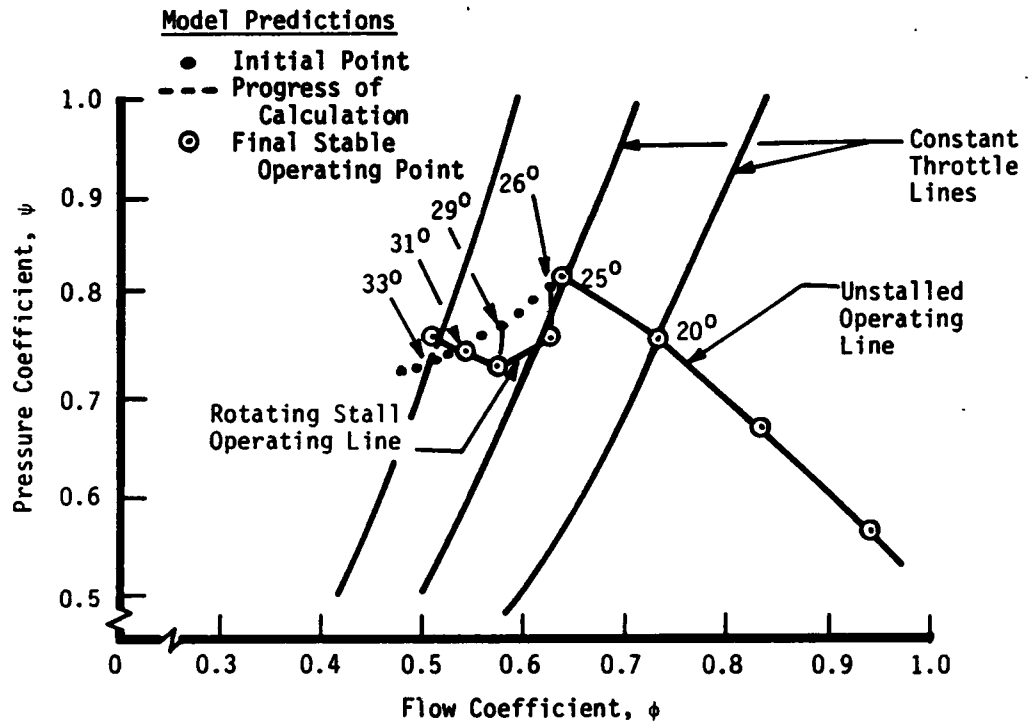

Figure 9. Model-Generated Compressor Stage Unstalled and Post-Stall Characteristic; Input Data for 65 Series Cascade, 25° Stagger [25].

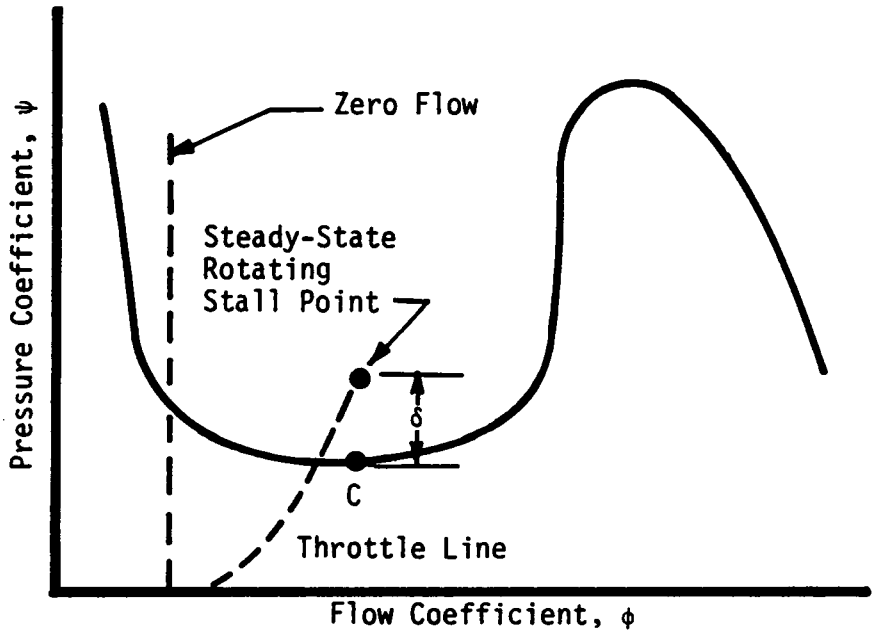

Figure 10. Constant-Speed Compressor Axisymmetric Characteristic in the Absence of Rotating Stall [26].

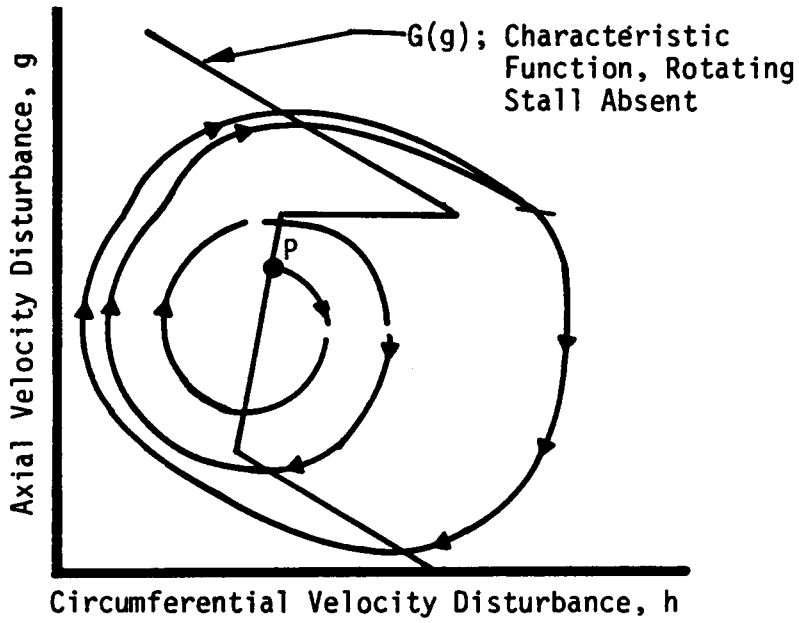

Figure 11. Development of Limit Cycle in Moore's Model [26].

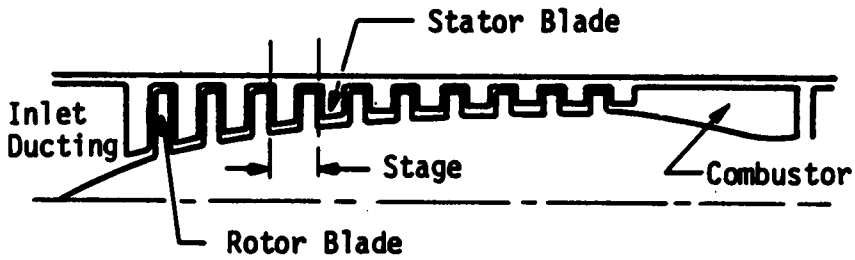

a. Compressor and Ducting System

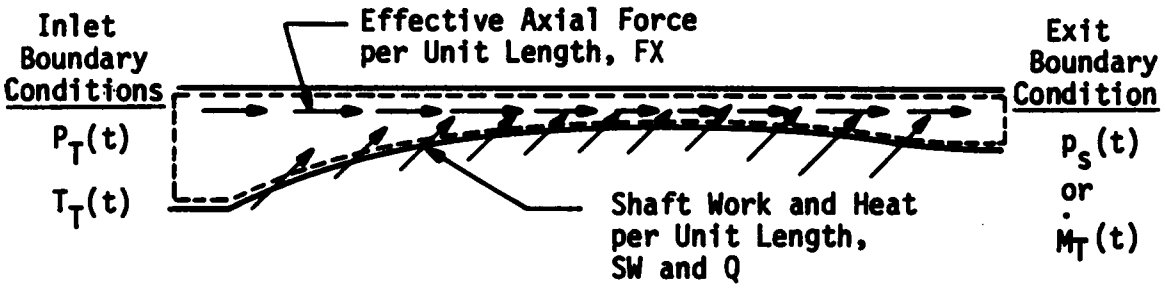

b. Overall Control Volume

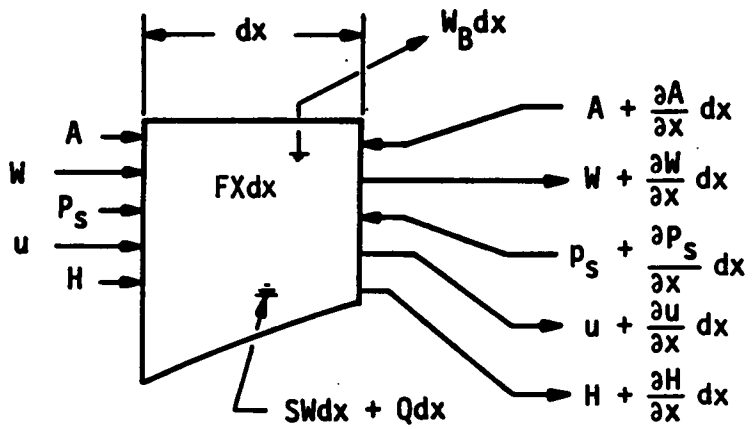

c. Elemental Control Volume

Figure 12. Physical Compression System Modeled and Control Volume Concepts.

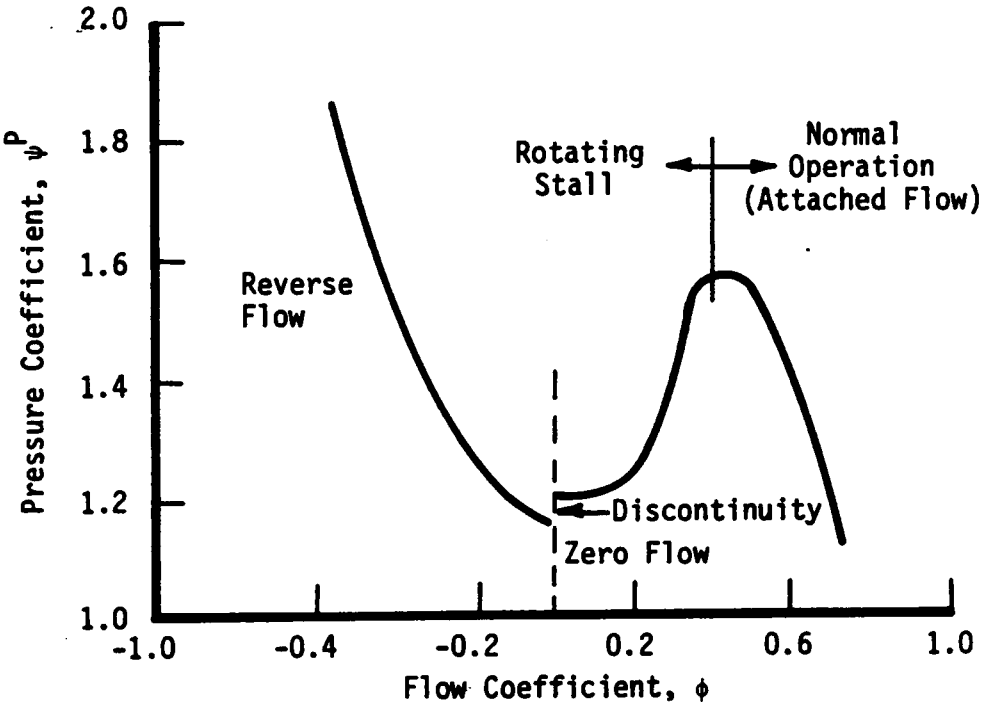

a. Pressure Coefficient

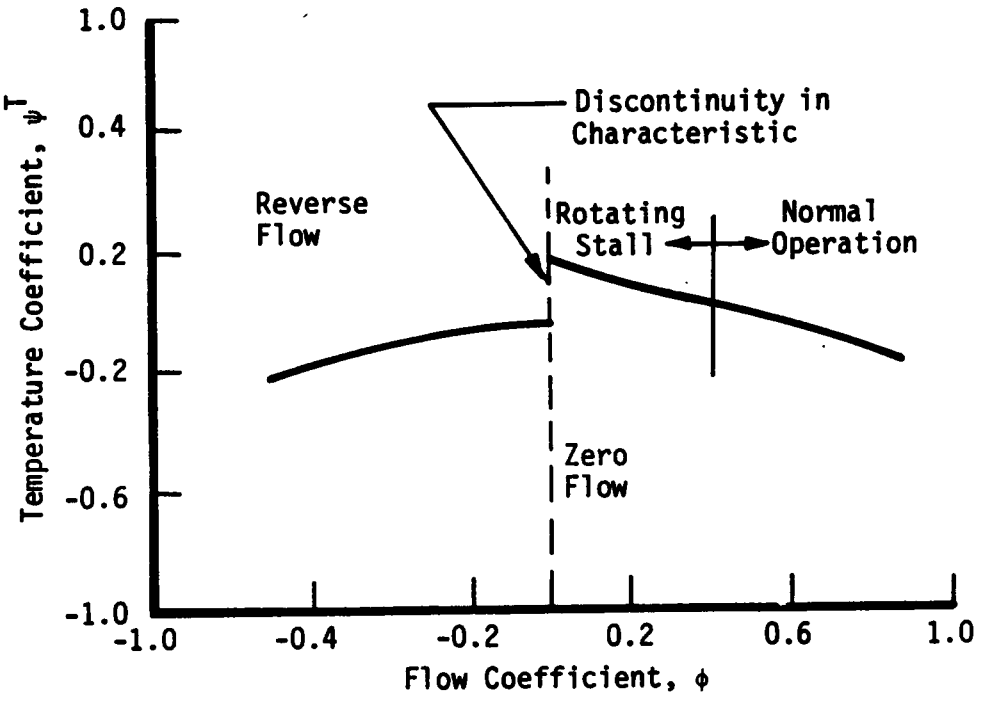

b. Temperature Coefficient

Figure 13. Typical Stage Characteristics.

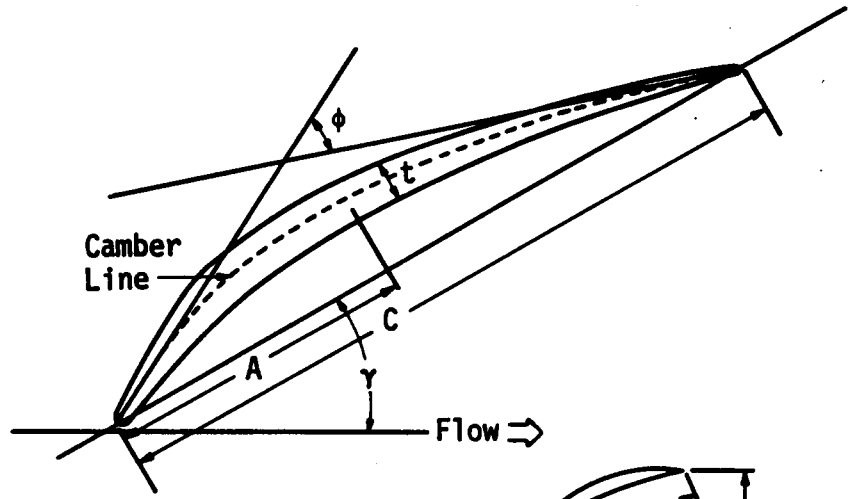

As a Function of Radial Position:

- γ - Stagger
- ϕ - Camber
- t/C - Thickness-to-Chord Ratio
- C/S - Solidity
- A/C - Position of Point of Maximum Camber
- Blade Profile Shape Description
- Flowpath Geometry and Blade Row Placement

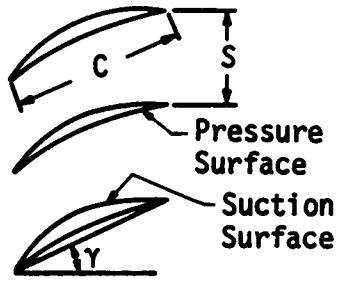

Figure 14. Blading Geometry Information Required for COCODEC.

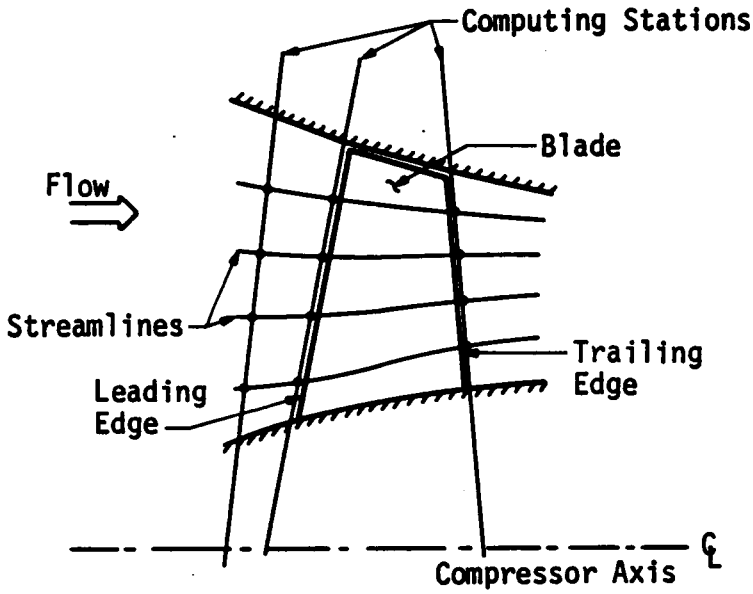

Figure 15. COCODEC Computing Mesh.

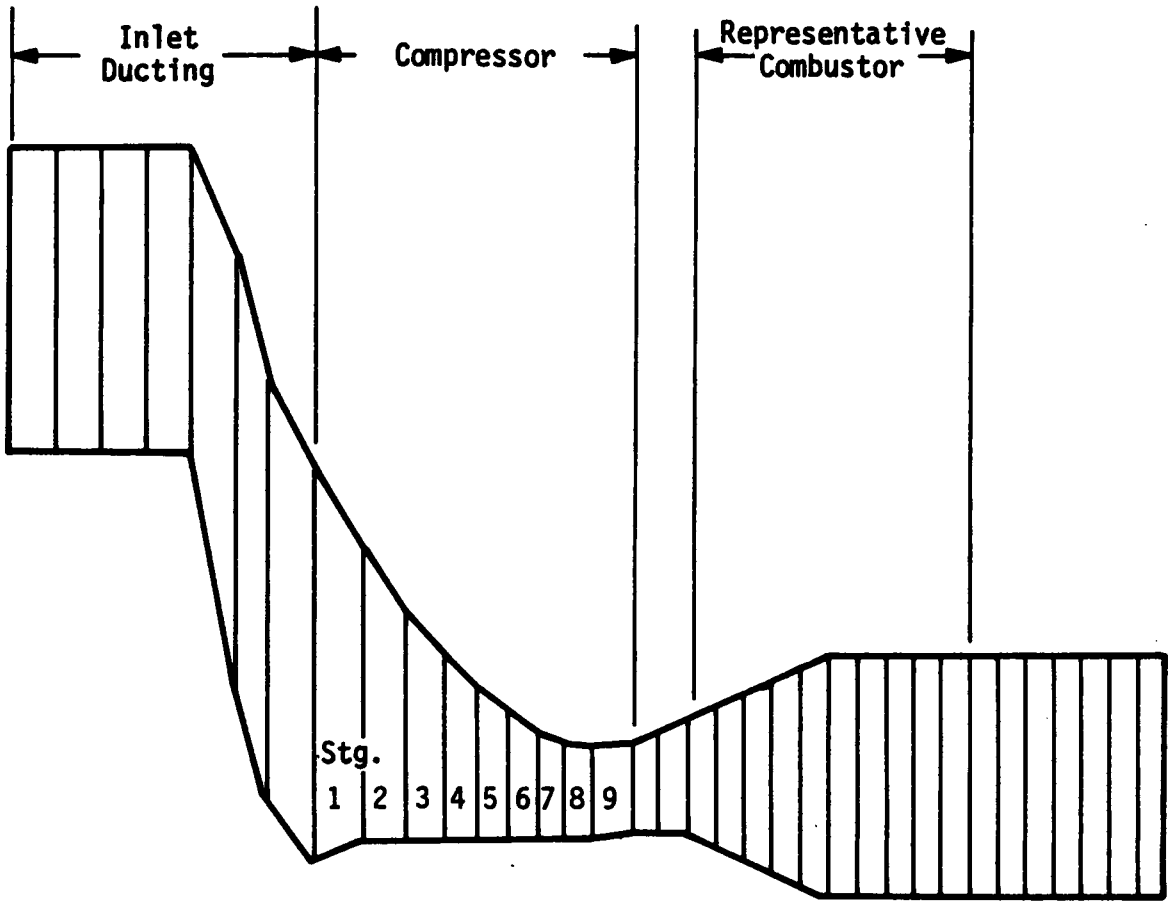

Figure 16. Control Volume Schematic of Nine-Stage Compressor with Representative Combustor.

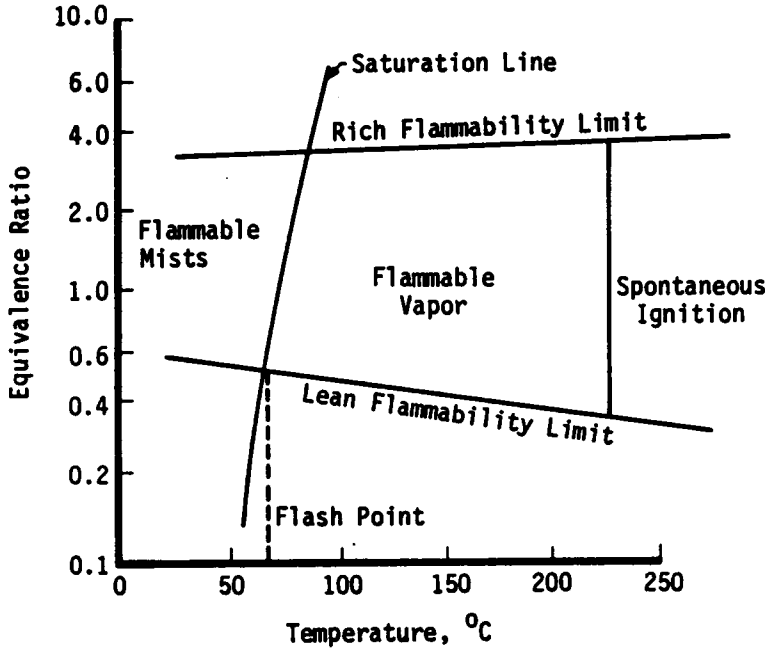

Figure 17. Flammability Characteristics for a Kerosene-Type Fuel in Air at Atmospheric Pressure [31].

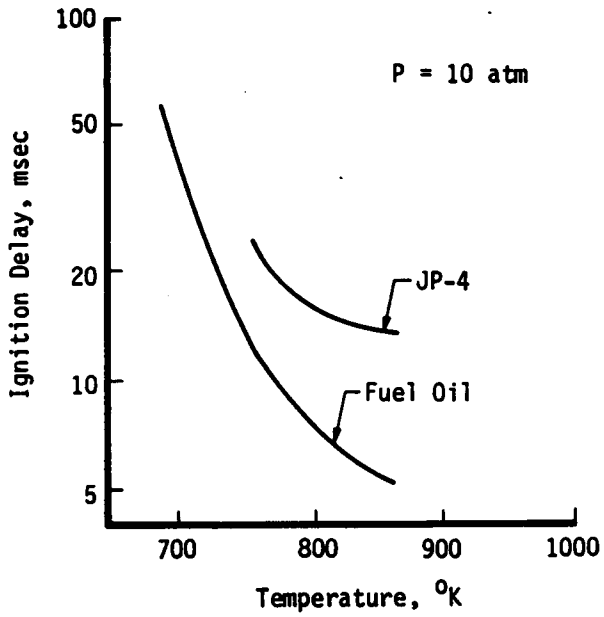

Figure 18. Ignition Delay Times for Practical Fuels [31].

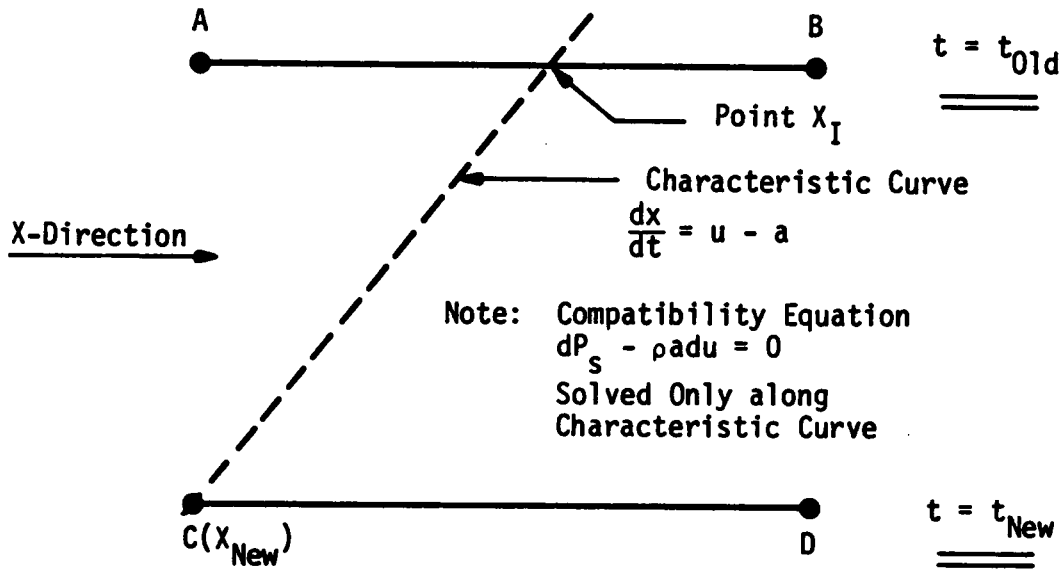

Figure 19. Schematic of Inlet Characteristic Boundary Scheme.

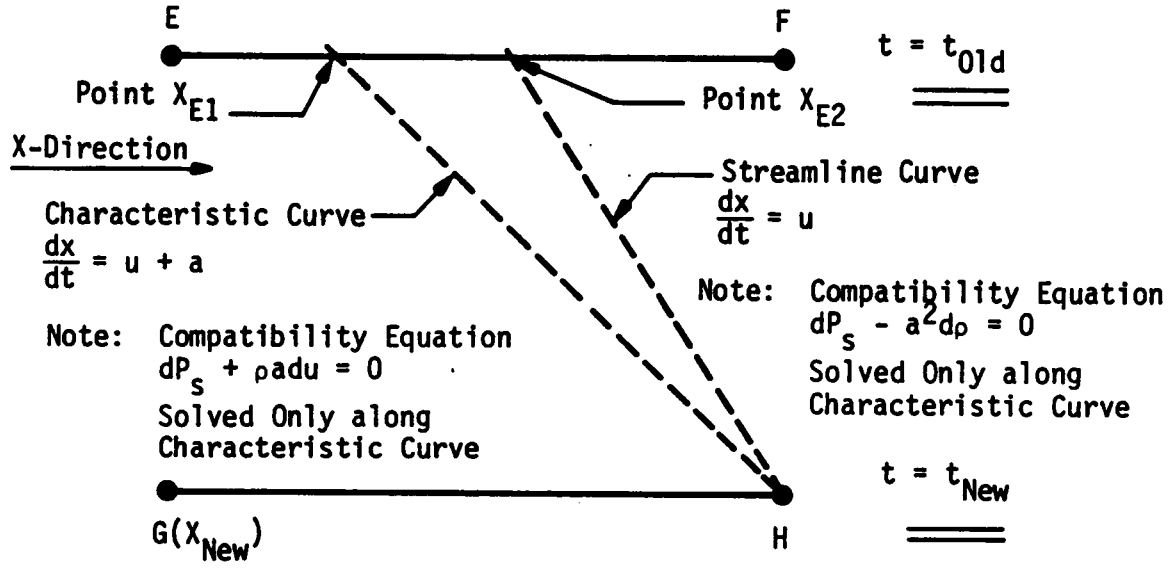

Figure 20. Schematic of Exit Characteristic Boundary Scheme.

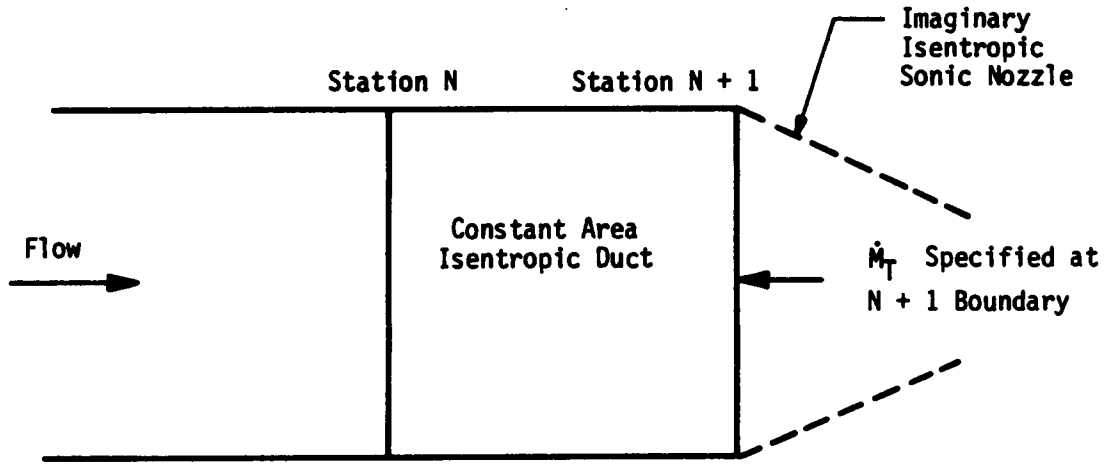

Figure 21. Sonic Nozzle Exit Boundary Condition.

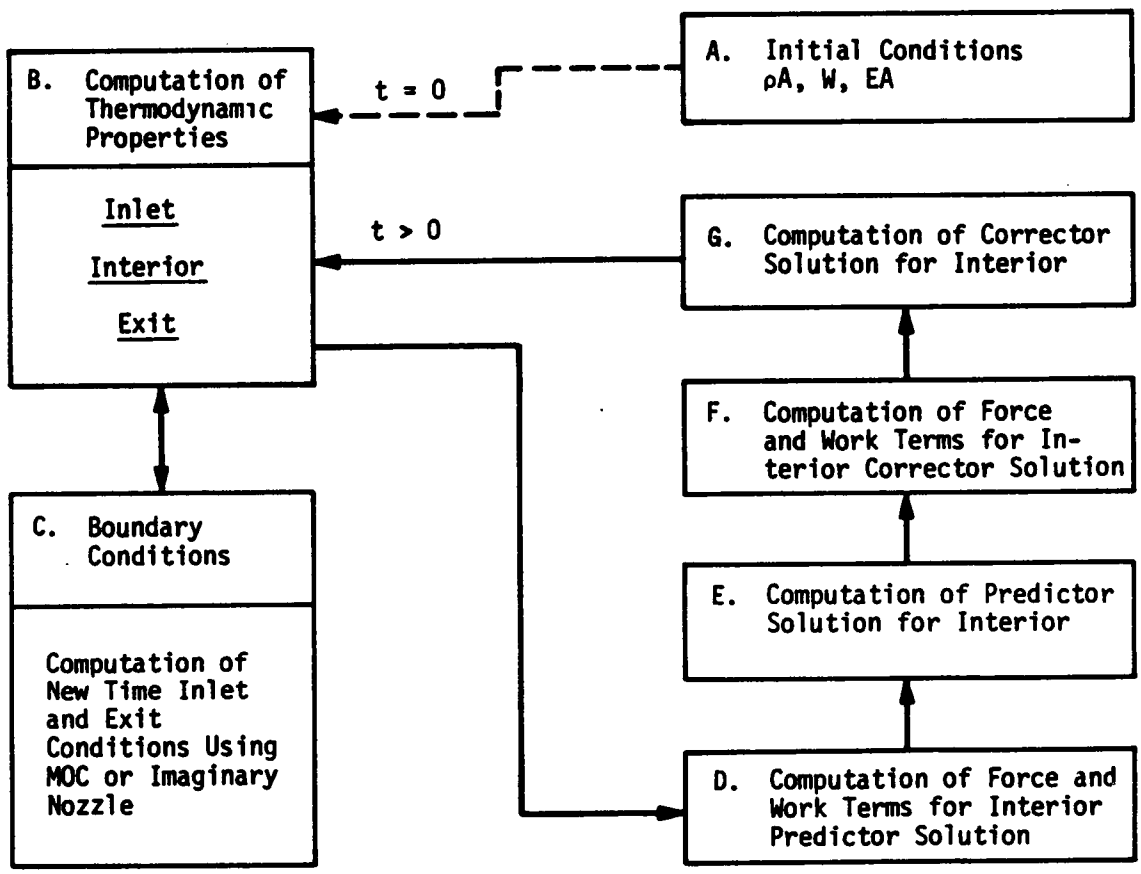

Figure 22. Time-Dependent Compressor Model Solution Procedure.

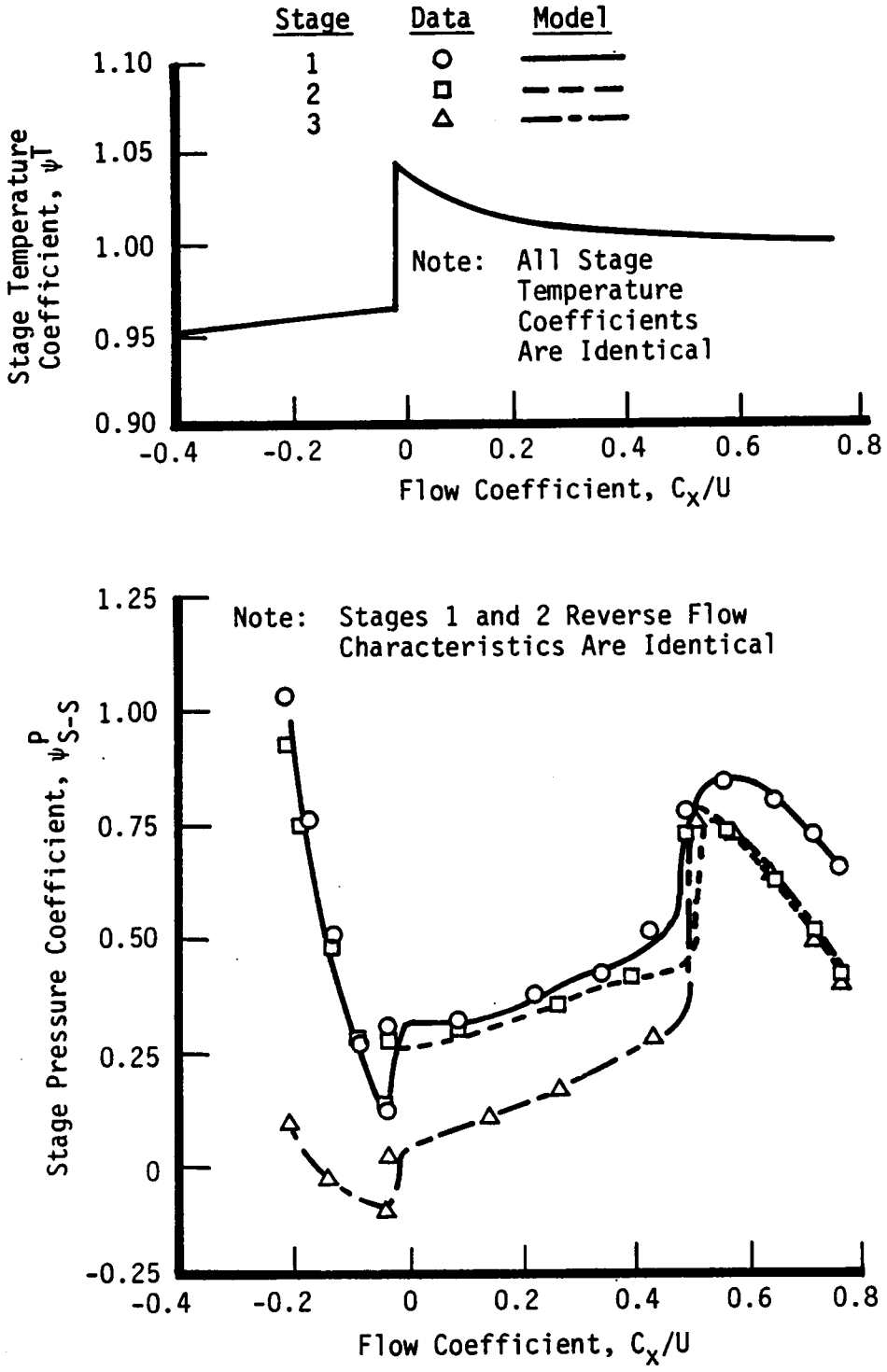

Figure 23. Synthesized Stage Characteristics for a Three-Stage, Low-Speed, Experimental Compressor Rig and Comparison to Experimental Results [5].

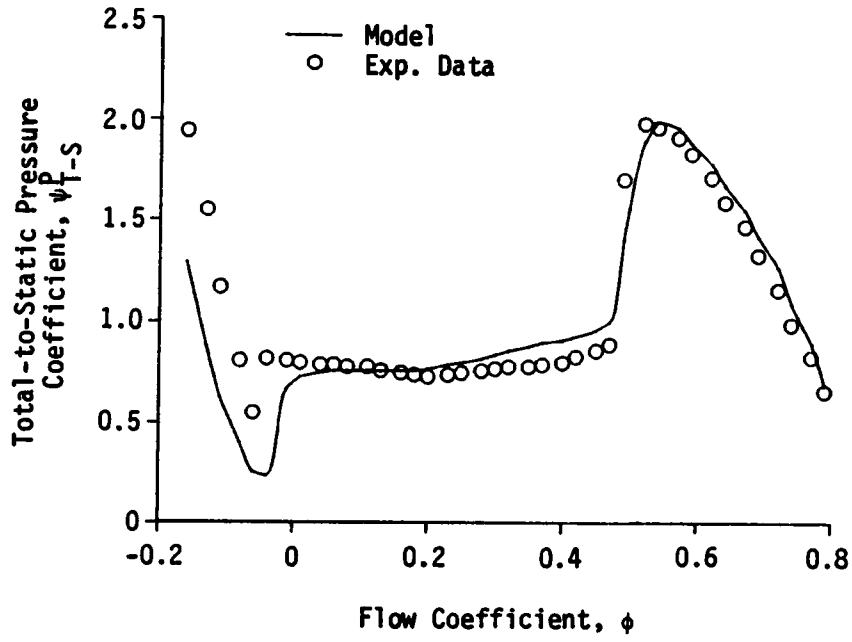

a. Total-to-Static Pressure Coefficient

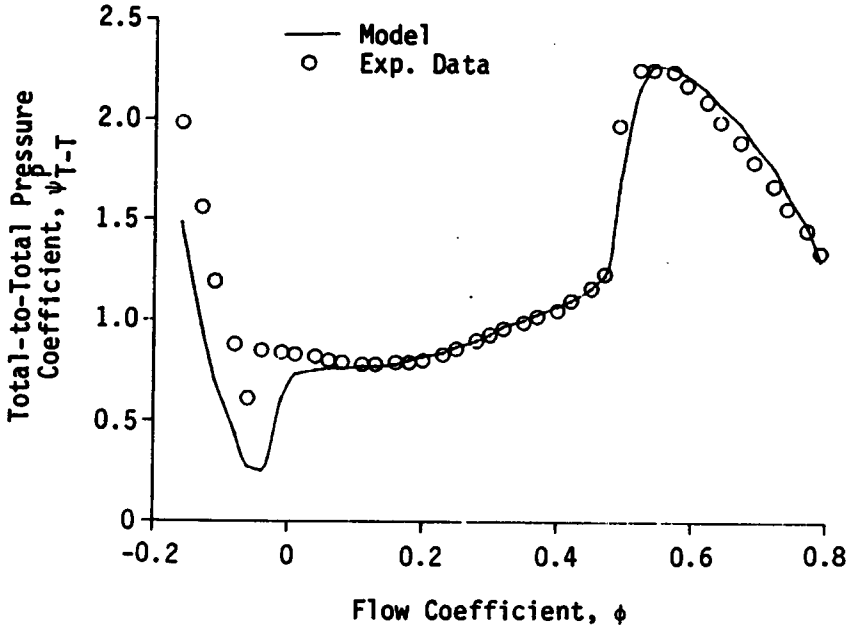

b. Total-to-Total Pressure Coefficient

Figure 24. Three-Stage Compression System Model Overall Steady Performance and Comparison to Experimental Data [5].

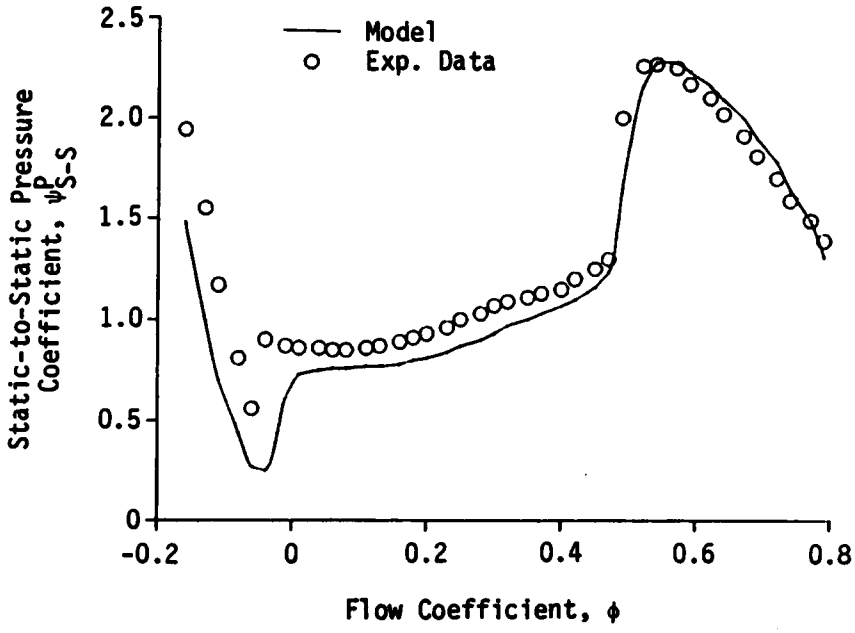

c. Static-to-Static Pressure Coefficient

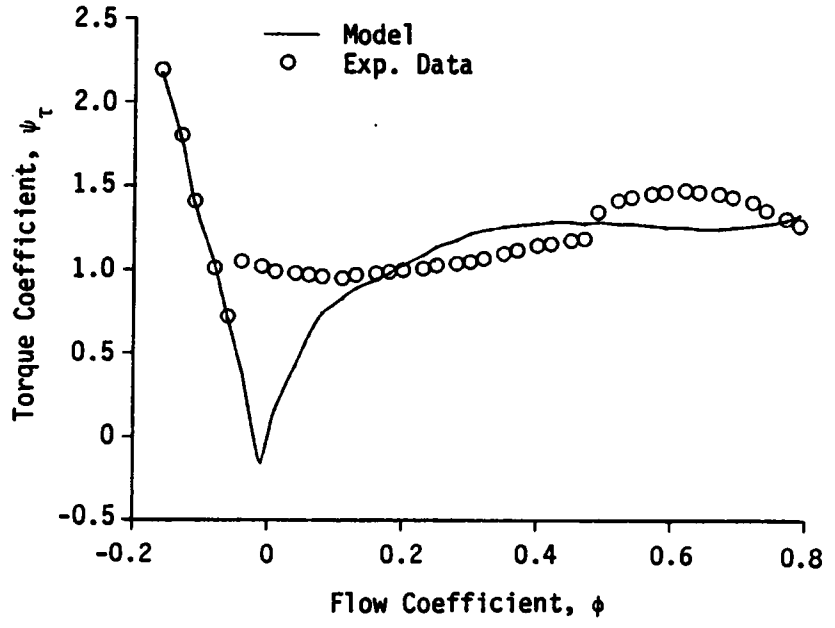

d. Torque Coefficient

Figure 24. (continued)

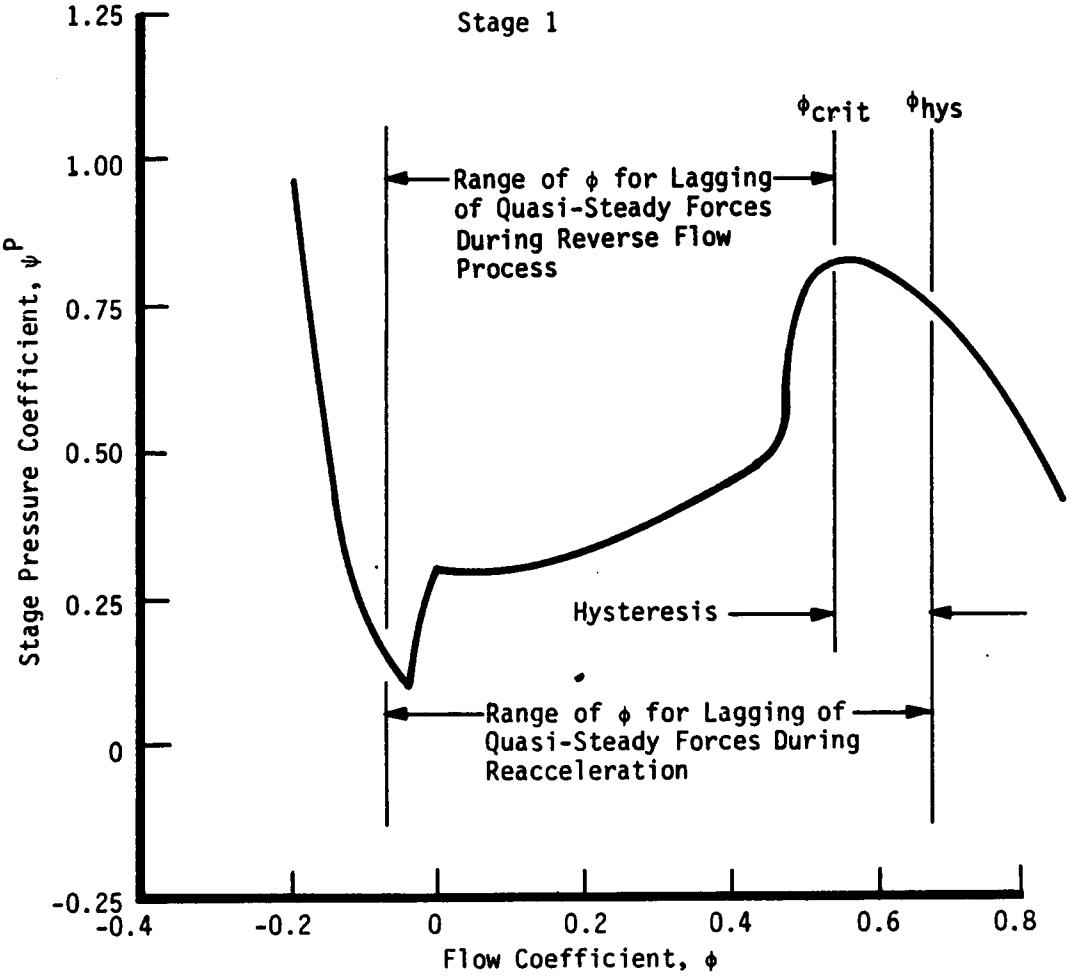

Figure 25. Flow Regions for Application of Dynamic Lagging Equation to Produce Dynamic Forces [5].

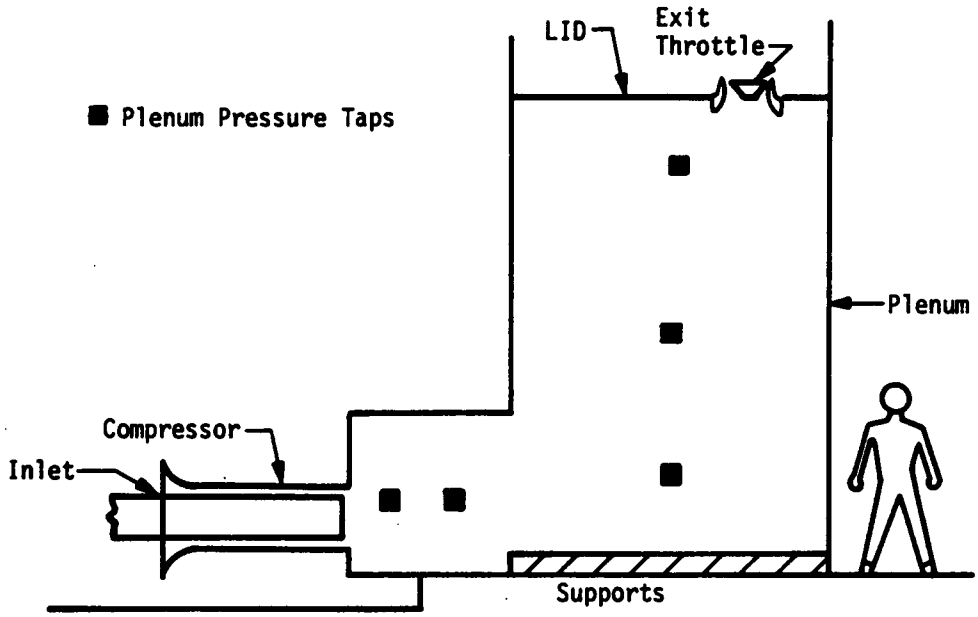

Figure 26. Schematic of Greitzer's Compressor Rig [1].

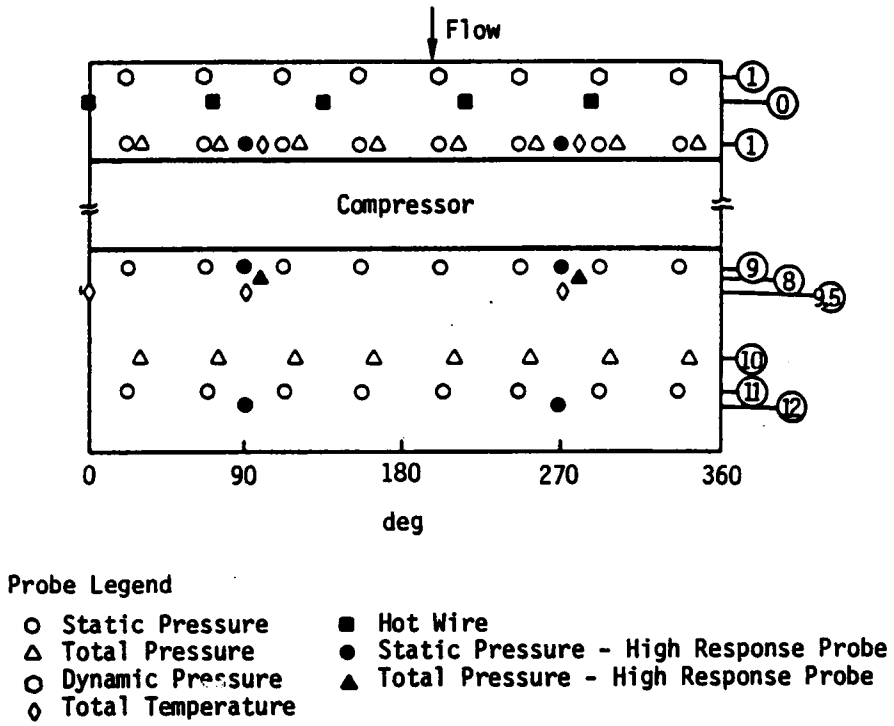

Figure 27. Instrumentation Location for Greitzer's Compressor Rig [1].

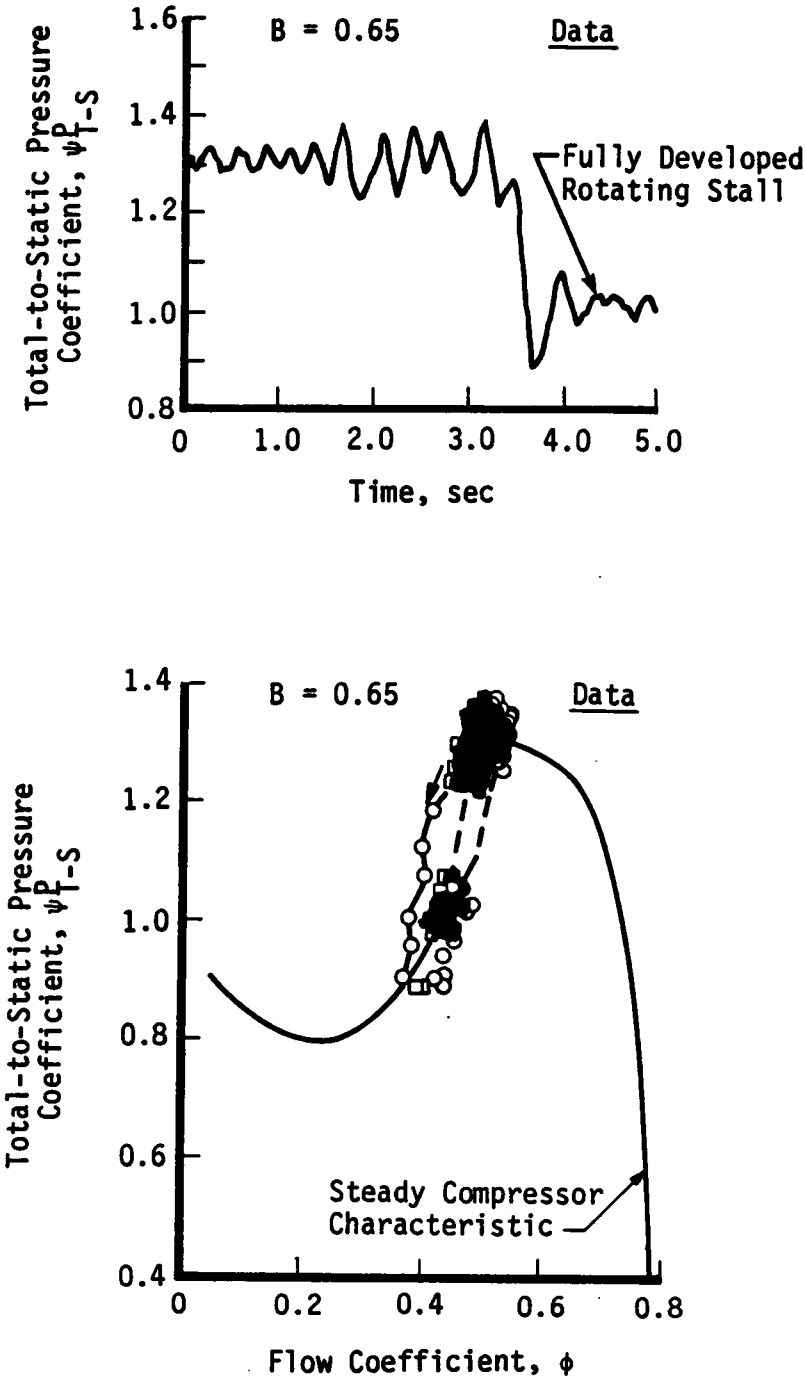

Figure 28. Post-Stall Behavior of Greitzer's Compressor Rig: B=0.65 [1].

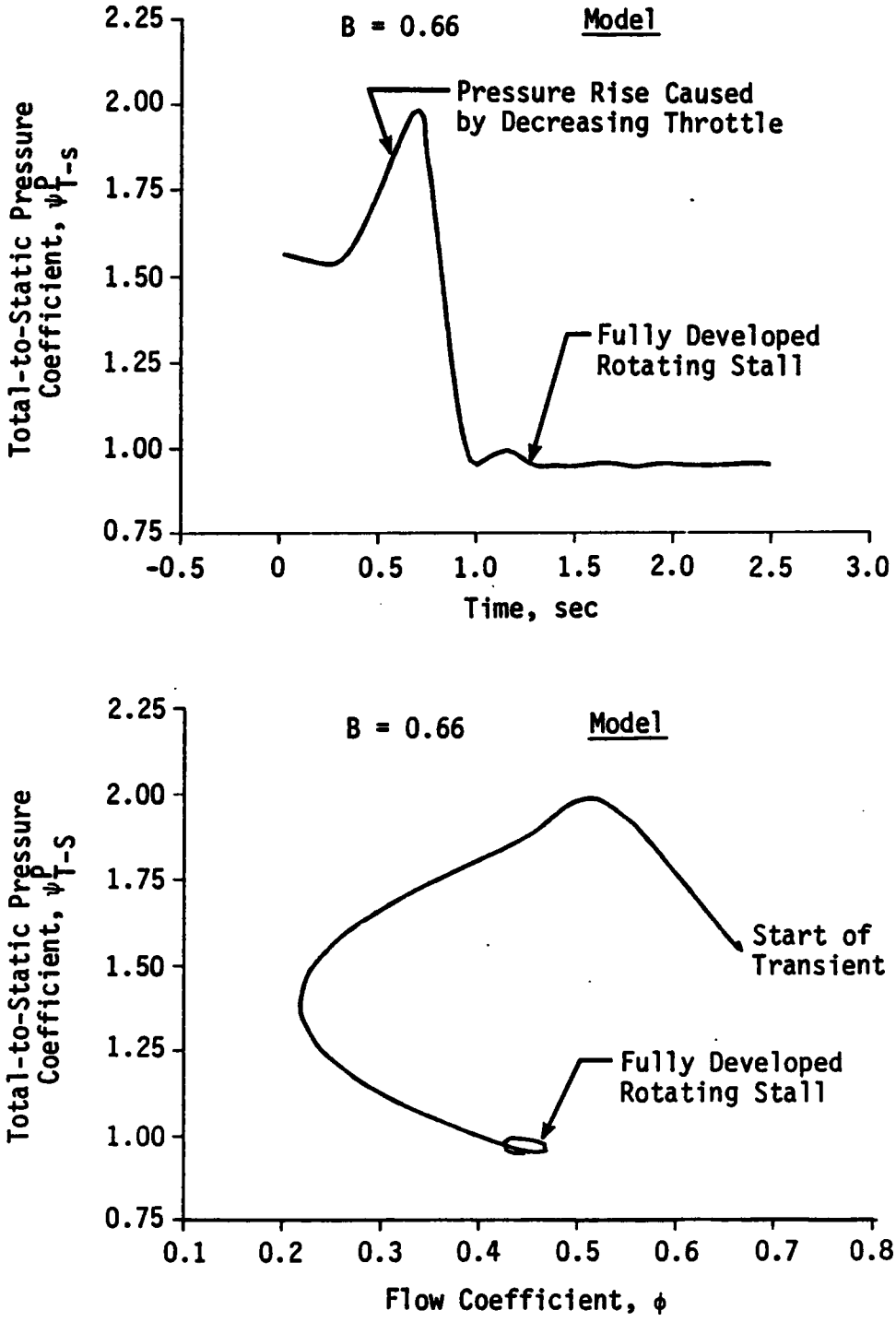

Figure 29. Three-Stage Model Overall Compression System Post-Stall Behavior: B=0.66.

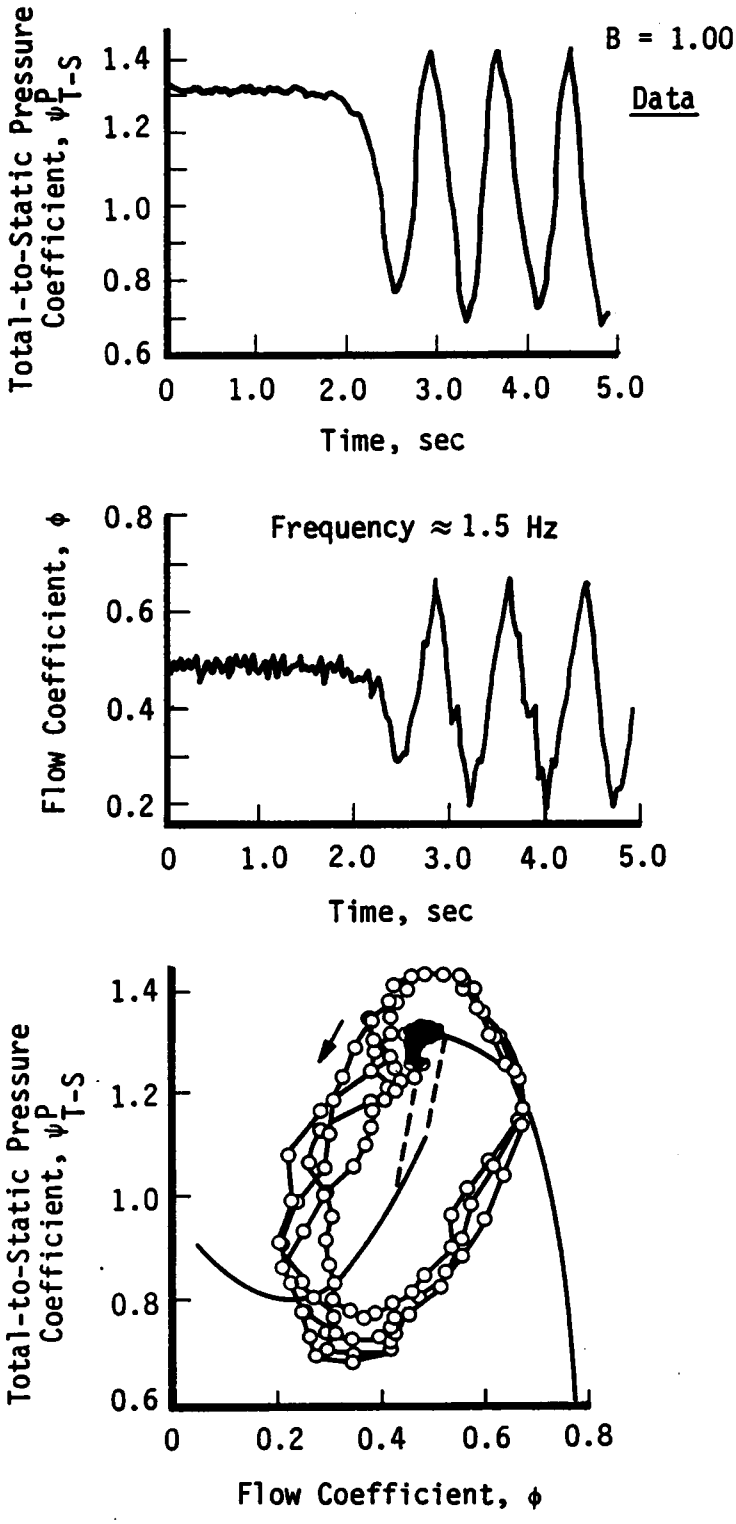

Figure 30. Post-Stall Behavior of Greitzer's Compressor Rig: B=1.00; Low-Speed, Large Volume [1].

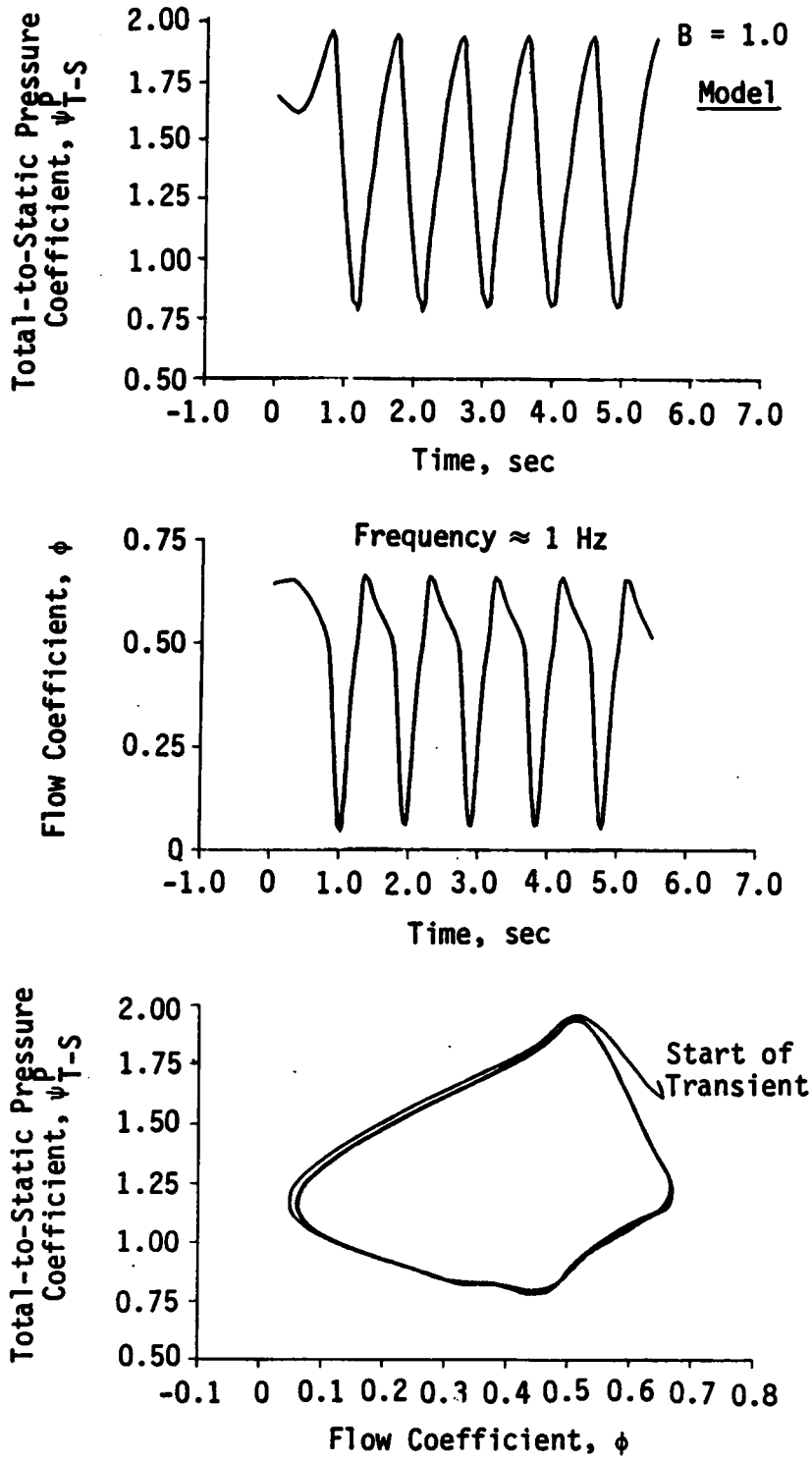

Figure 31. Model Overall Compression System Behavior: B=1.00; Low-Speed, Low Volume.

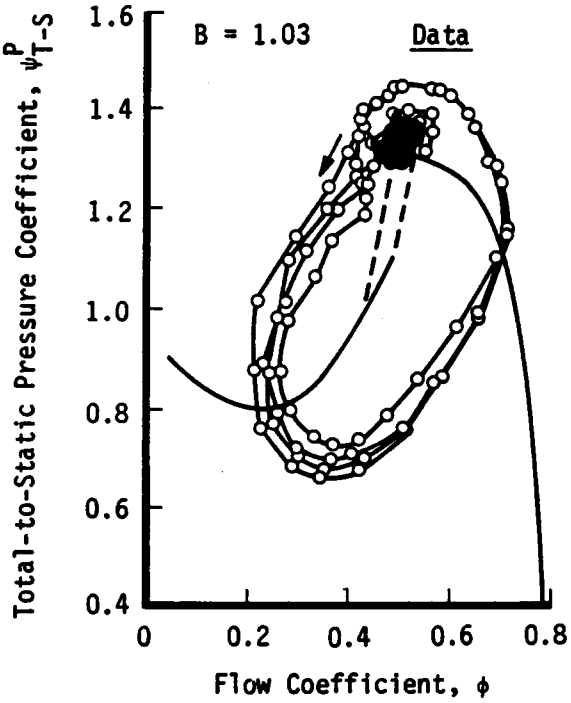

Figure 32. Post-Stall Behavior of Greitzer's Rig: B=1.03; High-Speed, Small Volume [1].

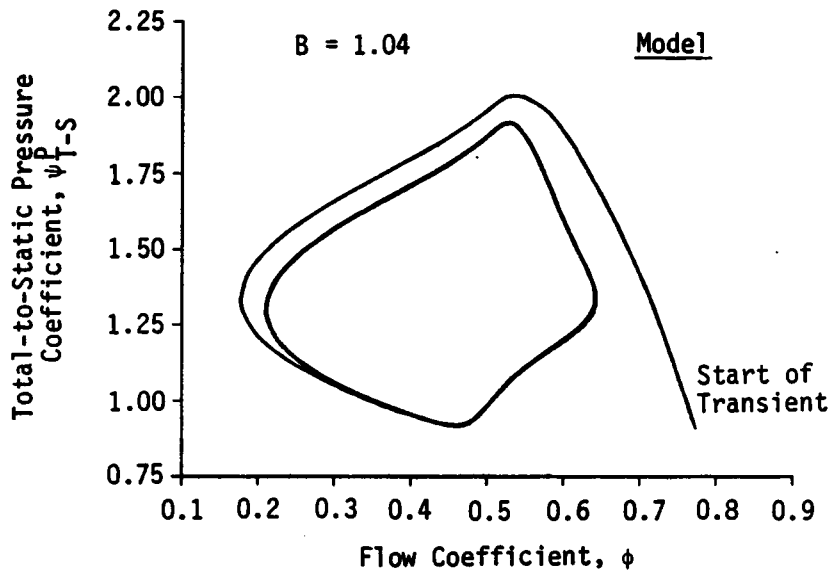

Figure 33. Model Overall Compression System Behavior: B=1.04; High-Speed, Small Volume.

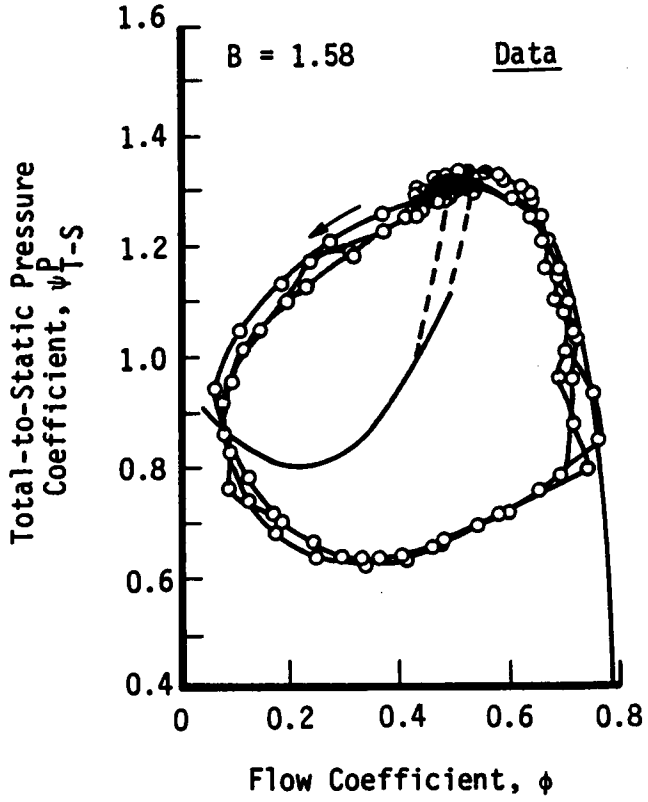

Figure 34. Post-Stall Behavior of Greitzer's Rig with Throttle at Minimum Closure to Cause Instability: B=1.58 [1].

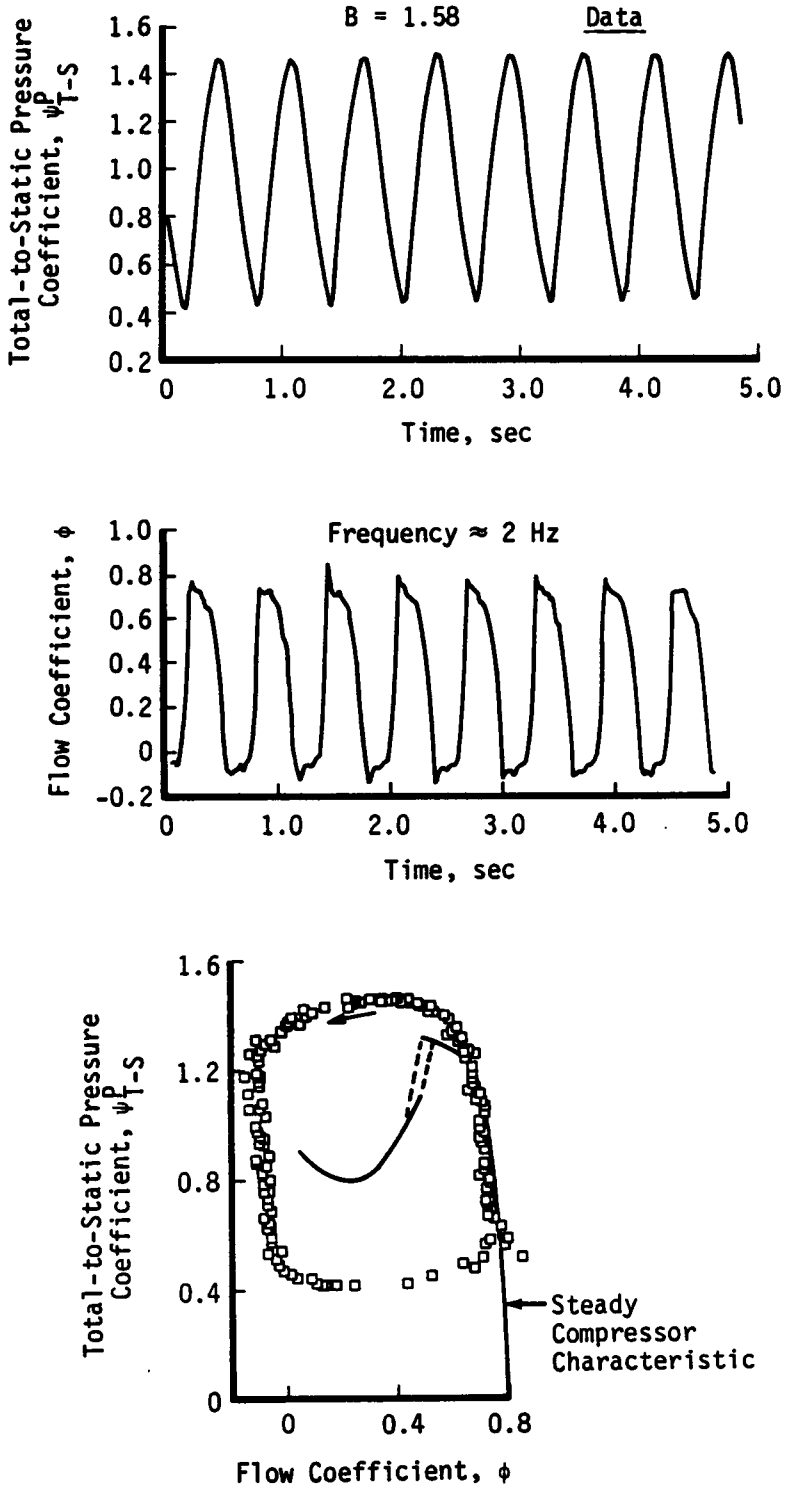

Figure 35. The Effect of Throttle Closure on Compression System Post-Stall Behavior: Greitzer's Rig: B=1.58 [1].

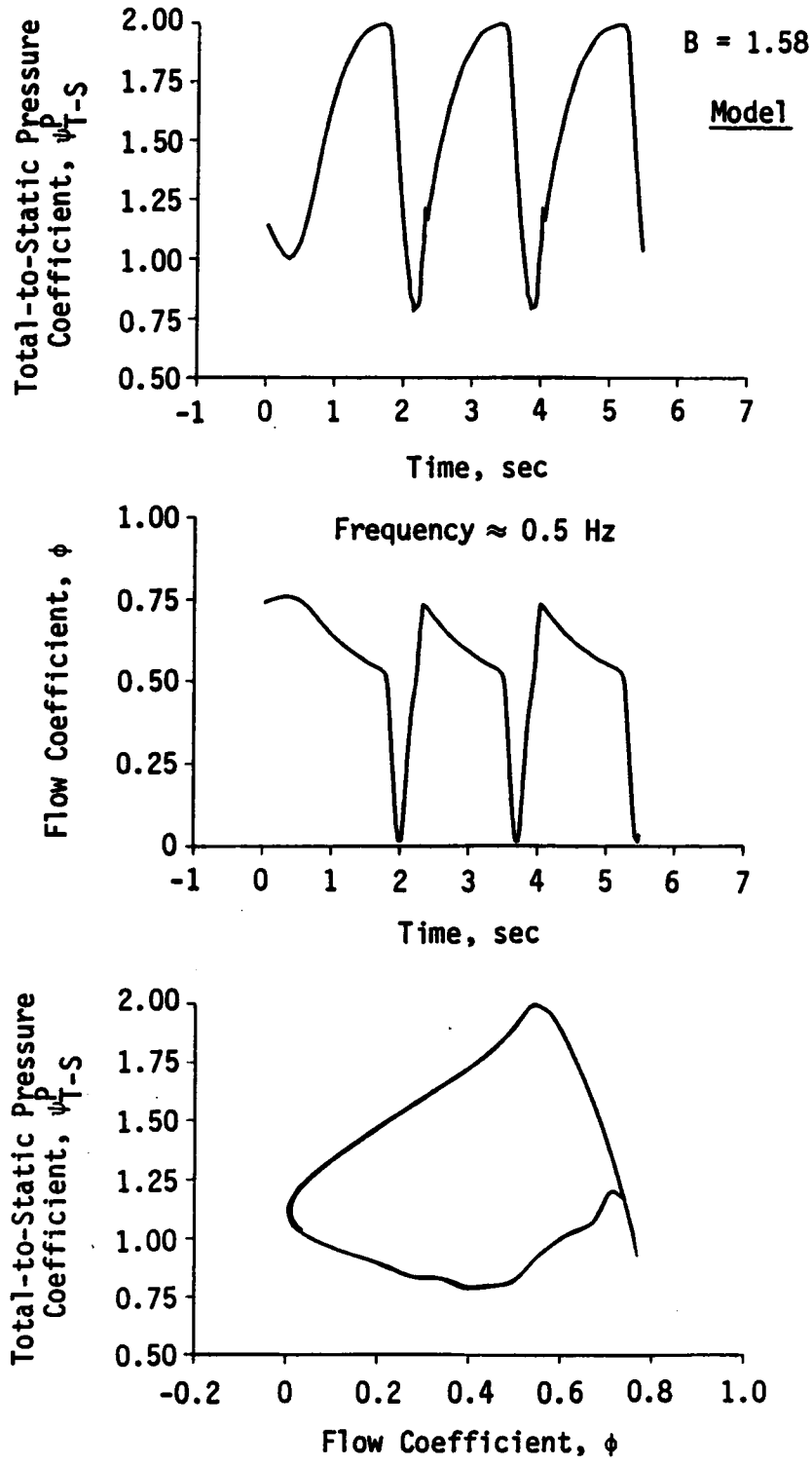

Figure 36. Model System Behavior with Throttle at Minimum Closure to Cause Instability: B=1.58.

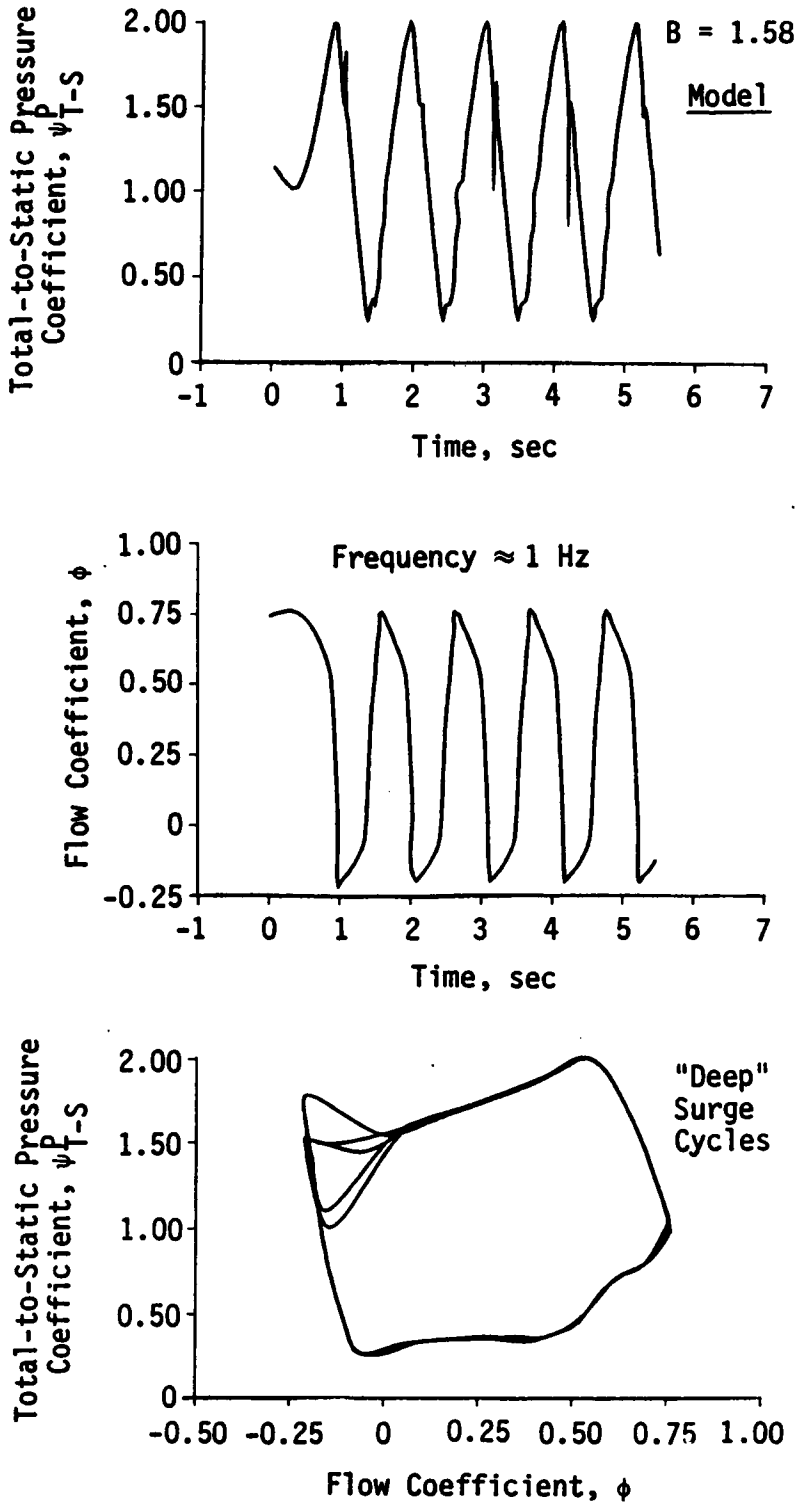

Figure 37. Model Prediction of the Effect of Throttle Closure on Compression System Post-Stall Behavior: B=1.58.

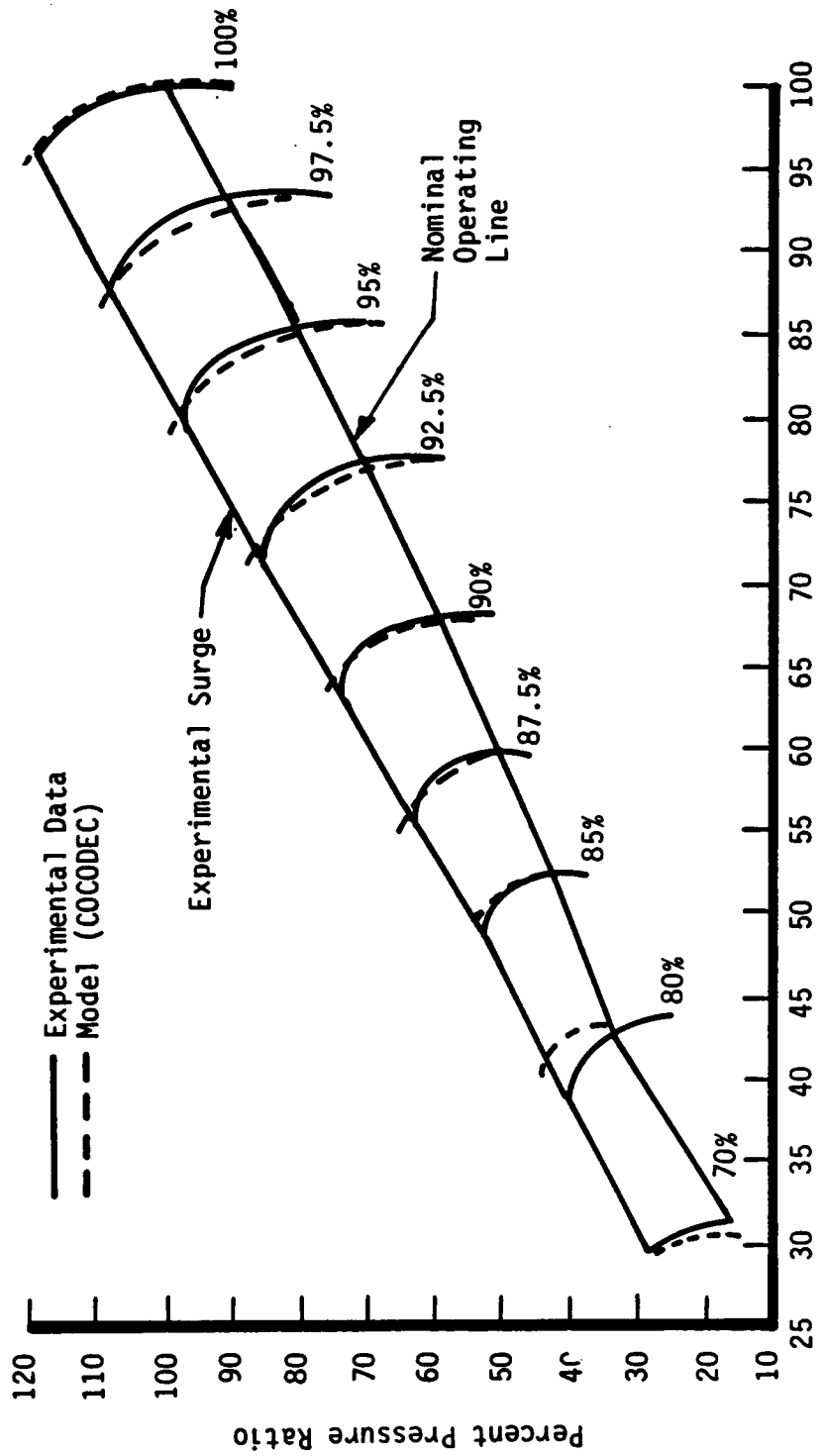

Figure 38. Model Prediction of Prestall Overall Compression System Performance and Comparison to Experimental Results for the Nine-Stage, High-Pressure Compressor (HPC).

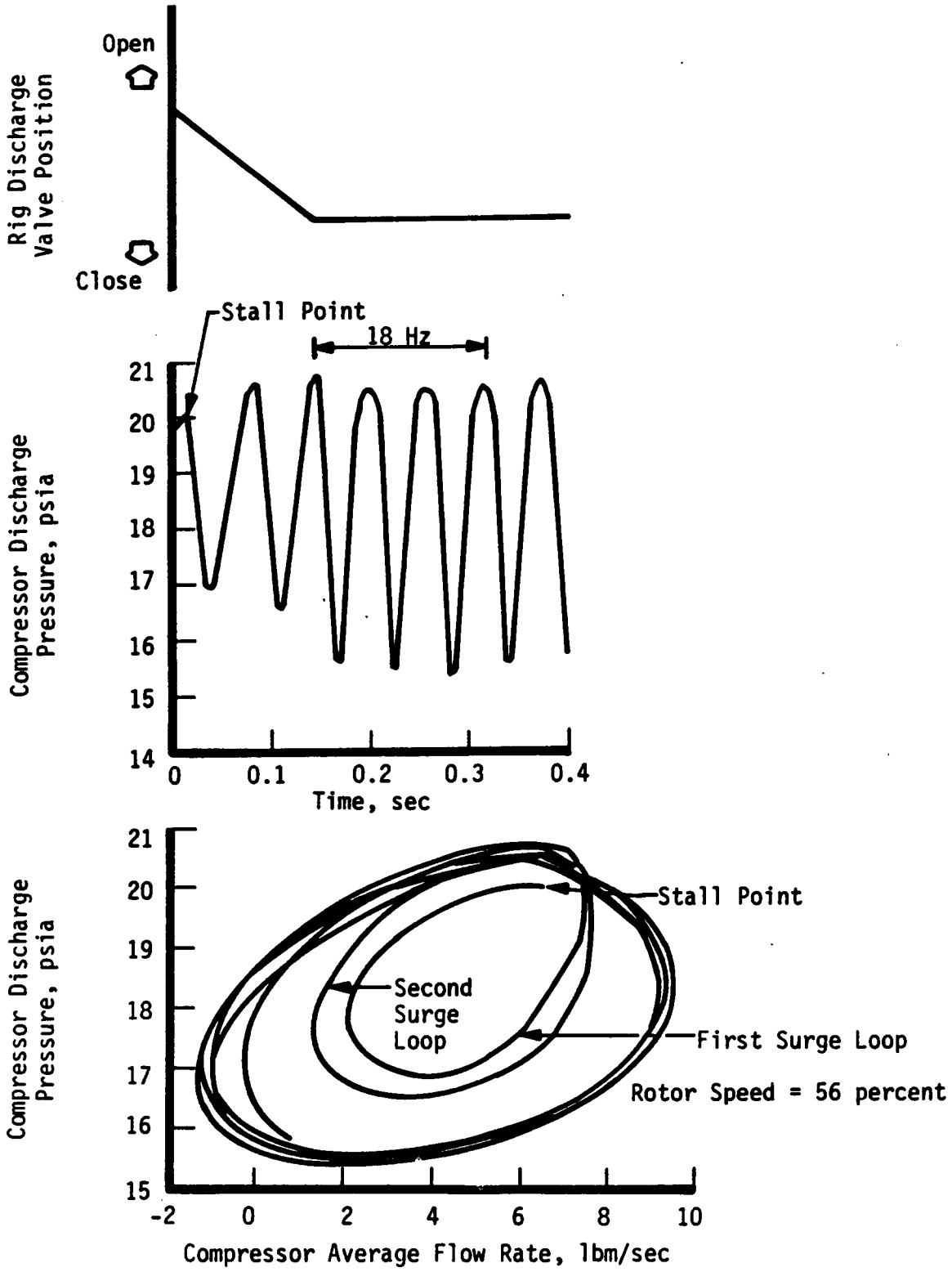

Figure 39. Recoverable Stall Data for Pratt and Whitney Research Compressor Rig [4].

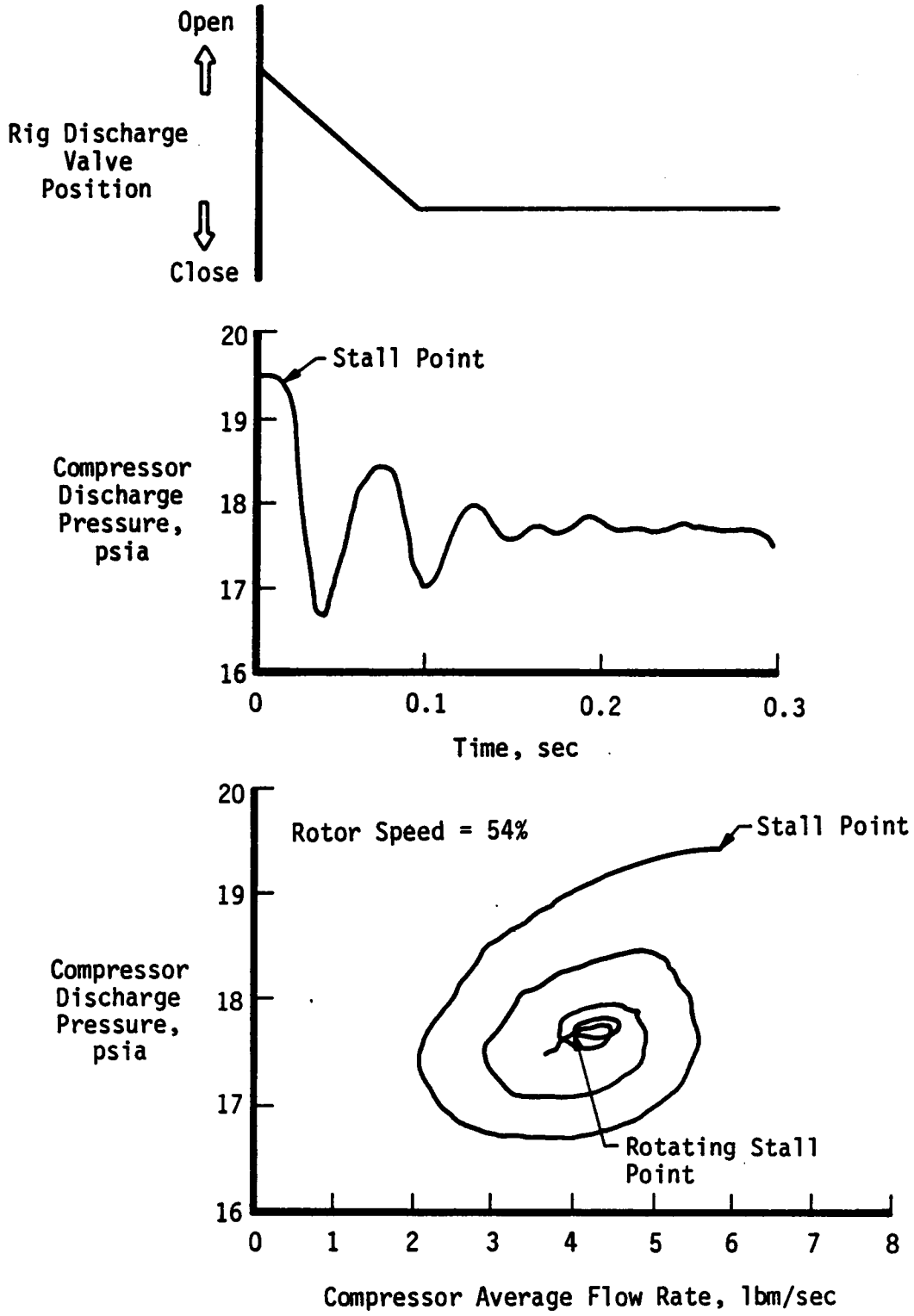

Figure 40. Nonrecoverable Stall Data for Pratt and Whitney High-Speed Research Compressor Rig [4].

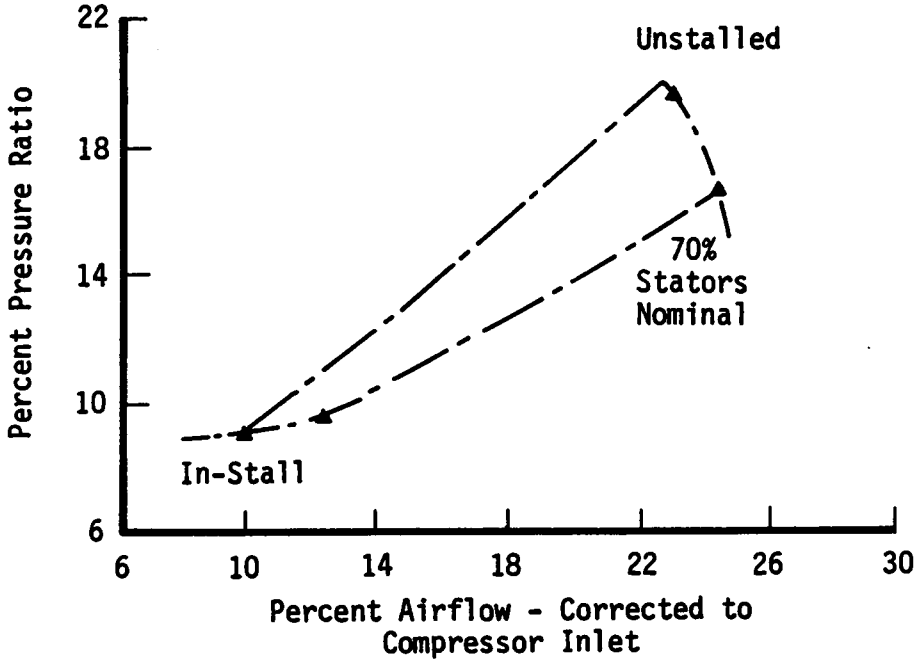

Figure 41. Energy Efficient Compressor Post-Stall Performance at 70 Percent Speed [39].

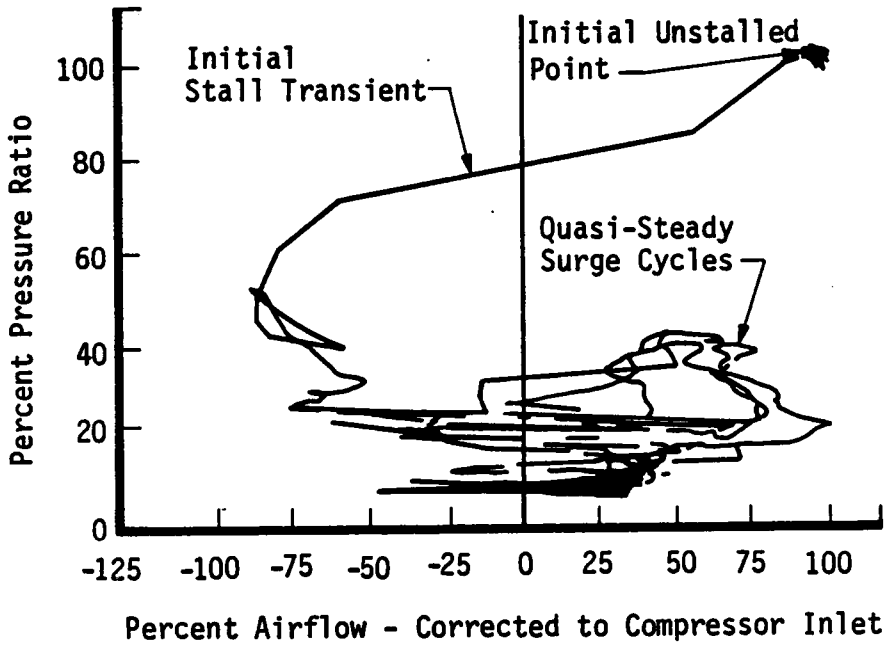

Figure 42. General Electric Energy Efficient Compressor Surge Transient at 98.5 Percent Speed [39].

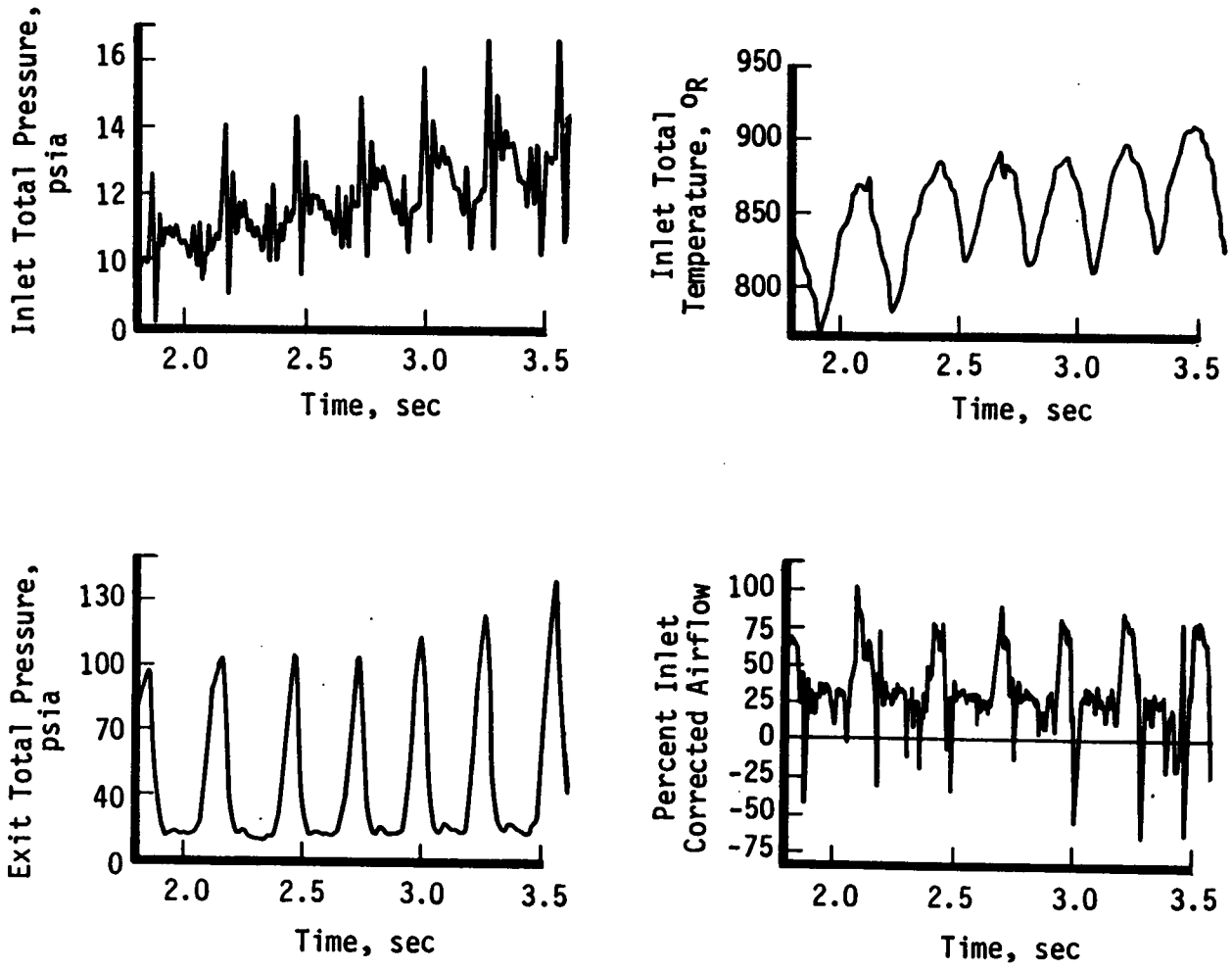

Figure 43. General Electric Energy Efficient Post-Stall Key Performance Parameters During a Surge Event Initially at 98.5 Percent Speed [39].

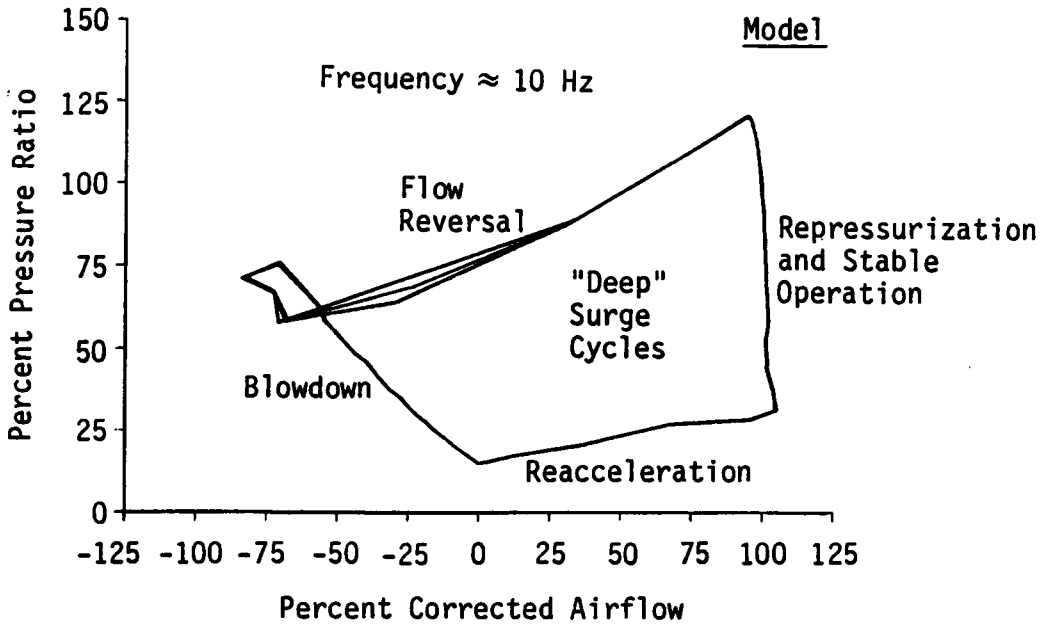

Figure 44. Model Surge Trajectories of a Nine-Stage, High-Pressure Compressor (HPC) with Representative Combustor Volume No Combustion, at 100 Percent Speed.

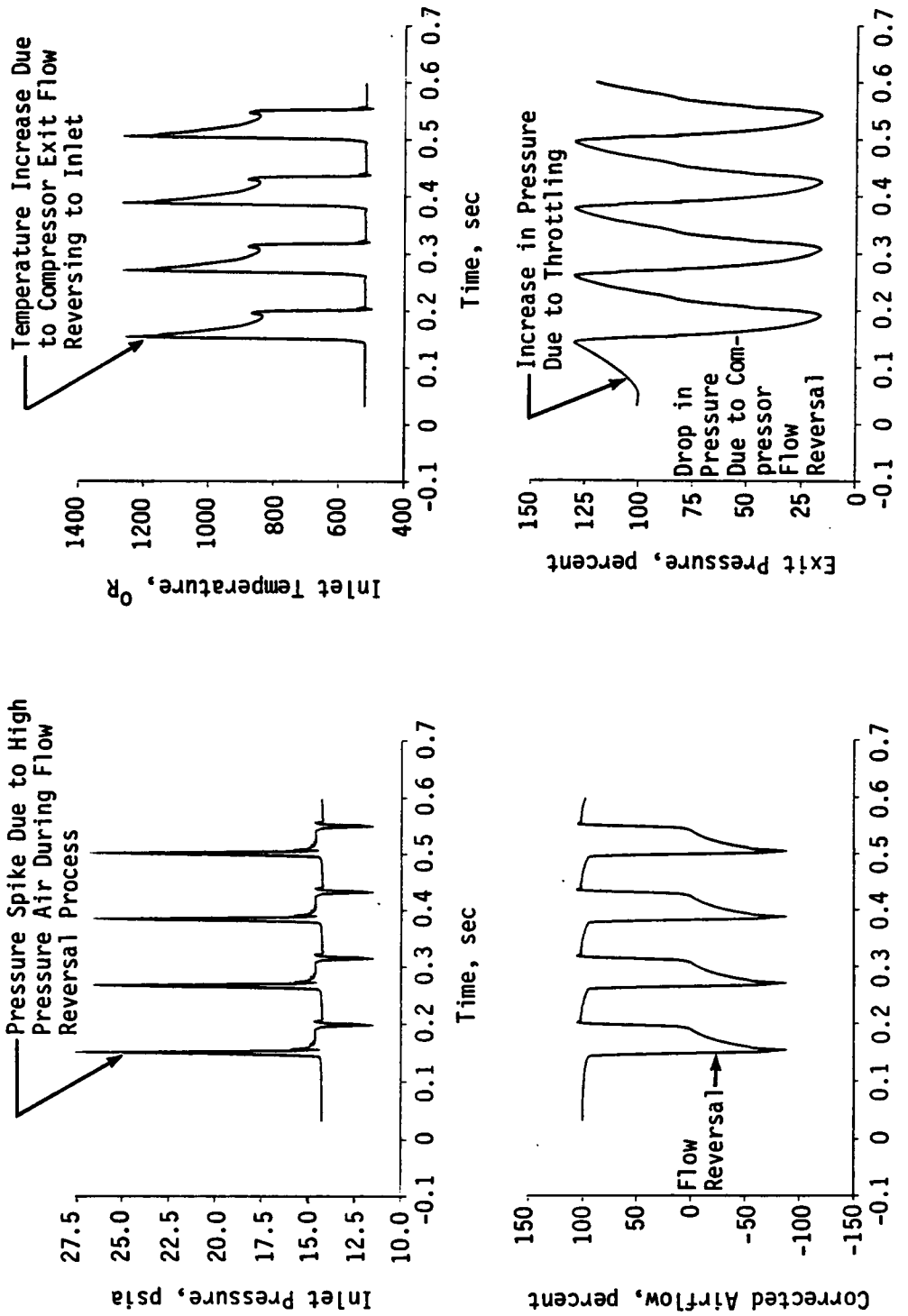

Figure 45. Model Compression System Performance During Surge of a Nine-Stage HPC with Representative Combustor Volume, No Combustor, at 100 Percent Speed.

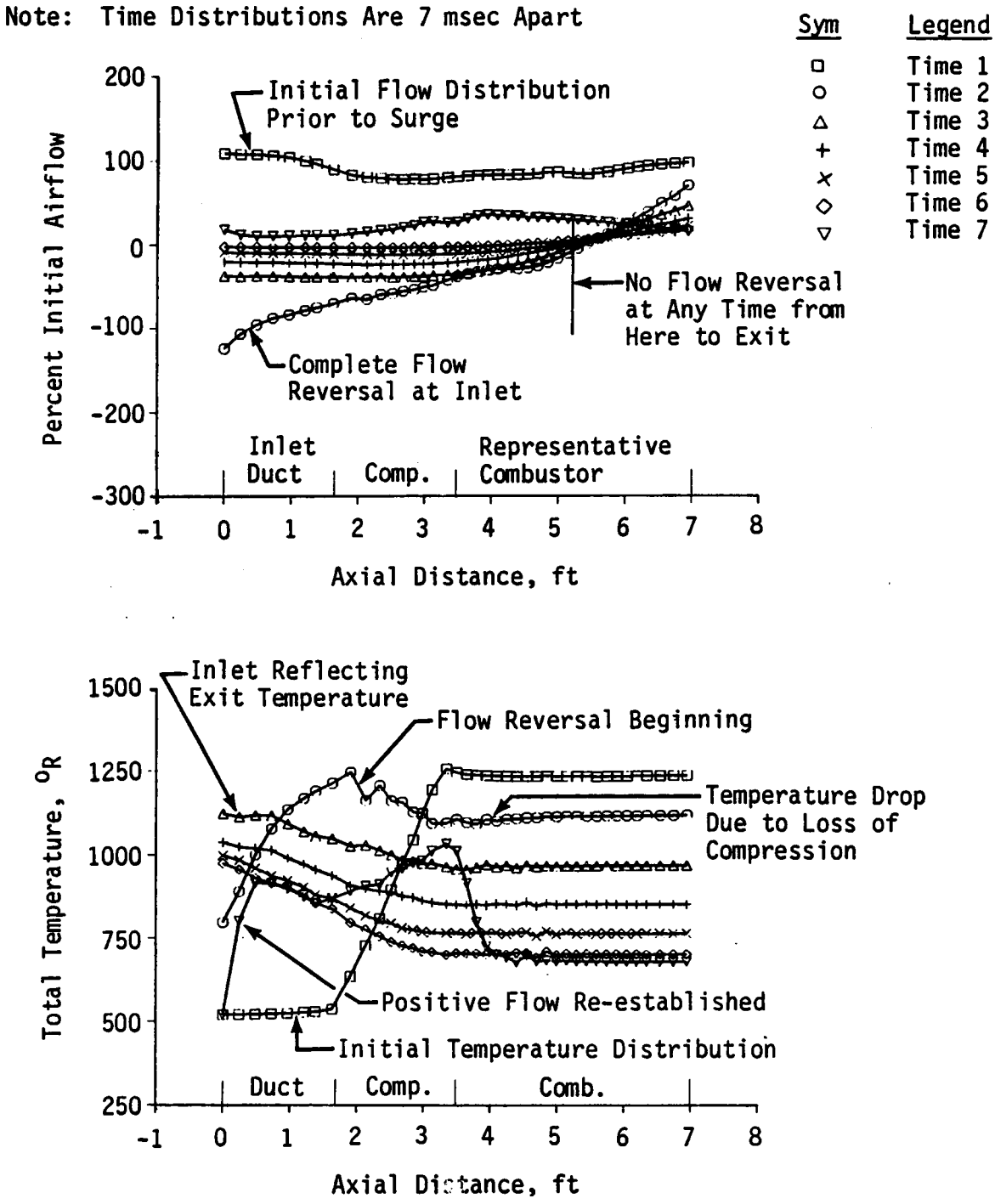

Figure 46. Model Prediction of Airflow and Temperature Distribution During a Single Surge Cycle of the Nine-Stage HPC at 100 Percent Speed, No Combustion.

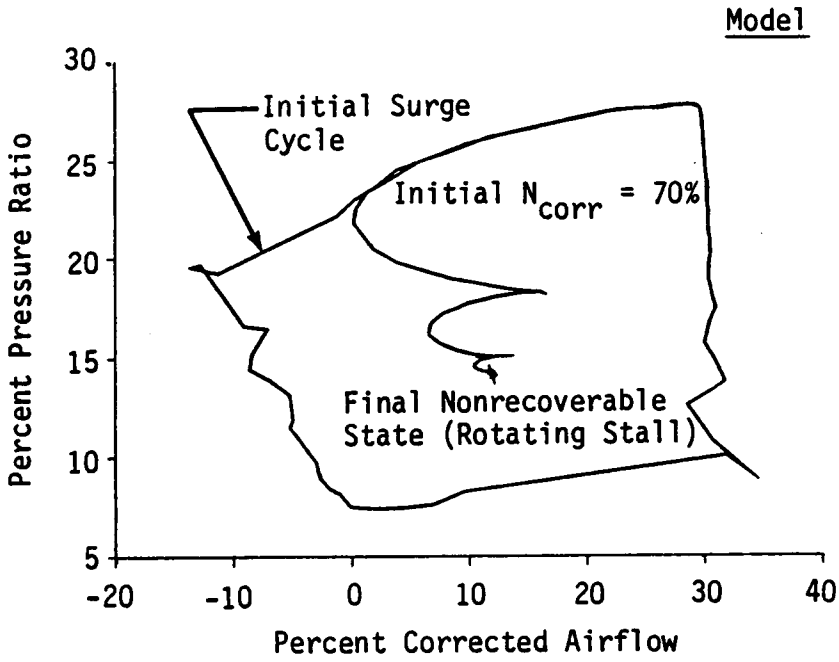

Figure 47. Model Prediction of Nonrecoverable Stall for the Nine-Stage HPC with Representative Combustor, No Combustion, 70 Percent Speed.

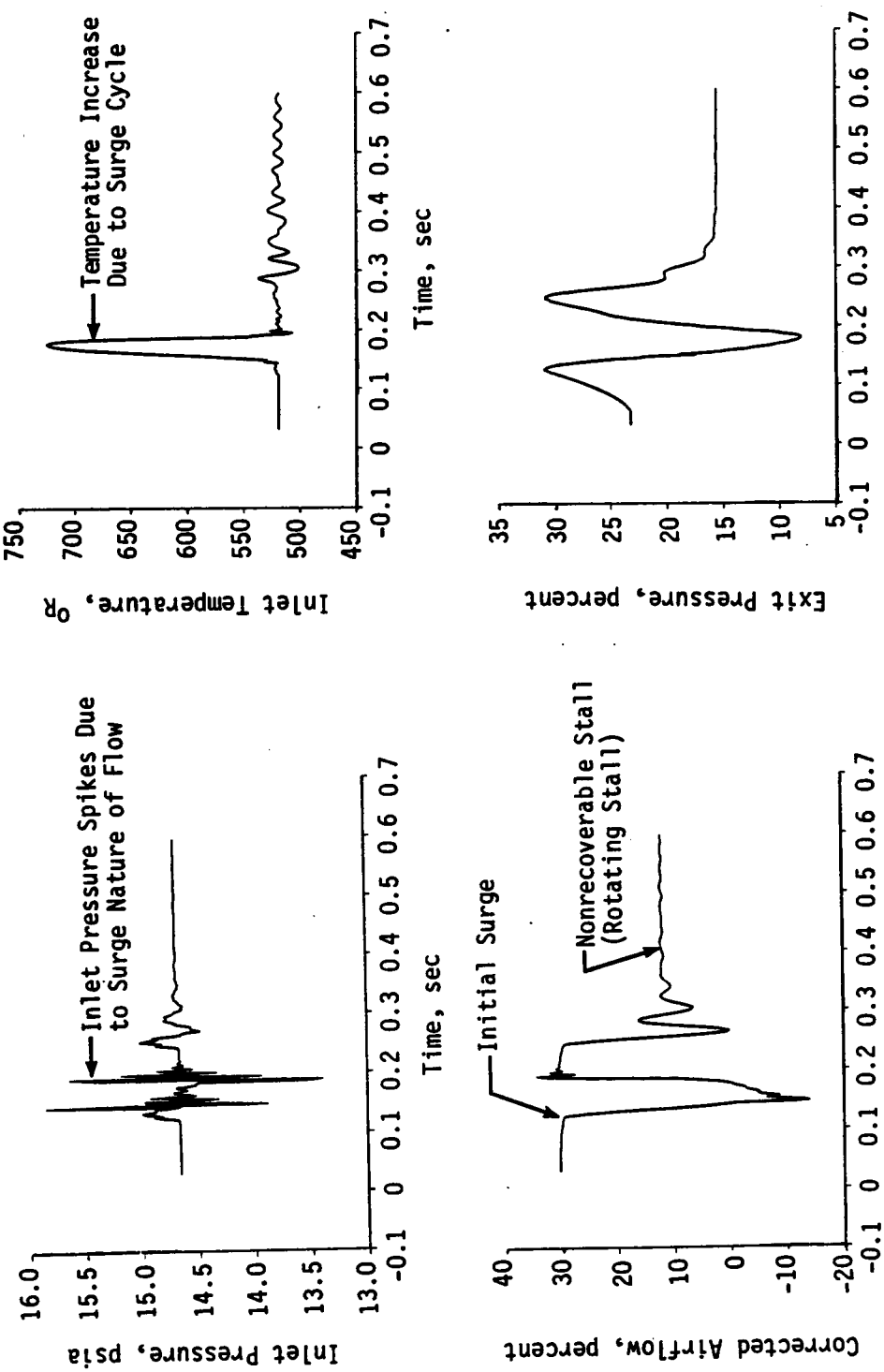

Figure 48. Model Compression System Performance During Nonrecoverable Stall of a Nine-Stage HPC with Representative Combustor, at 70 Percent Speed.

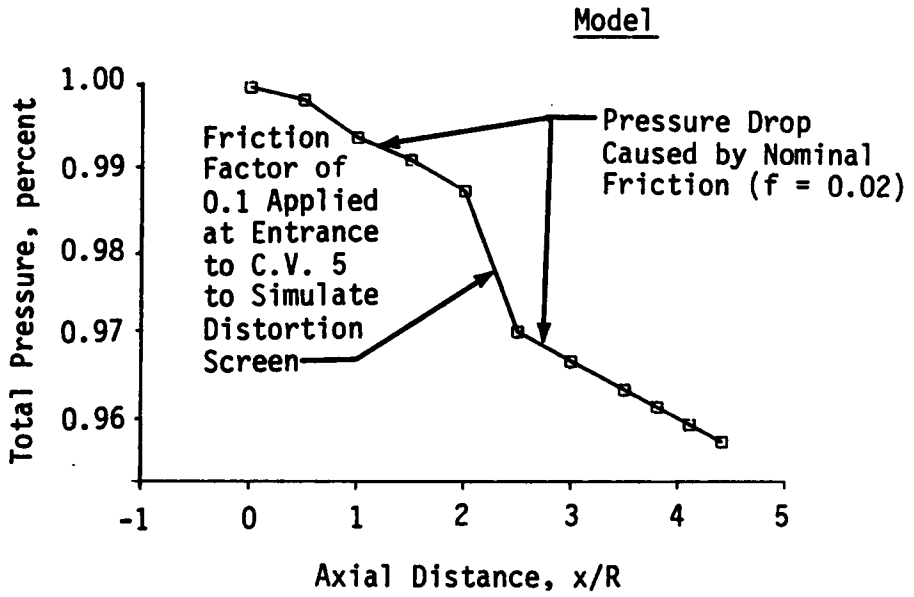

Figure 49. Pressure Distribution in Inlet Ducting with Distortion Screen Simulation.

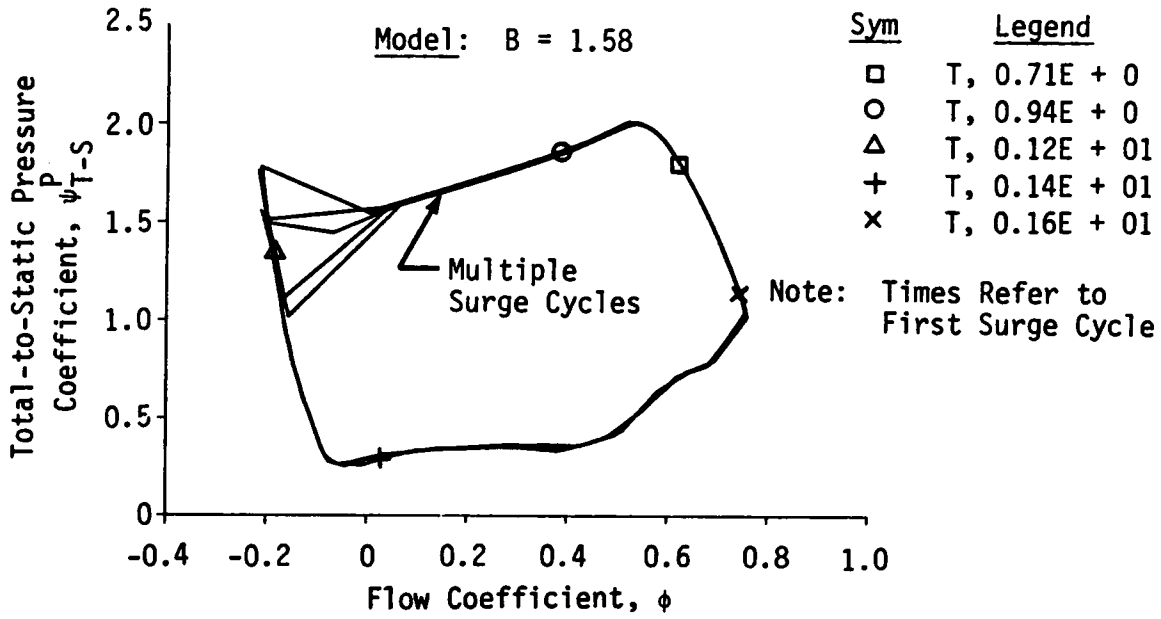

Figure 50. Three-Stage Model Post-Stall Results Without an Inlet Distortion Screen: B=1.58.

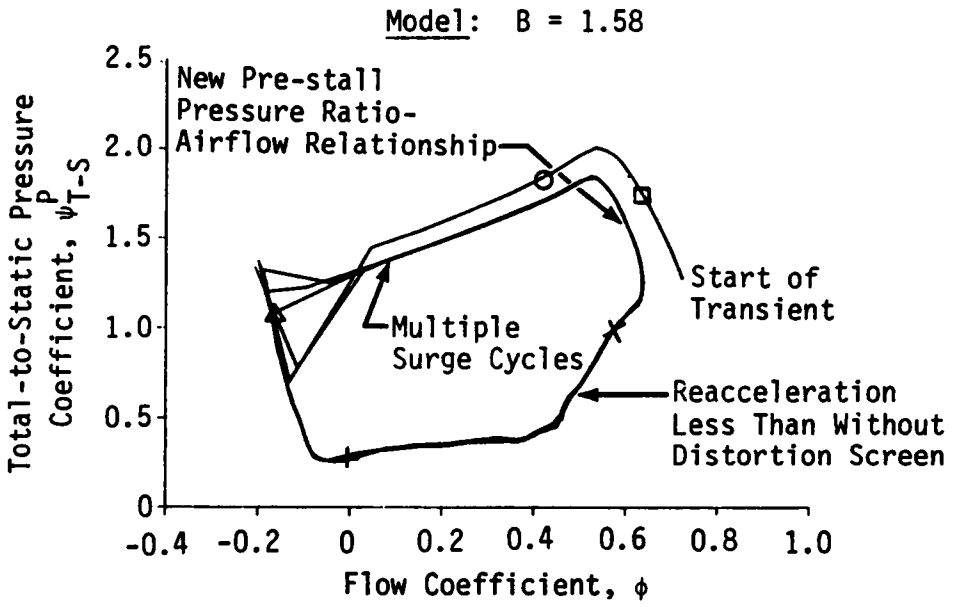

Figure 51. Three-Stage Model Post-Stall Results With Inlet Distortion Screen Present (f=0.1): B=1.58.

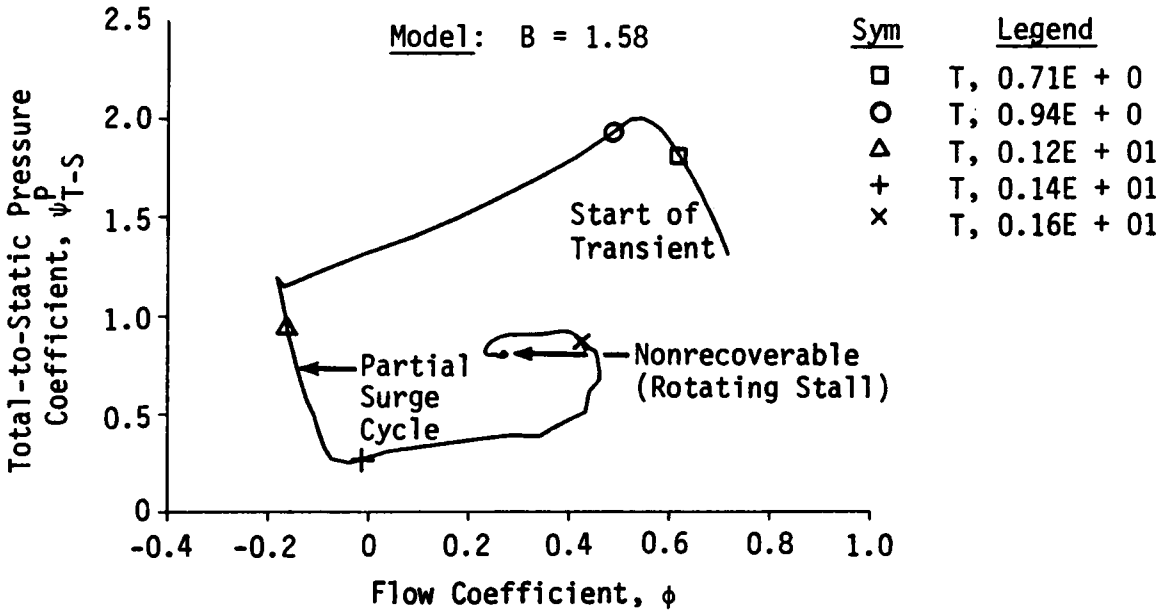

Figure 52. Three-Stage Model Post-Stall Results With Inlet Distortion Screen Simulation (f=0.15): B=1.58.

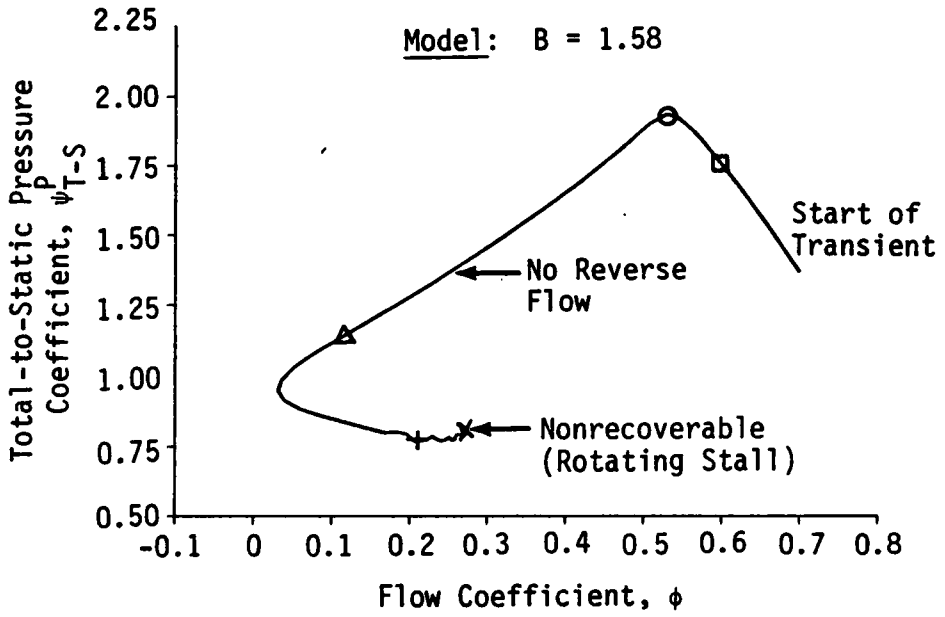

Figure 53. Three-Stage Model Post-Stall Results With Inlet Distortion Screen Simulation (f=0.3): B-1.58.

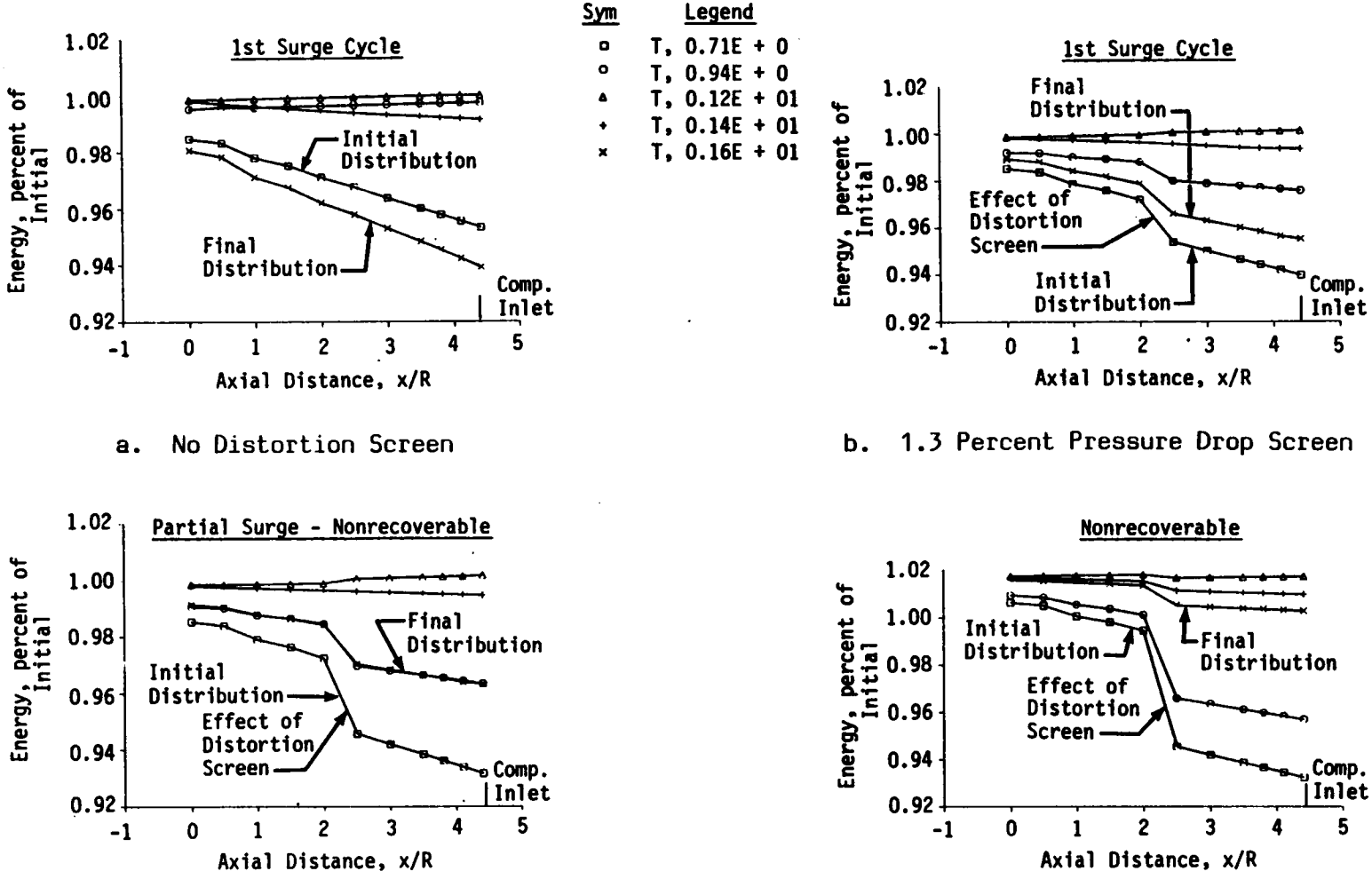

a. No Distortion Screen

b. 1.3 Percent Pressure Drop Screen

c. 2.8 Percent Pressure Drop Screen

d. 4.7 Percent Pressure Drop Screen

Figure 54. Inlet Energy Distribution for the Three-Stage Compressor Model With and Without the Distortion Screen Simulation.

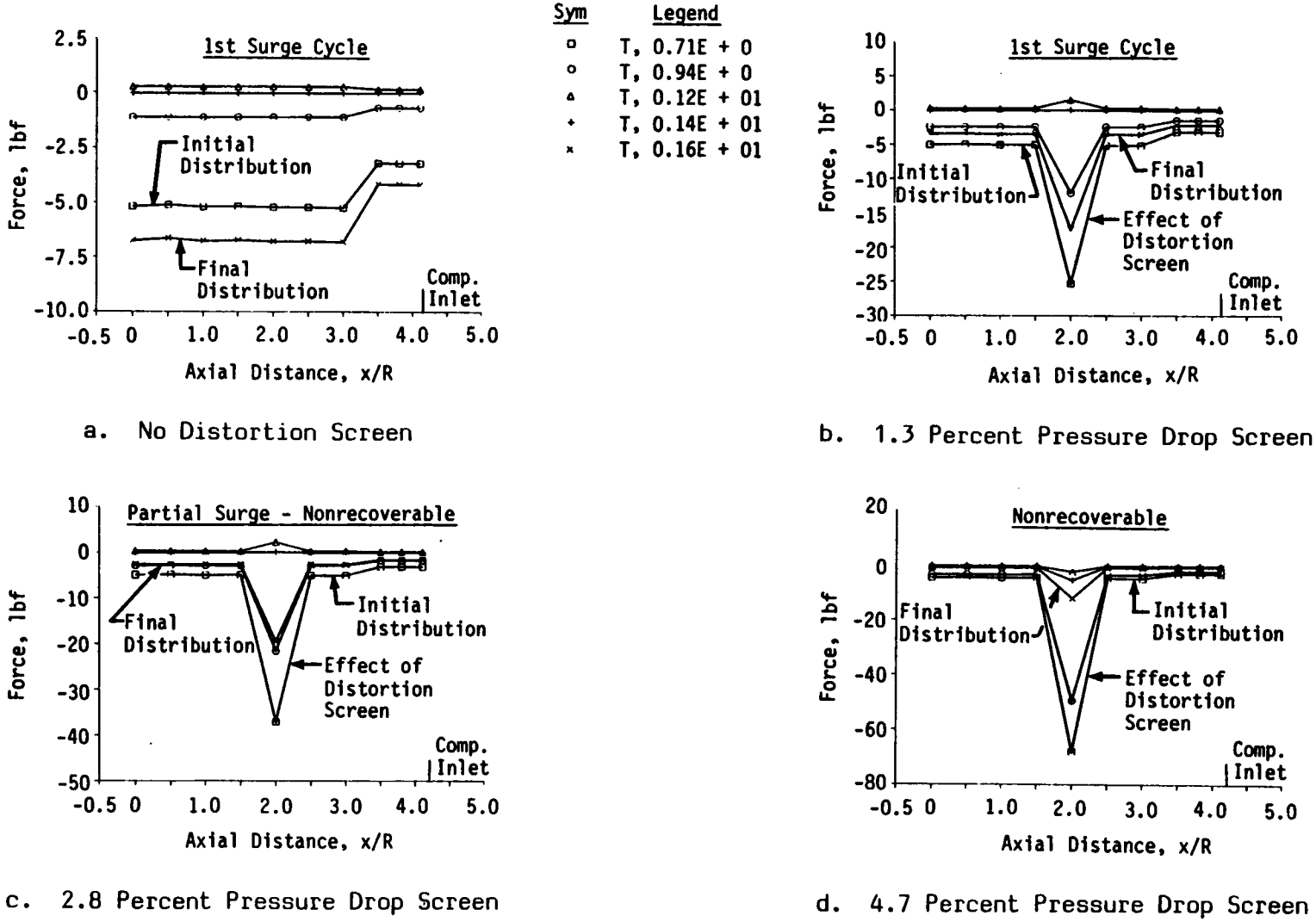

a. No Distortion Screen

b. 1.3 Percent Pressure Drop Screen

c. 2.8 Percent Pressure Drop Screen

d. 4.7 Percent Pressure Drop Screen

Figure 55. Inlet Force Distribution for the Three-Stage Compressor Model With and Without the Distortion Screen Simulation.

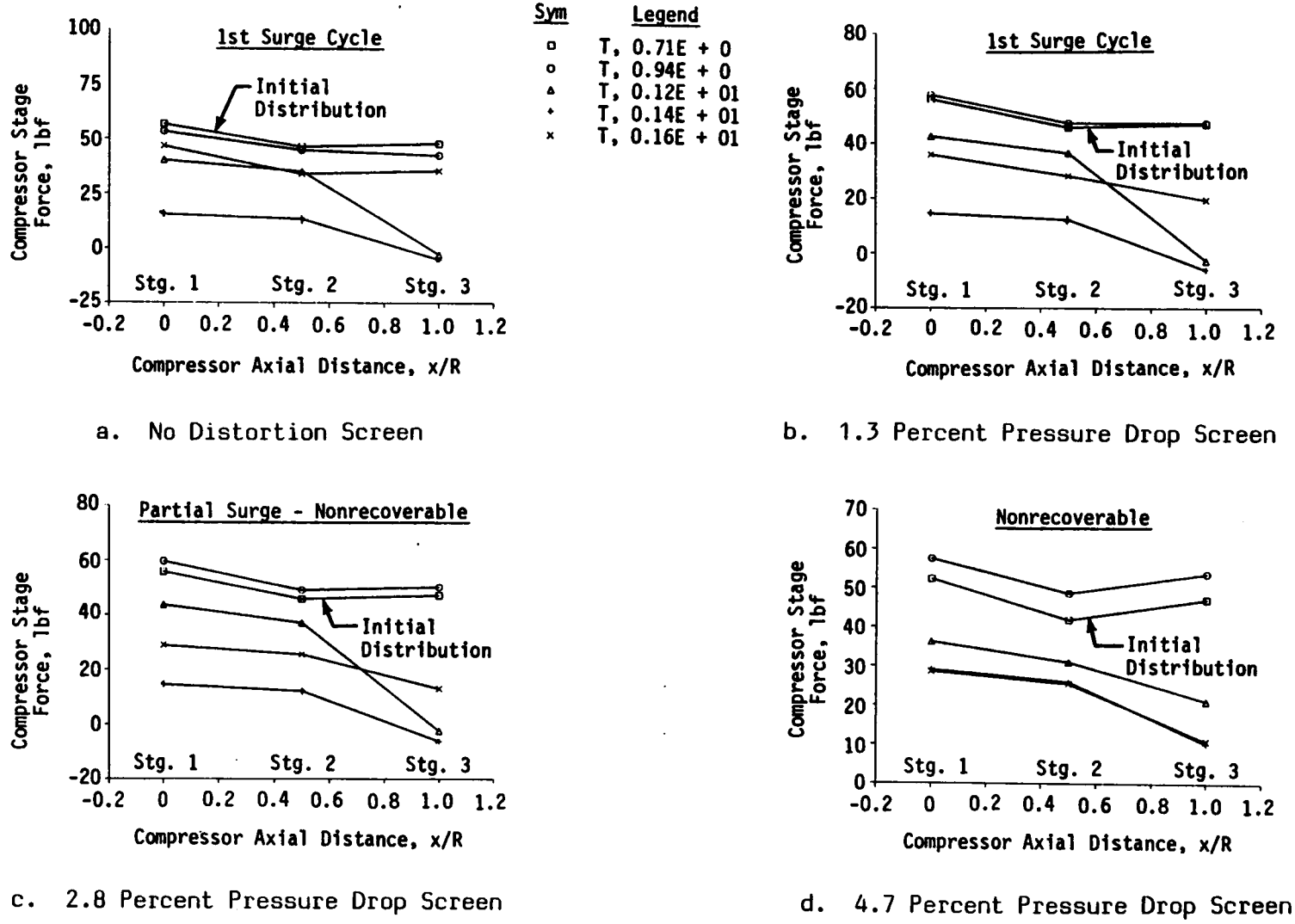

Figure 56. Three-Stage Compressor Stage Force Distribution With and Without the Distortion Screen Simulation.

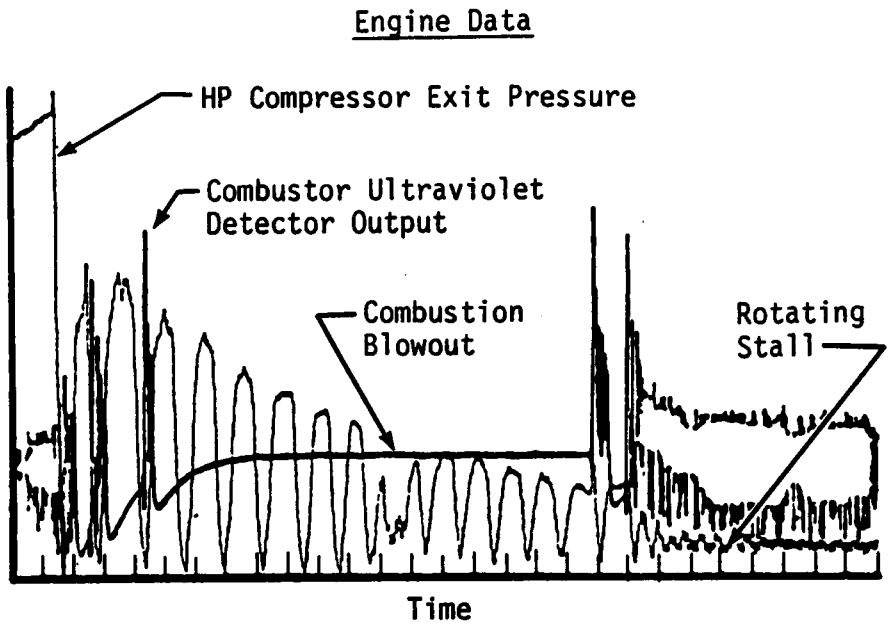

a. Complete Combustor Blowout

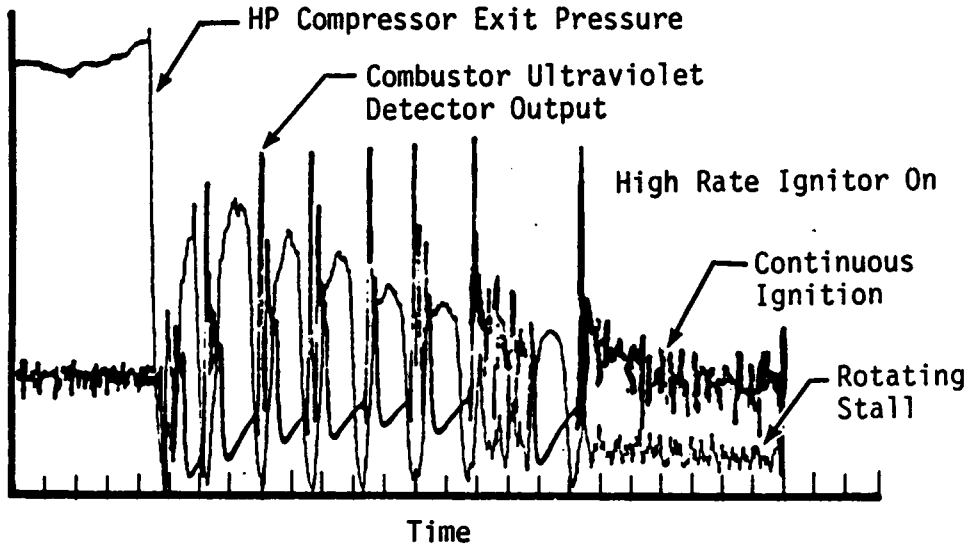

b. Intermittent Combustor Blowout

Figure 57. Actual Compressor/Combustor Interactions During Post-Stall Events [3].

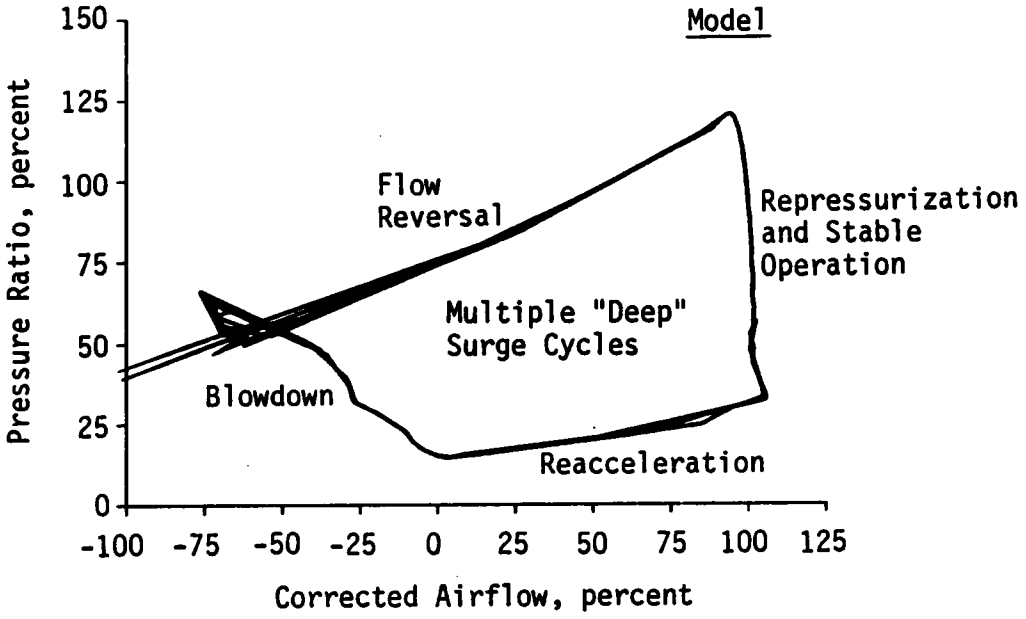

Figure 58. Model Surge Trajectories of a Nine-Stage HPC with Combustor Fuel Pulse at 100 Percent Speed.

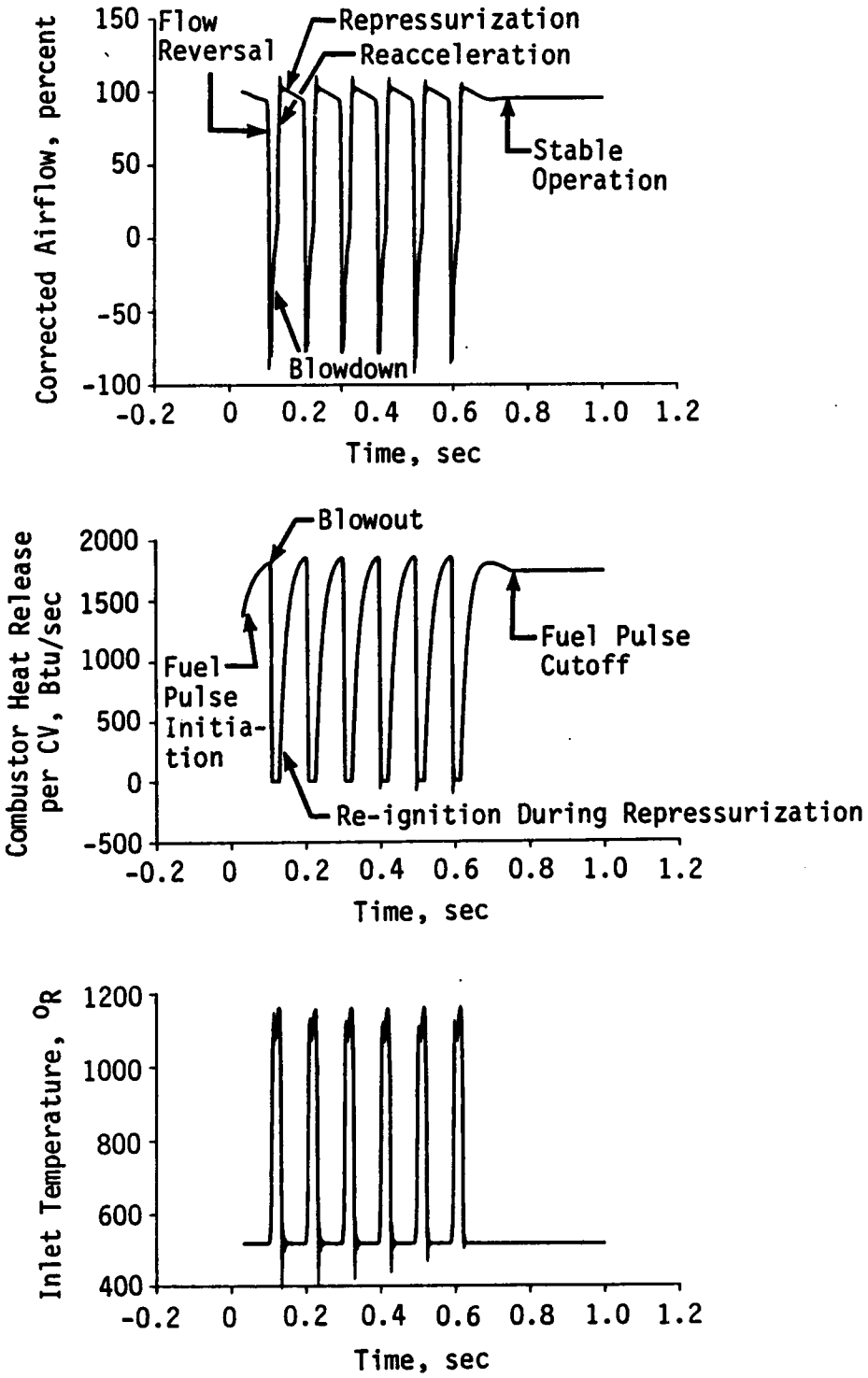

Figure 59. Model Indication of Combustor Blowout and Reignition During Fuel Pulse Driving Compression System Surge.

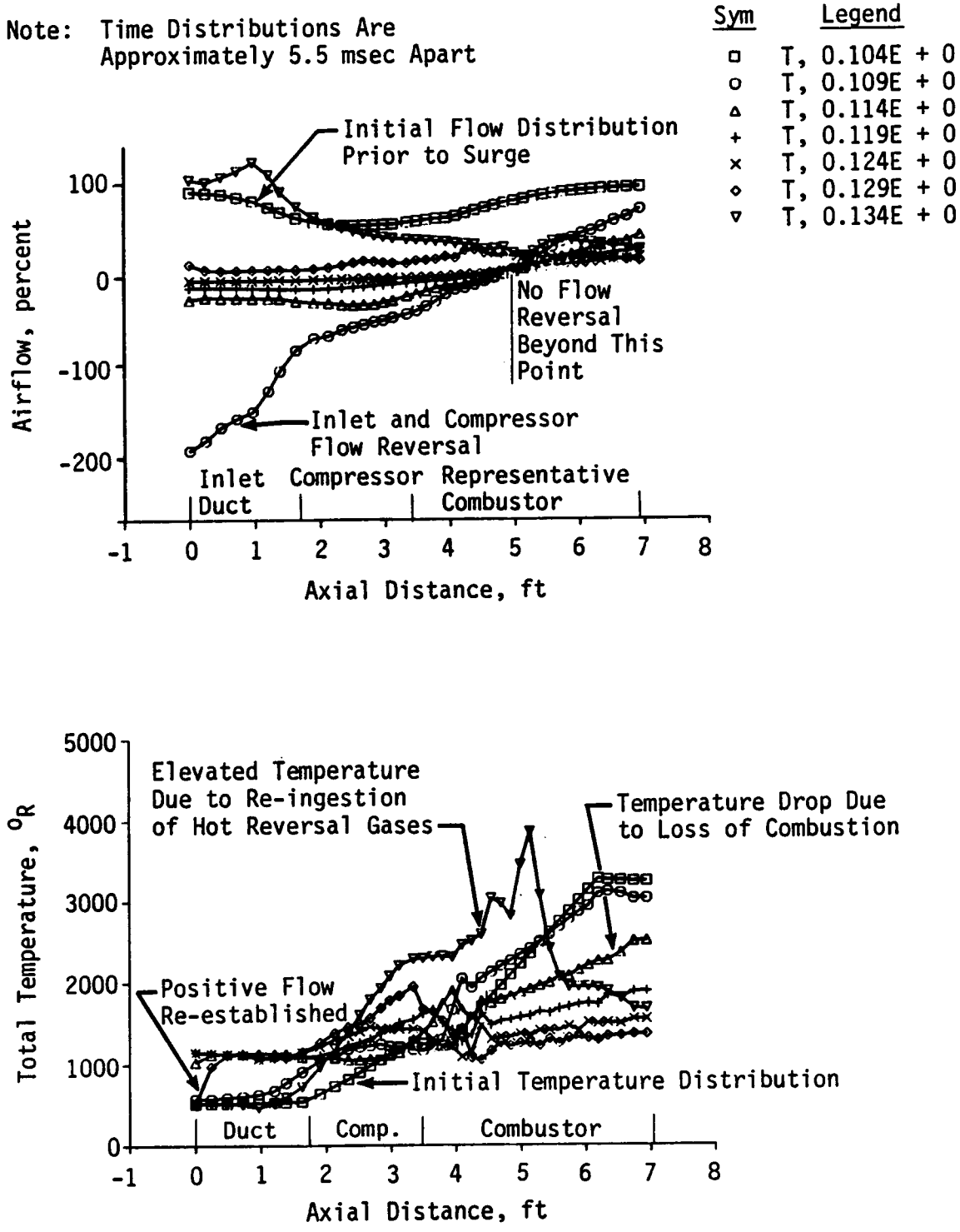

Figure 60. Model Prediction of Airflow and Temperature Distributions During a Surge of the HVC With Combustion at 100 Percent Speed.

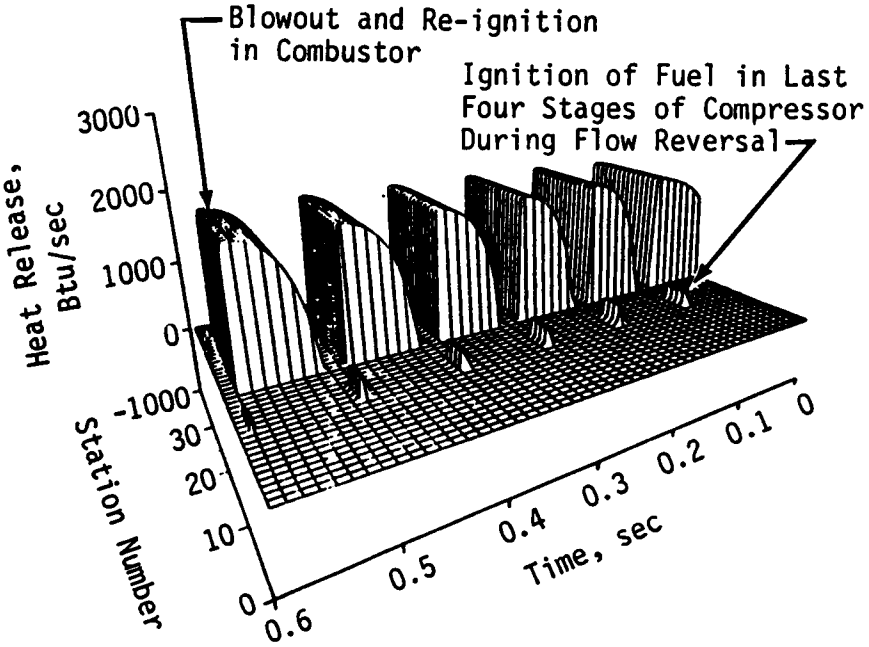

Figure 61. Heat Release in the Compressor Due to 10 Percent of the Combustor Fuel Flow Being Ingested During Flow Reversal of a Surge Cycle.

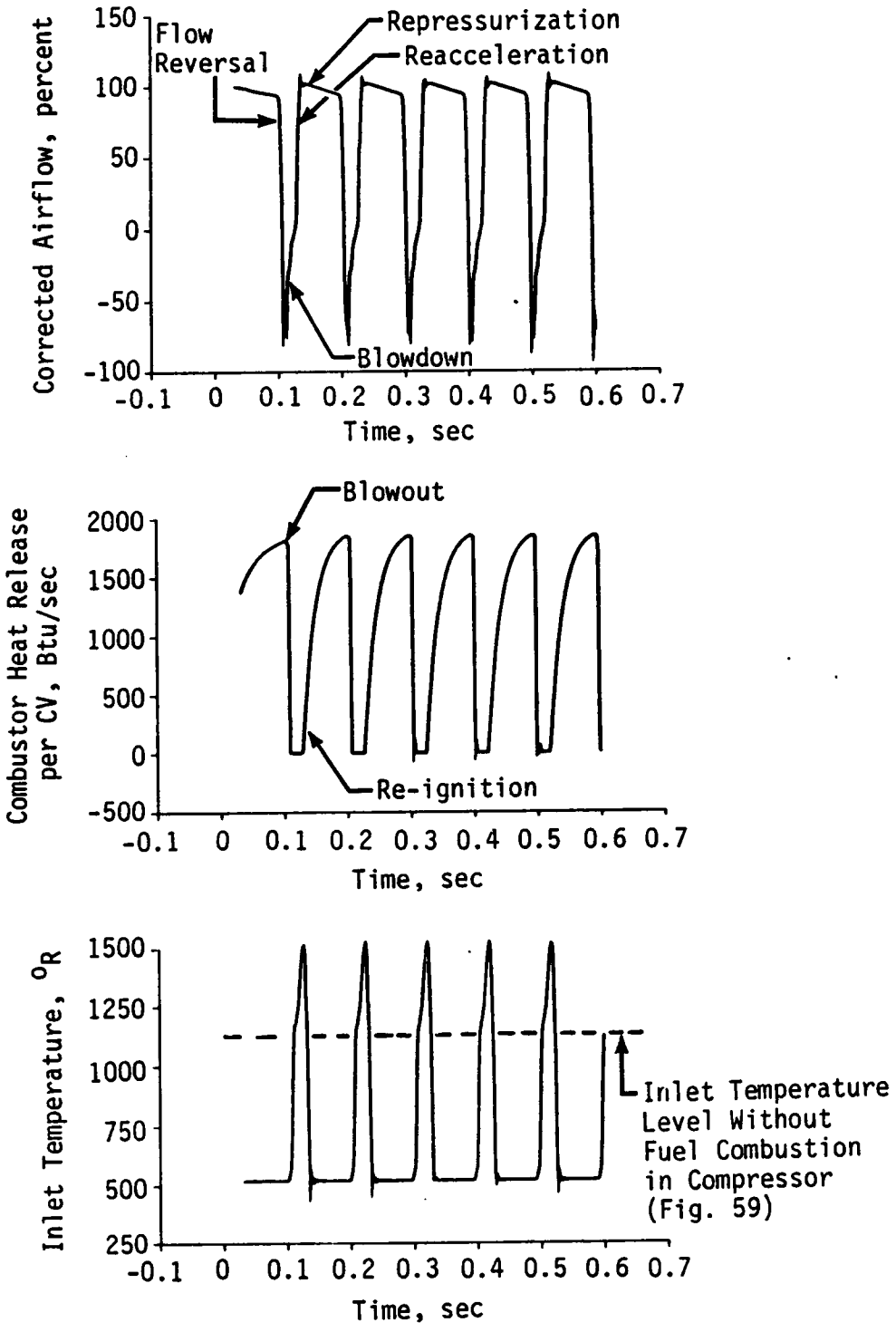

Figure 62. Model Prediction of the Effects of Ingesting 10 Percent of Initial Combustor Fuel Flow Into the Compressor During Flow Reversal Phase of a Surge Cycle.

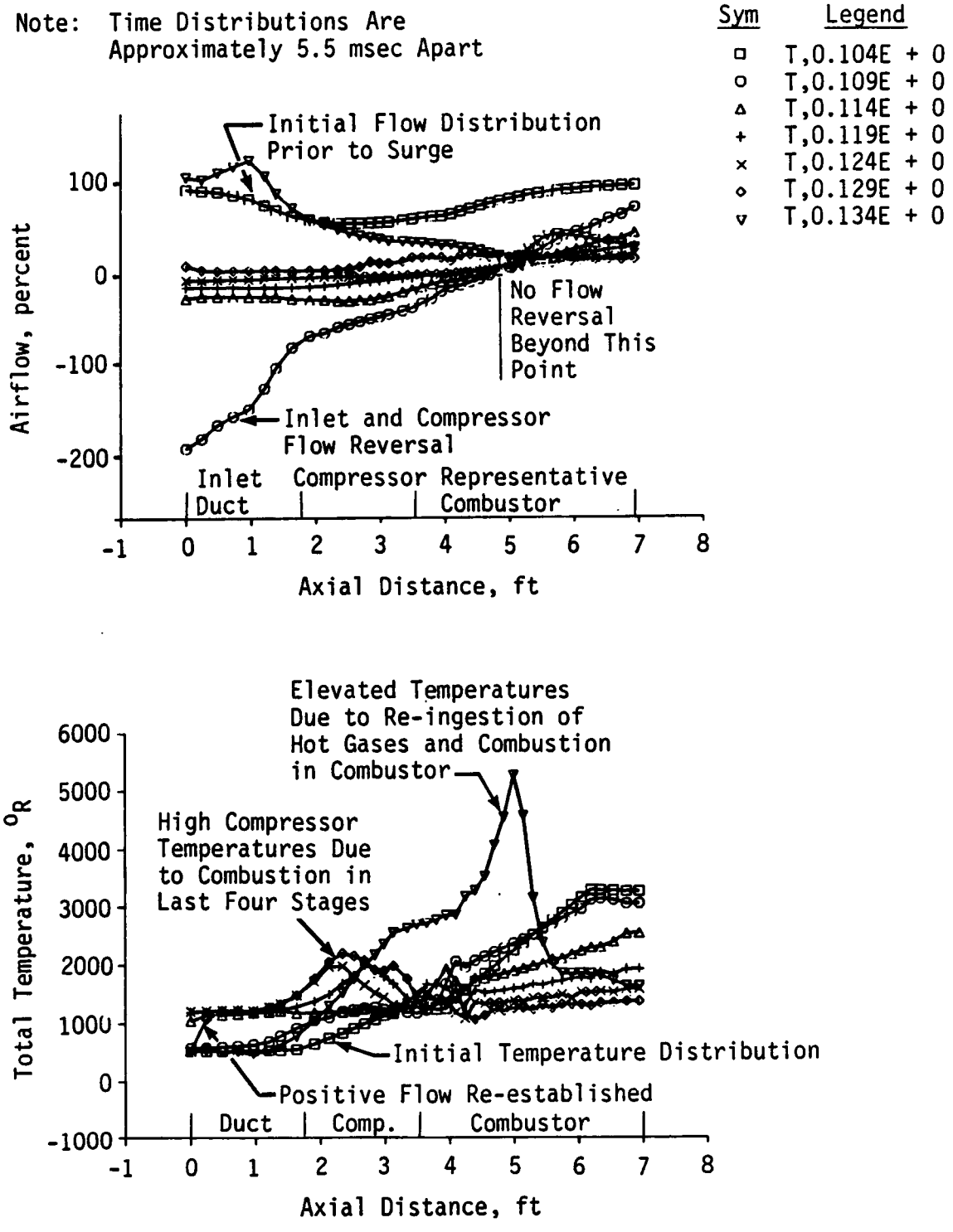

Figure 63. Model Predictions of Airflow and Temperature Distributions During a Surge Cycle with 10 Percent of the Initial Combustor Fuel Flow Being Ingested and Combusted in the Compressor During Flow Reversal.

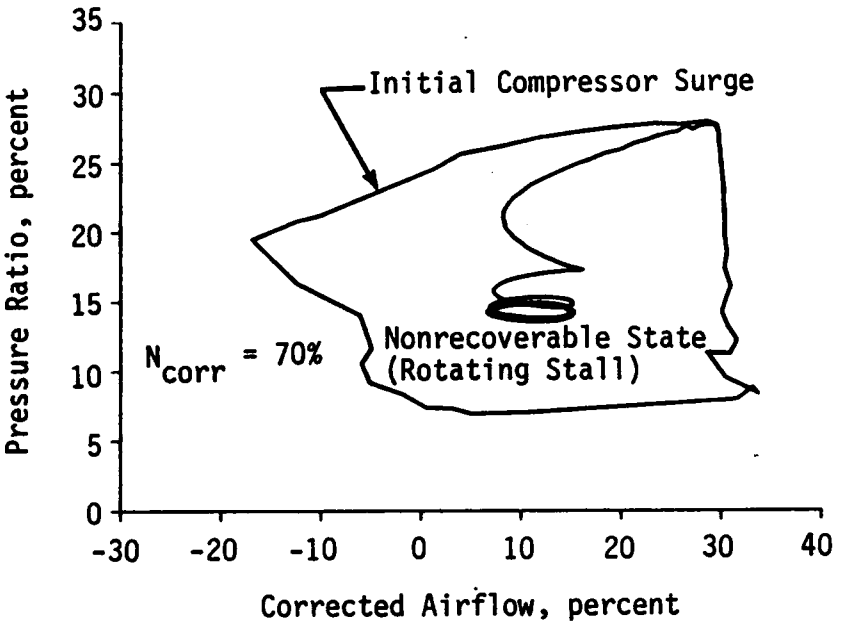

Figure 64. Model Prediction of Nonrecoverable Stall of the Nine-Stage HPC at 70 Percent Speed With Combustion.

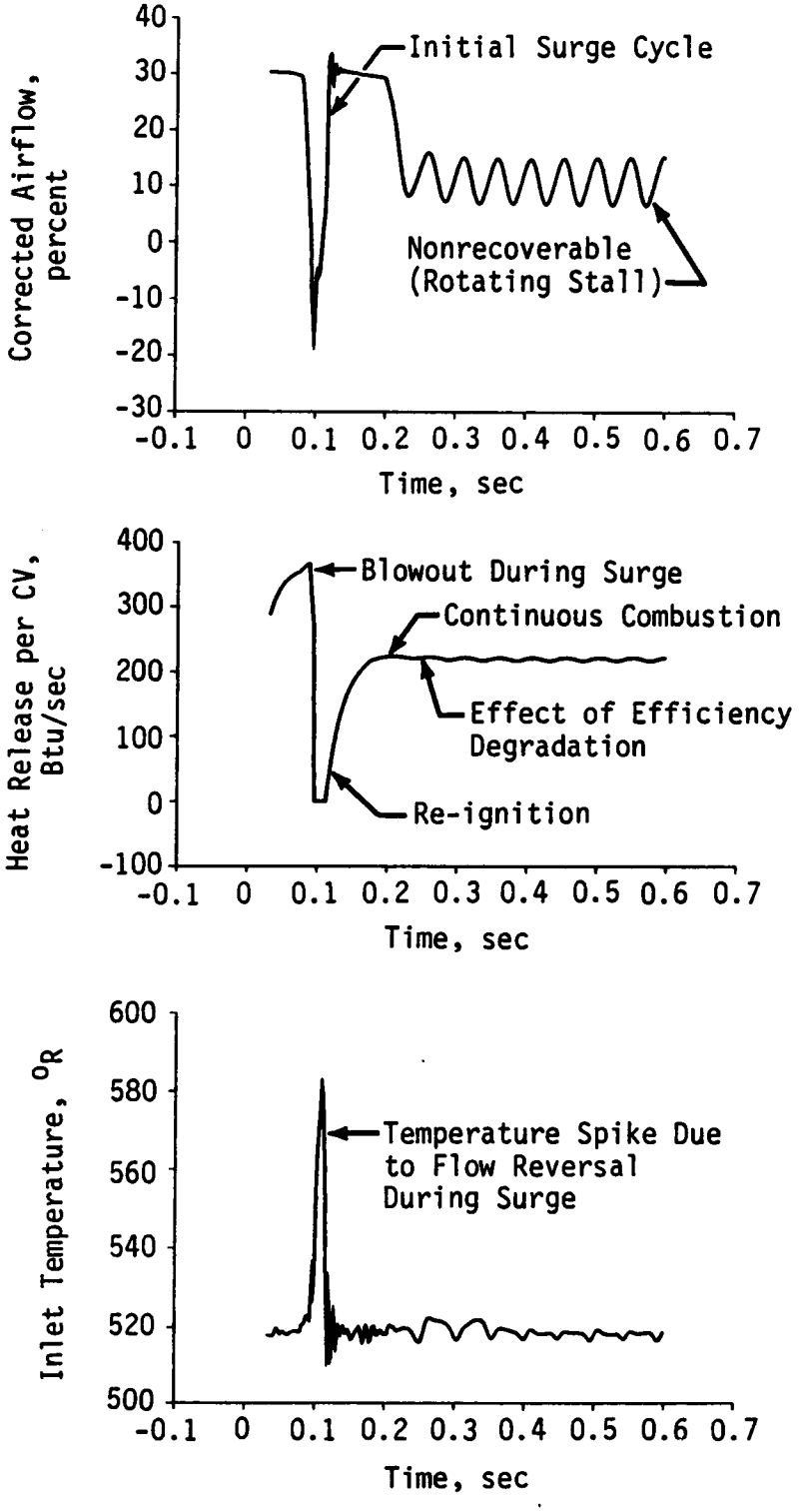

Figure 65. Model Prediction of Nonrecoverable Stall of a Nine-Stage HPC at 70 Percent Speed with Combustion.

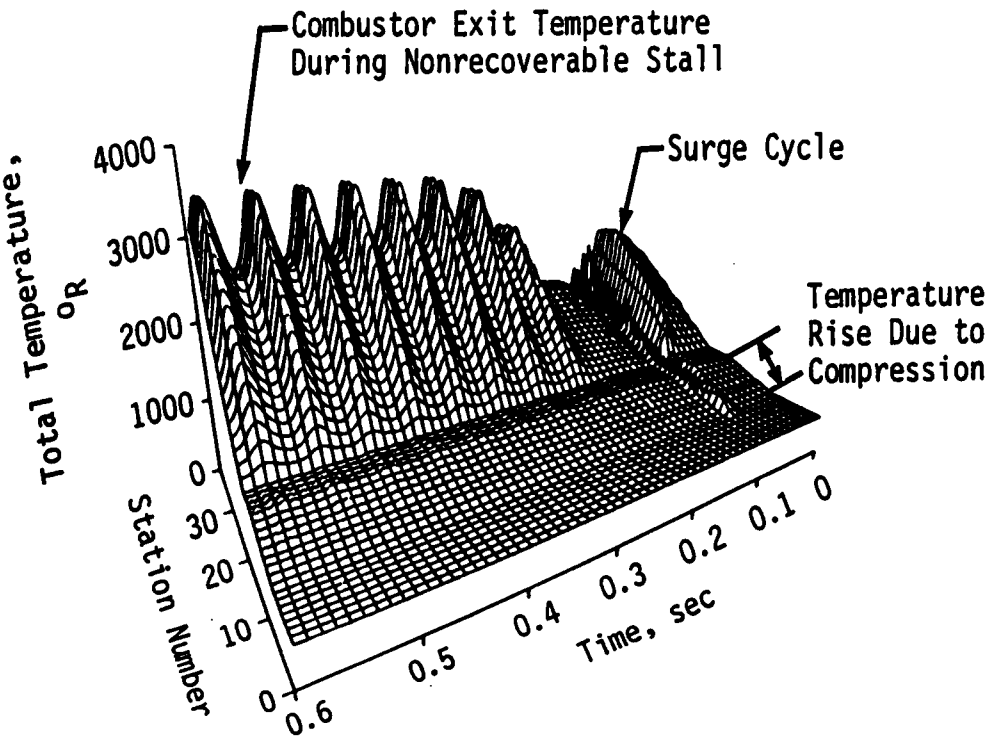

Figure 66. Model Prediction of Compression System and Combustion Temperature Distribution During Nonrecoverable Stall at 70 Percent Speed.

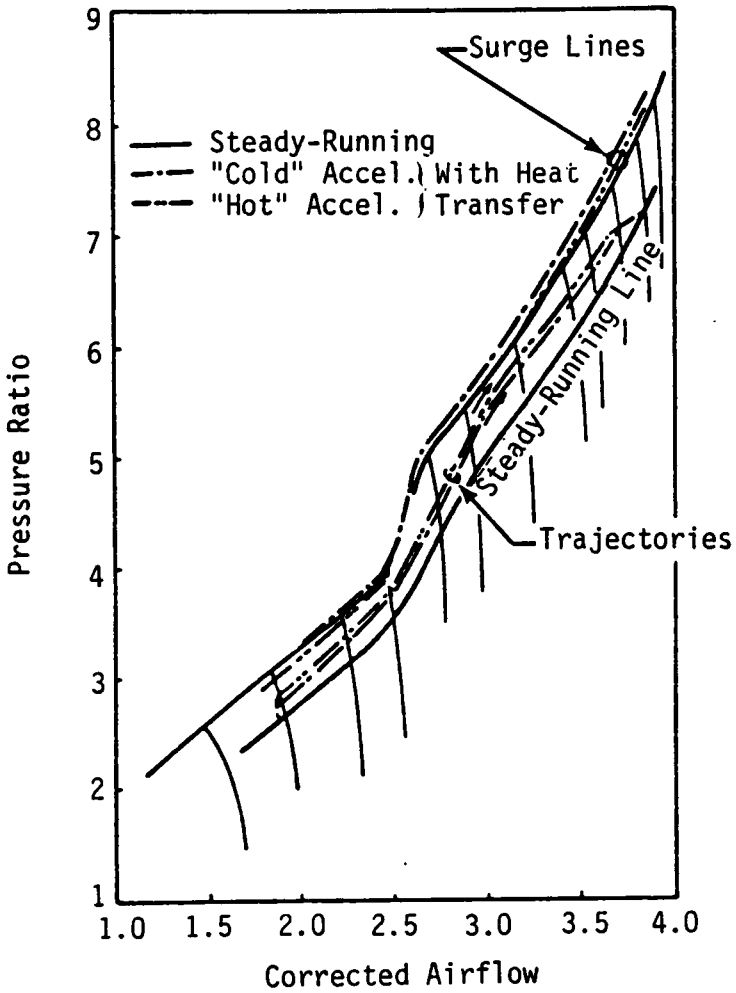

Figure 67. Predicted Trajectories and Surge Lines in HP Compressor- "Cold" and "Hot" Acceleration at Sea Level, [40].

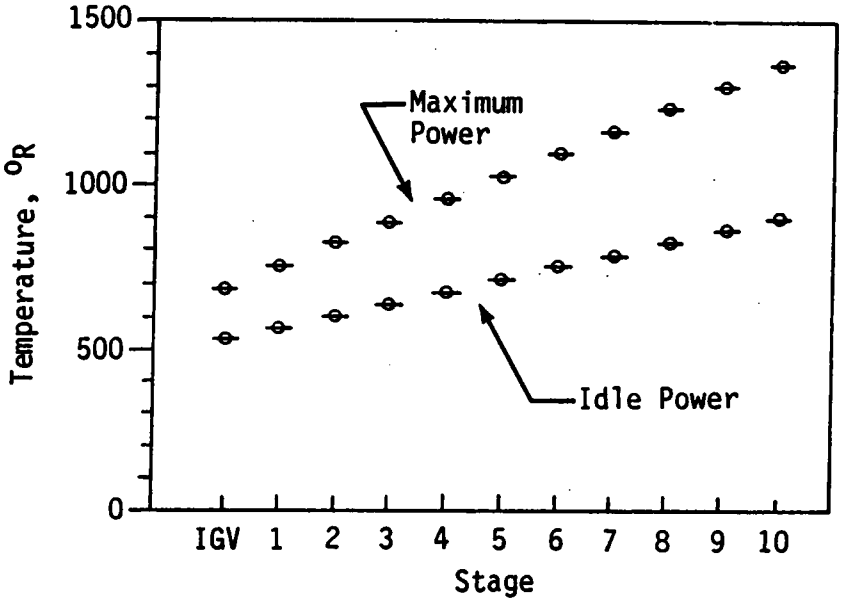

a. Core Compressor Temperature Distribution

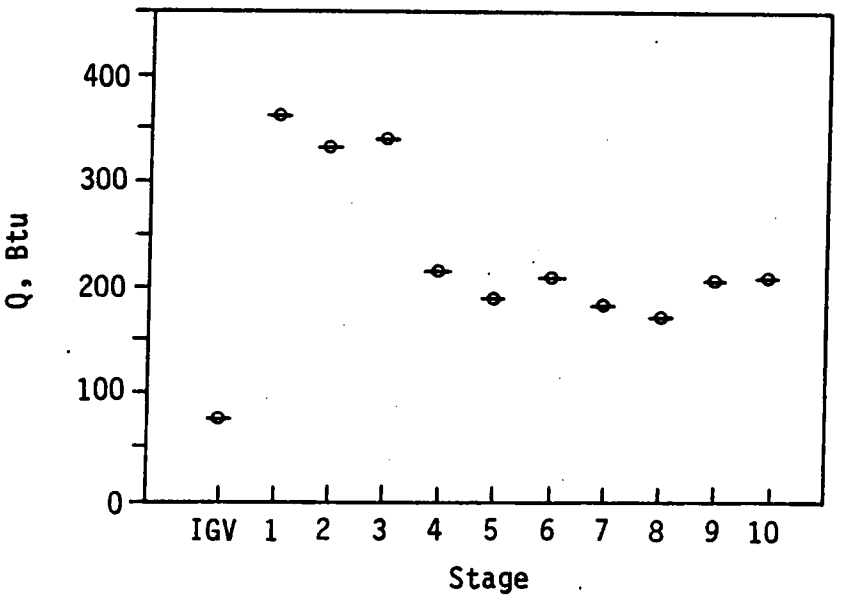

b. Stored Thermal Energy By Stage Blading

Figure 68. Predicted Stage Temperature Distribution at Maximum and Idle Power and Corresponding Blade Stored Thermal Energy in Each Stage [41].

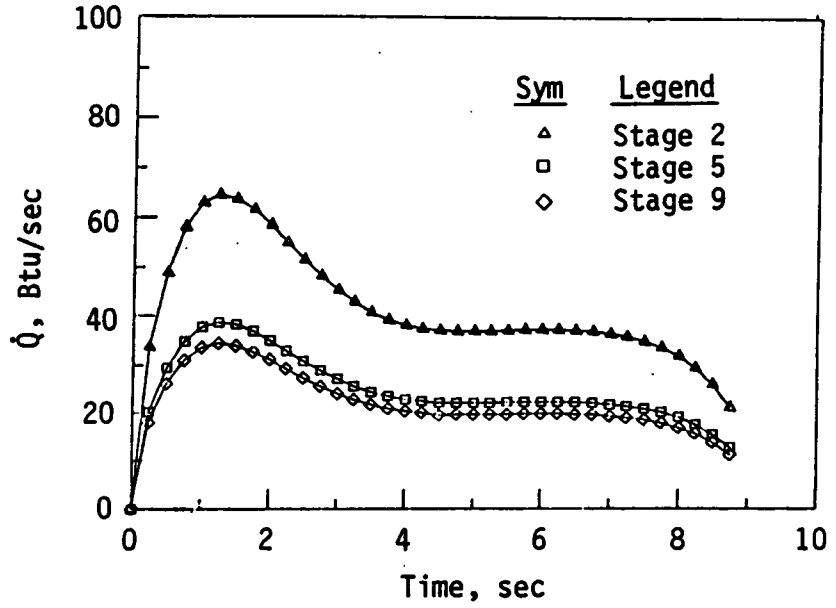

Figure 69. Typical Stage Heat Transfer Rates [41].

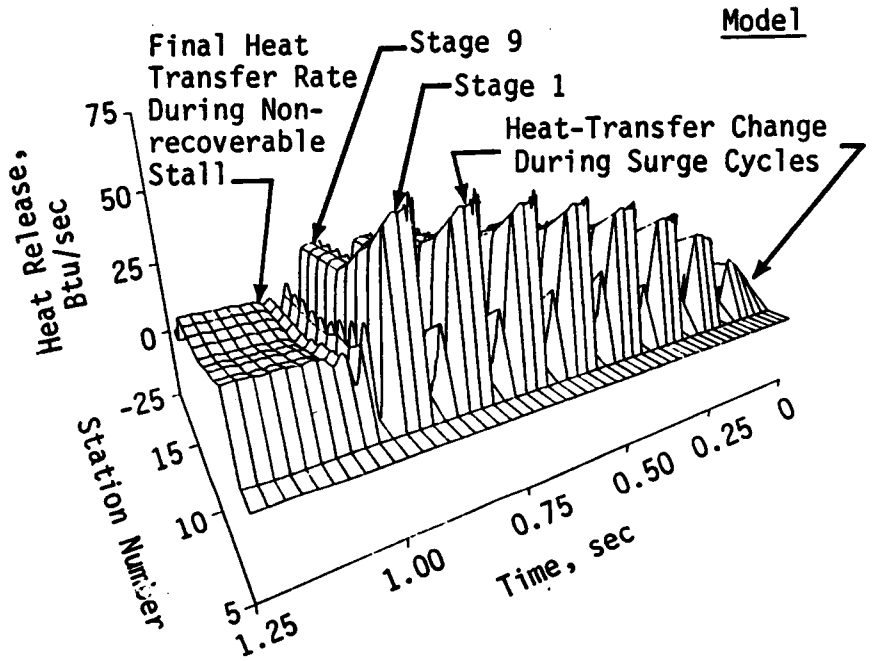

Figure 70. Heat Transfer Changes During Throttle Induced Surge Cycles of the Nine-Stage HPC at 70 Percent Speed.

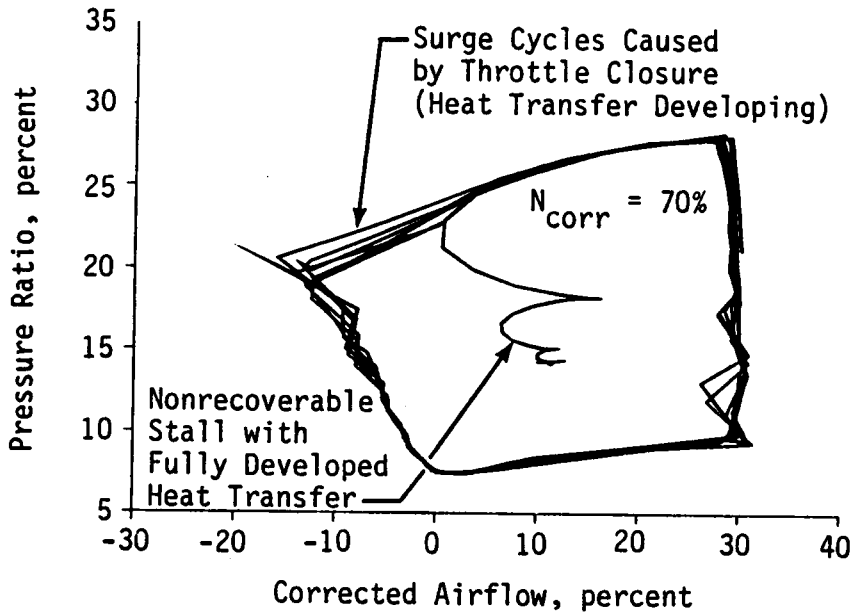

Figure 71. Effect of Compressor Heat Transfer (Blade to Gas Path) on Post-Stall Behavior, Nine-Stage HPC at 70 Percent Speed.

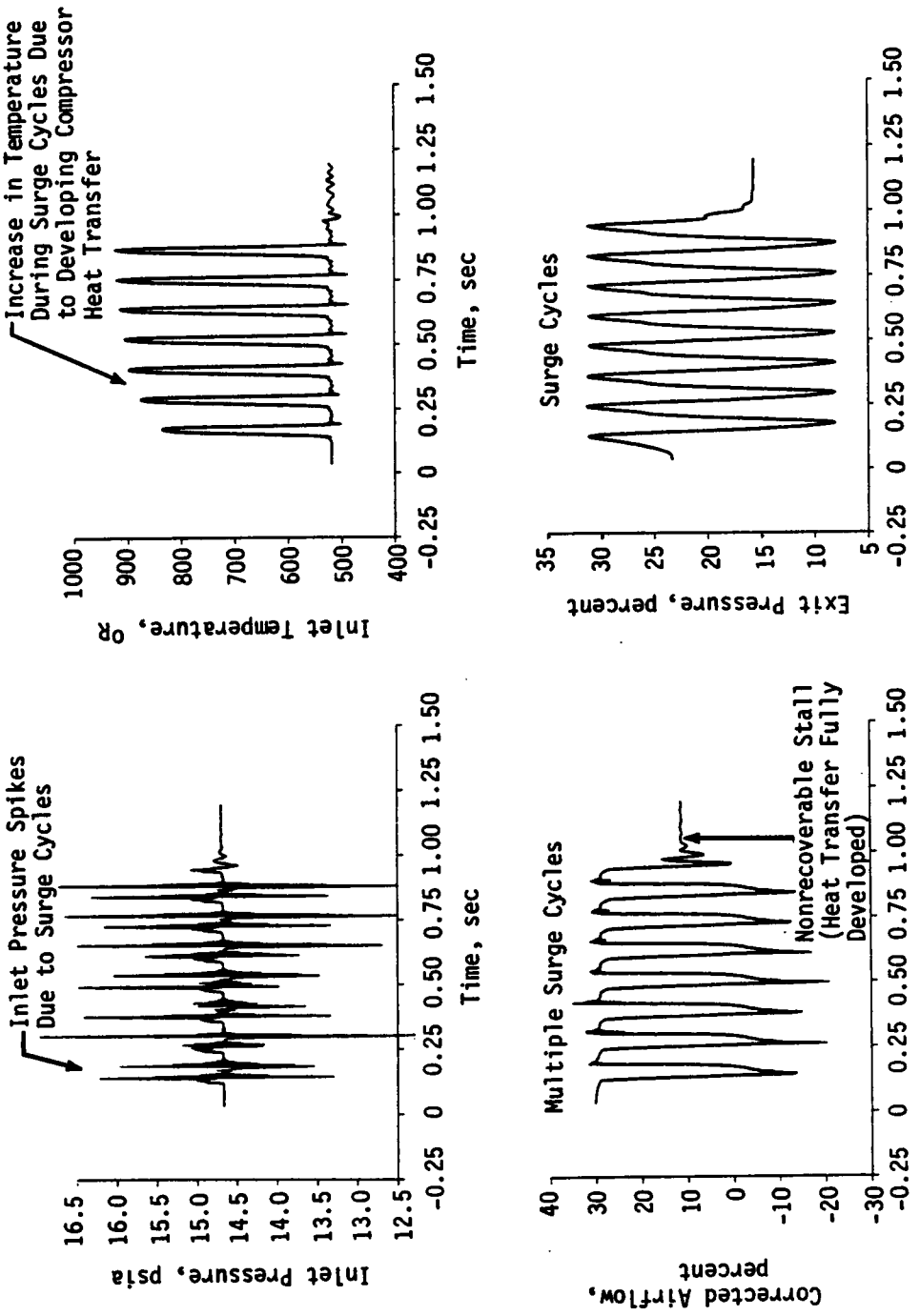

Figure 72. Model Compression System Performance During Throttle Induced Instability With Blade to Gas Path Heat Transfer Occurring.

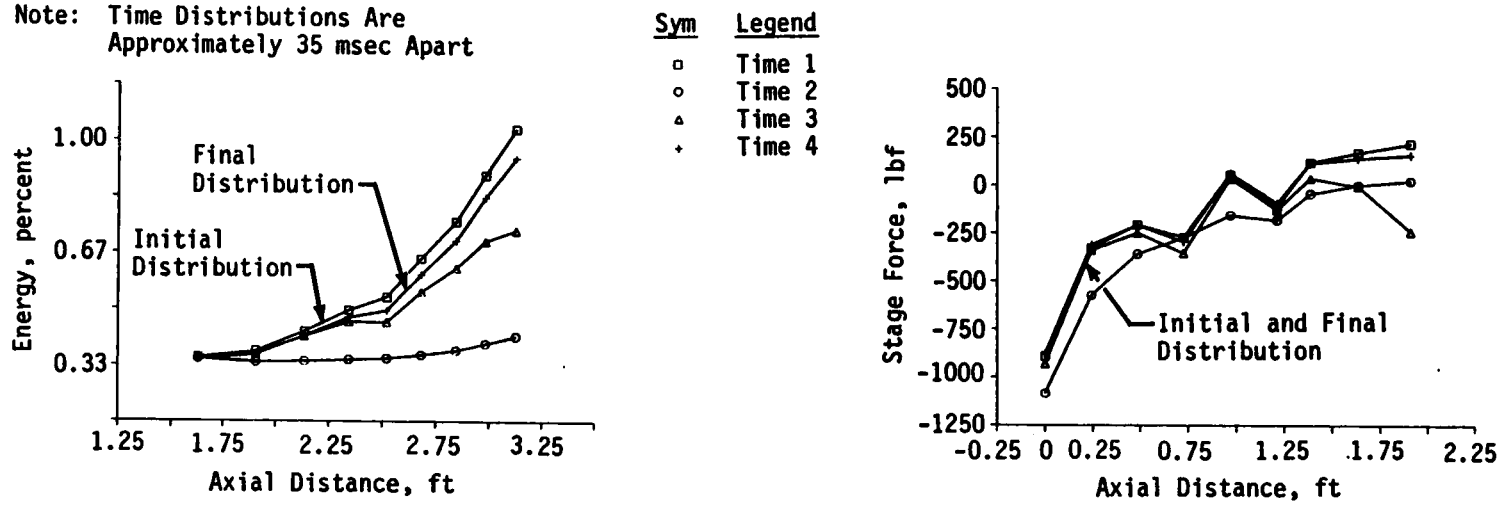

a. First Surge Cycle With Minimum Heat Transfer

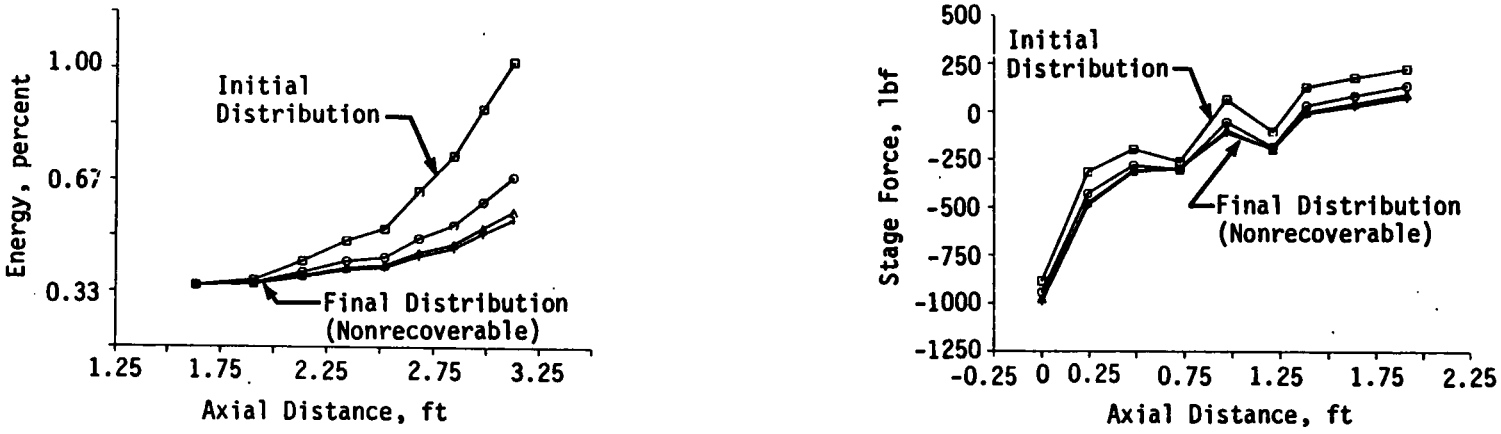

b. Last Surge Cycle and Nonrecoverable Stall With Maximum Heat Transfer

Figure 73. Stage Energy and Force During First and Last Surge Cycles of the Nine-Stage HPC at 70 Percent Speed With Compressor Heat Transfer.

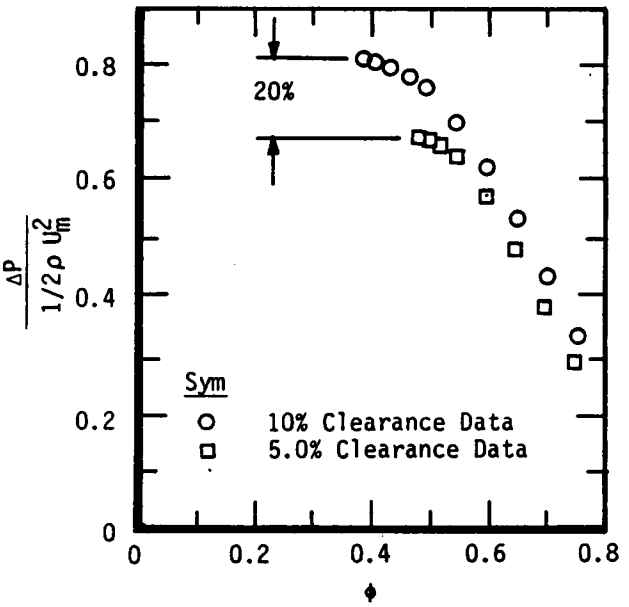

Figure 74. Effect of Tip Clearance on Stage Performance [42].

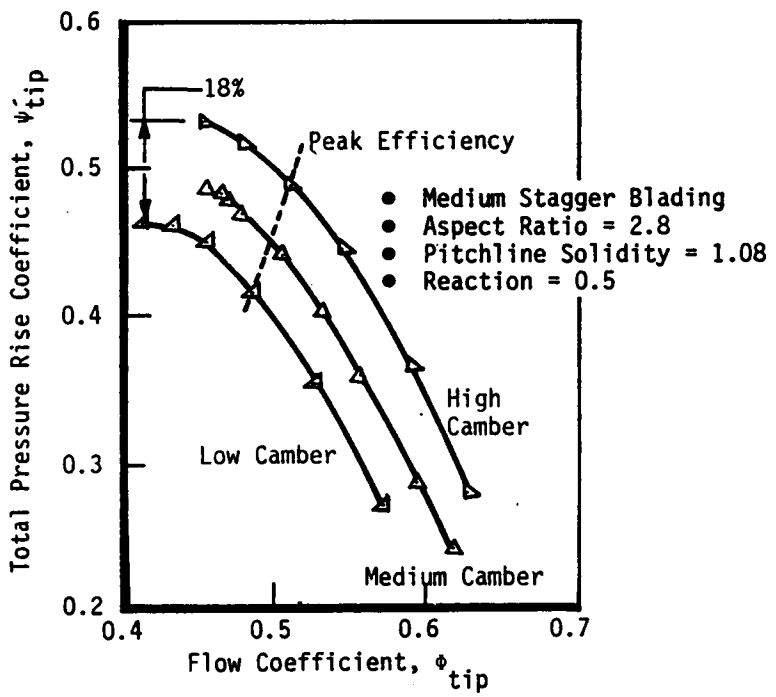

Figure 75. Effect of Camber on Stage Performance [43].

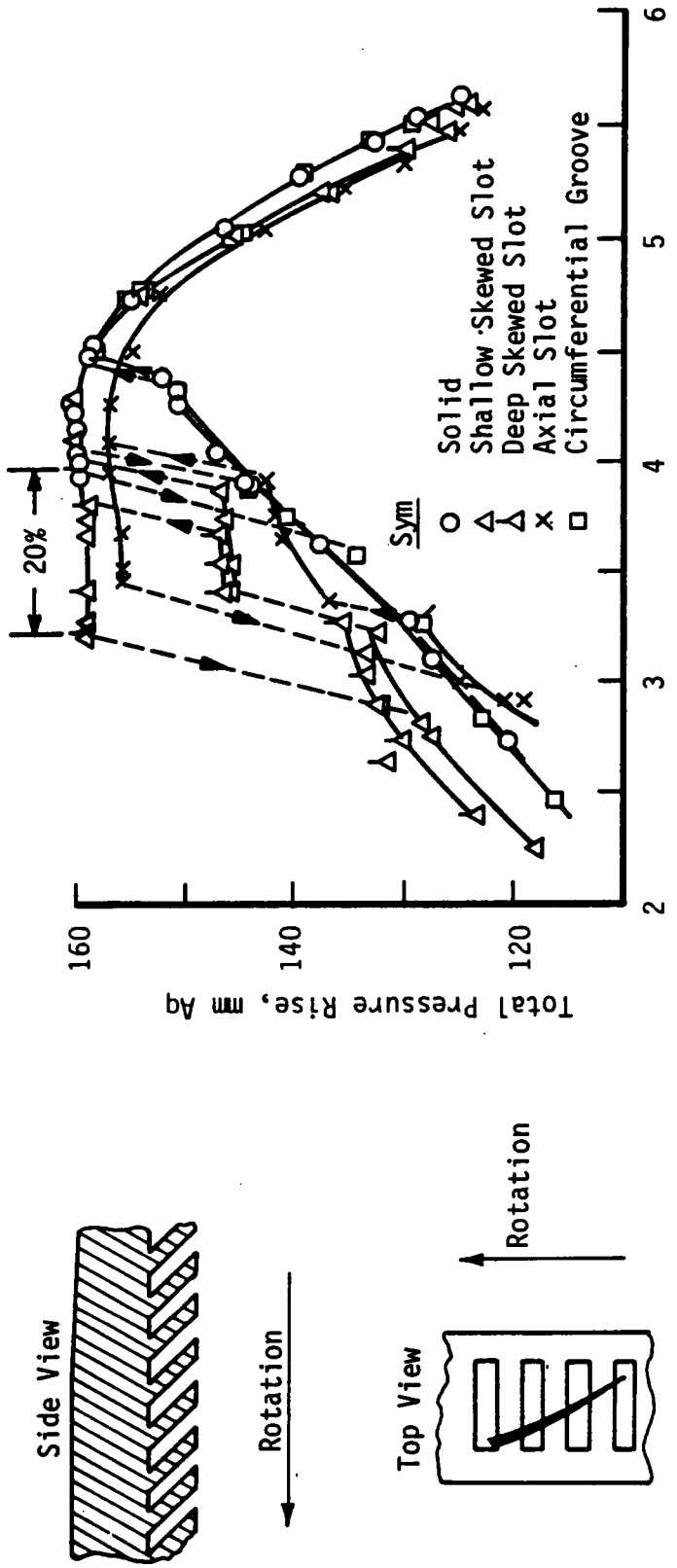

a. Tip Treatment Modification--Deep Skewed Slot Insert

b. Effects on Stage Characteristic

Figure 76. Possible Tip Treatment Modification and Its Effect On Stage Characteristic [44].

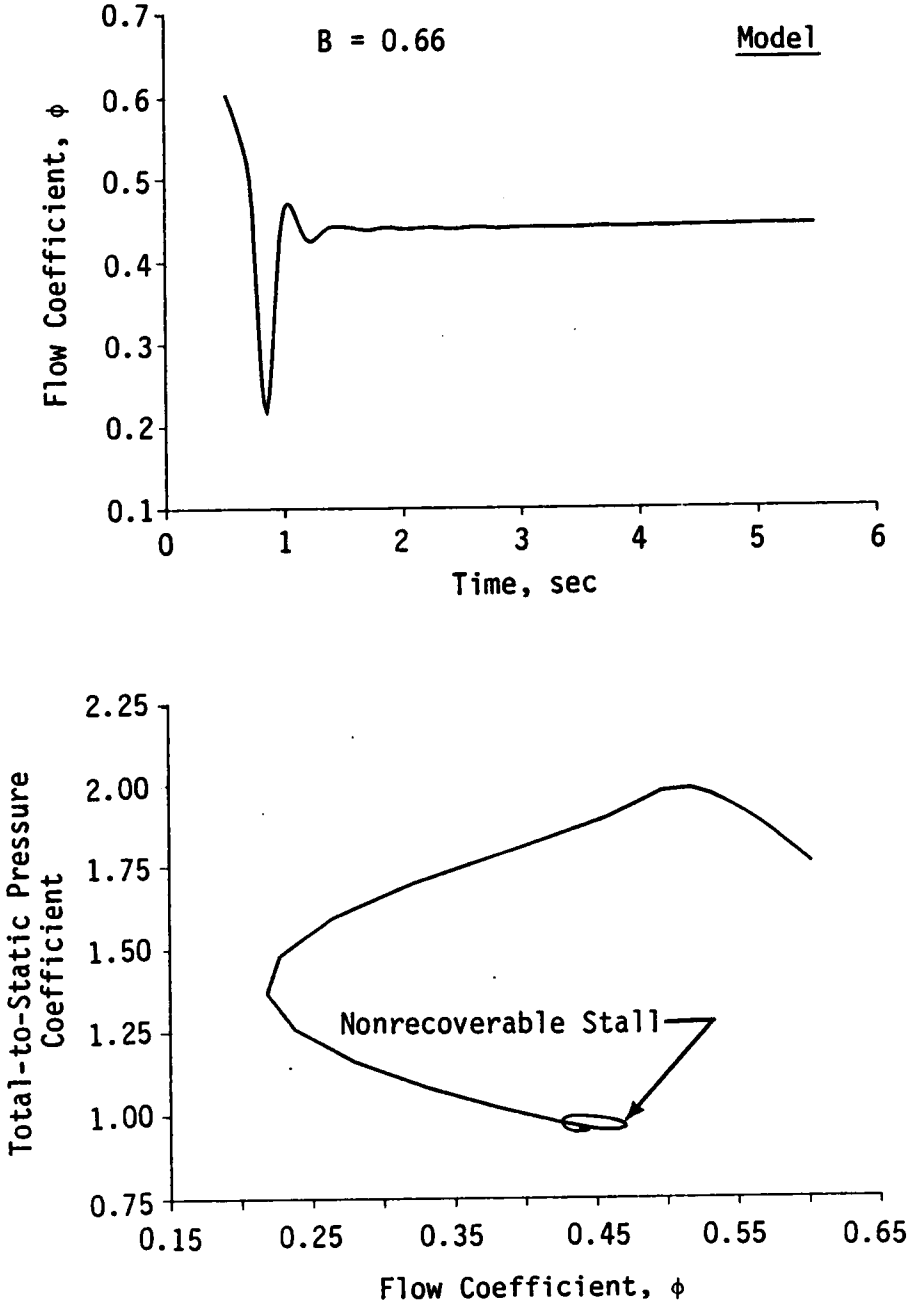

Figure 77. Three-Stage Compression System Model Prediction of Post-Stall Behavior: B=0.66.

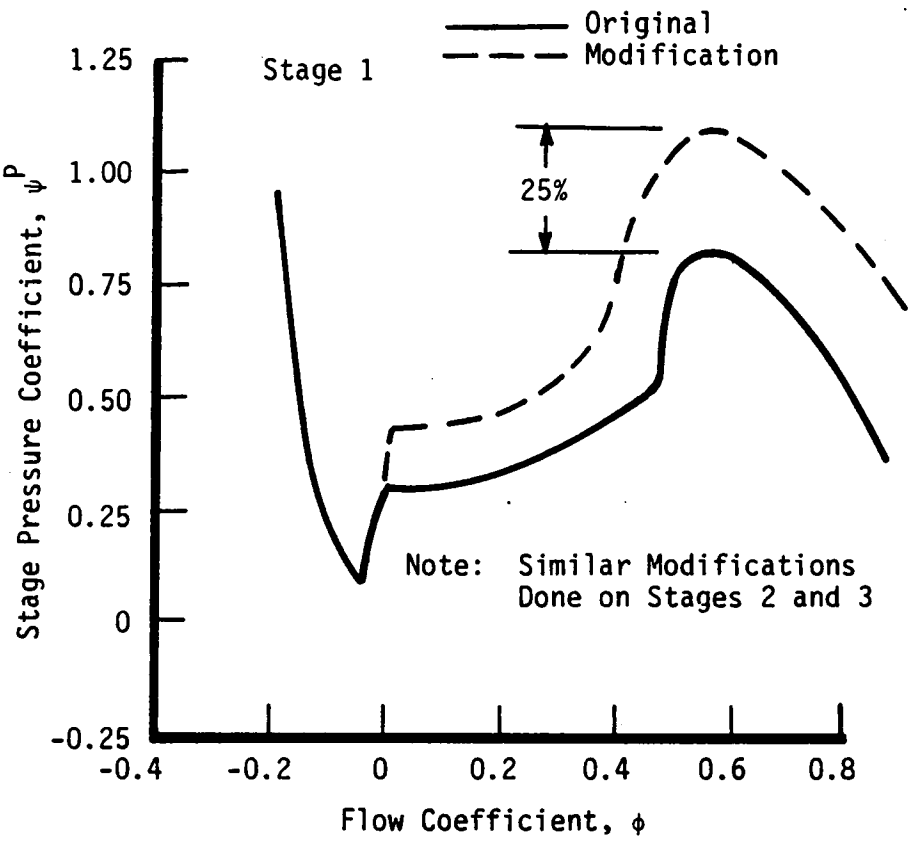

Figure 78. Possible Stage Pressure Characteristic Modification As a Result of Either Reducing Tip Clearance or Increasing Blade Camber.

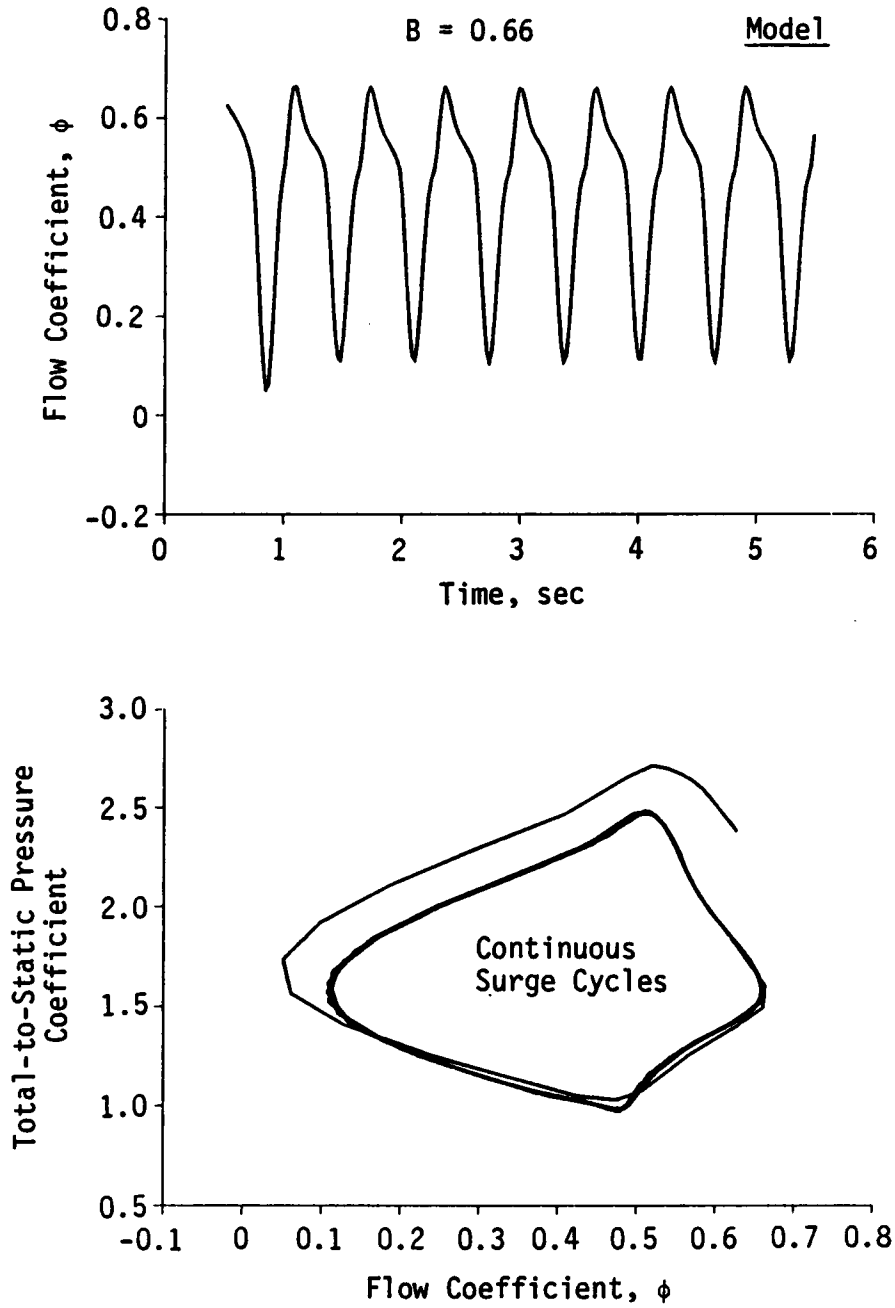

Figure 79. Model Prediction of the Effect of Reducing the Tip Clearance and/or Increasing the Blade Camber on Post-Stall Behavior: B=0.66.

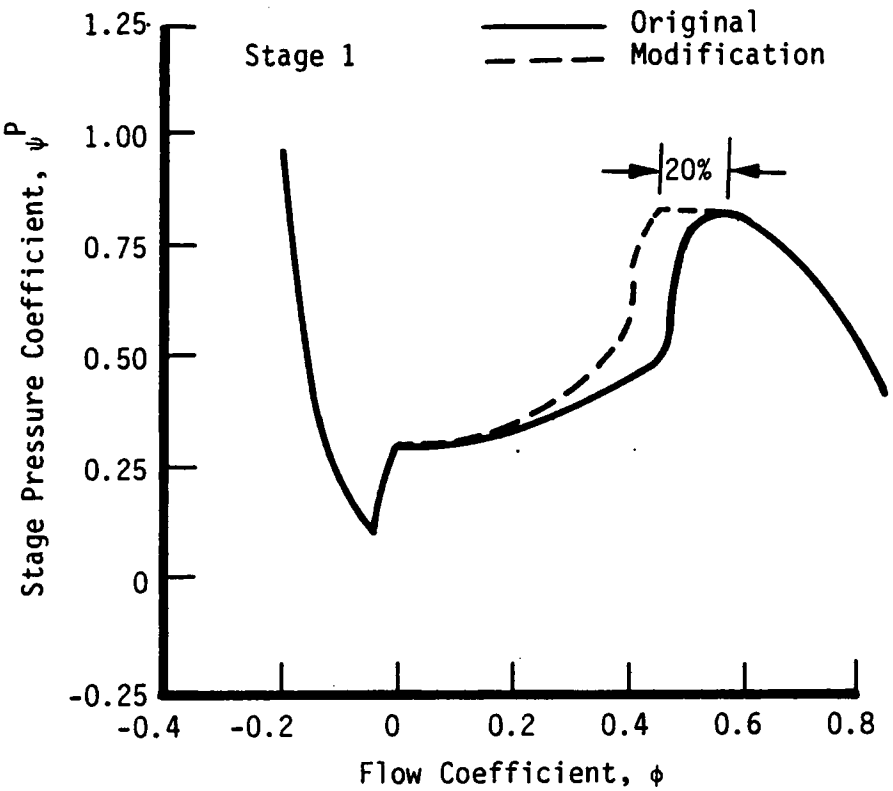

Figure 80. Postulated Stage Pressure Characteristic Modification As a Result of Tip Treatment.

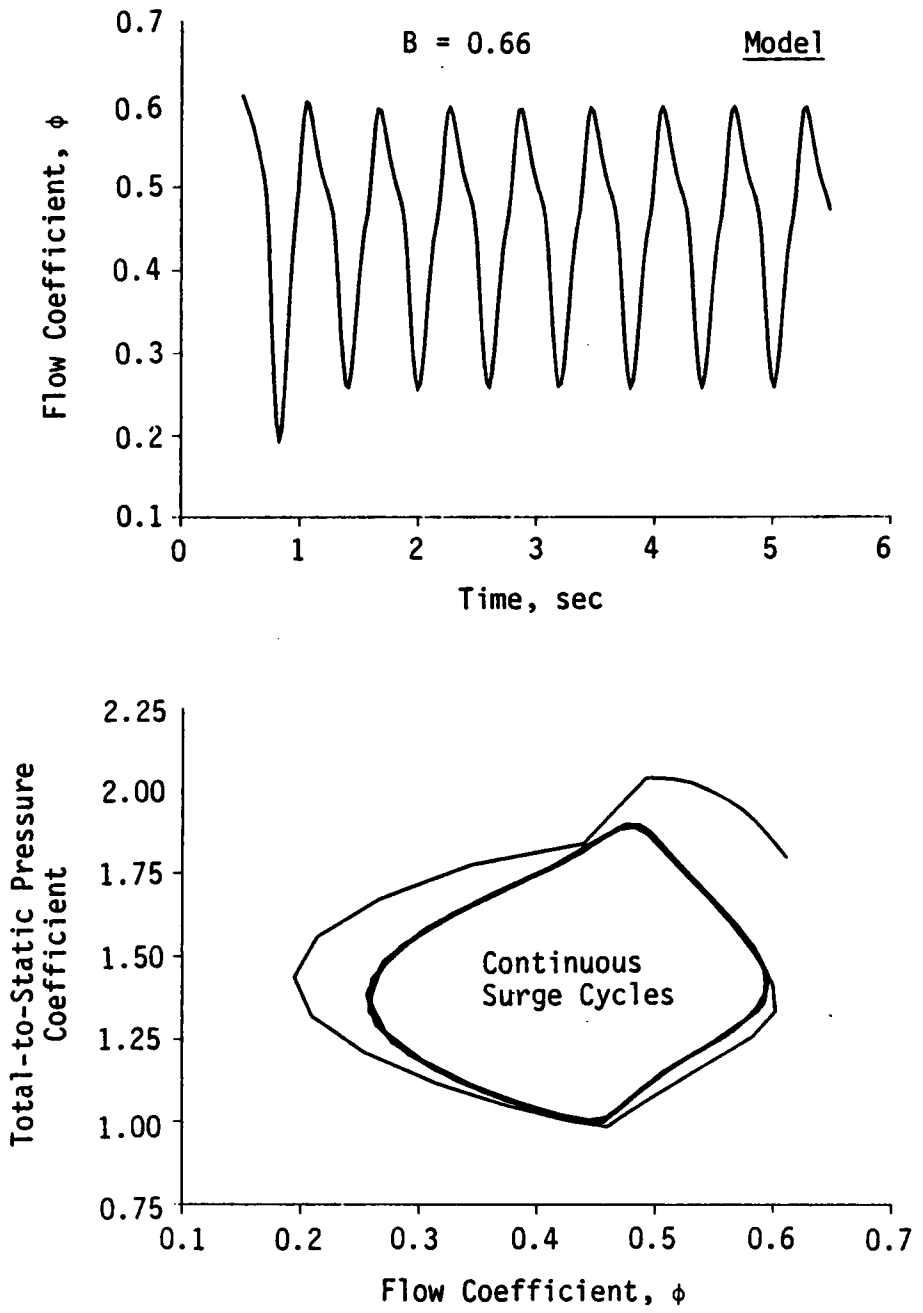

Figure 81. Model Prediction of the Effect of First Stage Tip Treatment on Post-Stall Behavior: B=0.66.

The two page vita has been removed from the scanned document. Page 1 of 2

The two page vita has been removed from the scanned document. Page 2 of 2